Ministry of Higher Education and Scientific Research
Hassiba Benbouali University of Chlef

Faculty of Technology

Department of Mechanical Engineering

THESIS

Presented for obtaining the diploma of

DOCTORAT

Field: Mechanical engineering

Specialty: Mechanical and production manufacturing

By

Abdelwahab KHLEDJ

Theme

Study of the aptitude for thermoforming of extruded sheets based on an ABS - 15% PMMA blend

Defended on --/--/----, before jury composed of :

ZAHLOUL Hamou	Professor	Chlef University	President
ZIDANE Ibrahim	Professor	Chlef University	Examinator
OULD CHIKH El Bahri	Professor	Mascara University	Examinator
MERIEM BENZIANE Madjid	Professor	Chlef University	Examinator
HADJ MILOUD Mohamed	MCA	Chlef University	Supervisor
MENDAS Mohammed	Professor	Chlef University	Co-Supervisor
BACHIR BOUIADJRA Bel Abbes	Professor	Sidi Bel Abbes University	Invited

Acknowledgment

<div dir="rtl">

الحمد لله الذي بنعمته تتم الصالحات

لا يشكر الله من لا يشكر الناس

</div>

I would like to express my deep gratitude to Dr. *Hadj Miloud Mohamed* for his continuing support, patience and motivation throughout my research career. His in-depth knowledge, insight and wise counsel have contributed significantly to the progress of this project. Dr. *Hadj Miloud's* encouragement and constructive comments were instrumental in guiding my research and the development of this thesis. I am deeply grateful for his dedication and the invaluable influence he has had on my academic development.

I am extremely grateful to Pr**.** *Mendas Mohammed* for his unwavering support and exceptional guidance throughout my work. His great expertise, strategic advice and enlightened views have played an essential role in the advancement of this research. Pr. *Mendas* encouragement and contributions have not only enriched this project, but have also fostered my personal and professional development. I deeply appreciate his mentorship and the significant impact it has had on this thesis.

I would also like to express my profound gratitude to Pr. *Zidane Ibrahim*, His dedicated supervision, generous availability, and insightful advice have been instrumental throughout my doctoral research. His expert guidance and unwavering support have significantly contributed to the success of this thesis.

I would like to express my sincere gratitude to all the members of the jury who generously dedicated their time to evaluate this work. I extend my heartfelt thanks to Mr. *Zahloul Hamou*, Professor at UHB Chlef, *Ould Chikh El Bahri*, Professor at the University of Mascara, *Meriem Benziane Madjid*, Professor at UHB Chlef, and **Bachir Bouiadjra Bel Abbes** Professor at the University of Sidi Bel Abbes Your expertise and support have been invaluable throughout this process

I extend my heartfelt thanks to all the faculty members and individuals who, through their words, advice, and constructive criticism, have guided and influenced my reflections. I am especially grateful to Mr. *Yakoubi Belkacem* for her invaluable contributions and support.

Finally, I wish to express my heartfelt gratitude to my family and friends for their unwavering support and encouragement throughout my academic journey and the process of researching and writing this thesis. While my father is no longer with us, his memory remains a source of inspiration. I am profoundly thankful to my mother for her constant encouragement and support. Their love and belief in me have been instrumental in making this achievement possible.

Abstract

The objective of this study is to investigate the effect of temperature and strain rate on the characterization of an ABS/PMMA bilayer polymer structure. The bilayer is composed of 85% Acrylonitrile Butadiene Styrene (ABS) and 15% Poly(Methyl Methacrylate) (PMMA). The theoretical section presents a review of the applications of this polymer and explores the potential of thermoforming for bathtub production. It is of great importance that the technology used in this process gains insight into the relationship between thermoforming processes and the thermal, mechanical, and tribological properties of the ABS/PMMA bilayer. The experimental phase comprises a series of methodically designed tests on ABS/PMMA bilayer sheets. The thermal properties, including thermal stability and glass transition temperature, were evaluated, as well as viscoelastic behavior through mechanical dynamic analysis. Tensile testing was performed at varying temperatures and deformation rates to determine the modulus of elasticity, stress limits, maximum stresses, and elongation at break. Charpy impact testing was done to assess the impact resistance of the material, followed by fractographic analysis to examine interlayer interactions, identify the characteristics of structural and fracture defects, and explain the fracture characteristics observed following tensile and impact testing. Bending strength evaluations were performed to compare the ABS/PMMA bilayer with pure ABS and PMMA. Furthermore, the hardness and tribological properties, including the coefficient of friction and specific wear rate, were investigated. The findings indicated that the ABS/PMMA bilayer exhibited notable thermal stability. The glass transition temperature of the bilayer was found to be 111 °C. The viscoelastic behavior was described by determining the storage and loss modulus. Additionally, the results demonstrate that the influence of temperature and strain rate parameters on the tensile behavior of the ABS/PMMA bilayer was also determined, indicating a high dependence of mechanical behavior on these two parameters. The bilayer structure exhibited good adhesion between the two layers, and the hardness and wear rate were determined.

Key words: ABS; PMMA; Bilayer polymer; Thermal and mechanical properties; Tribology; Fractography.

Résumé

L'objectif de cette étude est d'examiner l'effet de la température et de la vitesse de déformation sur la caractérisation d'une structure polymère bicouche ABS/PMMA. La bicouche est composée de 85% d'Acrylonitrile Butadiène Styrène (ABS) et de 15% de Poly(Méthacrylate de Méthyle) (PMMA). La section théorique présente une revue des applications de ce polymère et explore le potentiel du thermoformage pour la production de baignoires. Il est très important pour la technologie utilisée dans ce processus de comprendre la relation entre les processus de thermoformage et les propriétés thermiques, mécaniques et tribologiques de la bicouche ABS/PMMA. La phase expérimentale comprend une série de tests méthodiques sur la feuille bicouche ABS/PMMA. Les propriétés thermiques, y compris la stabilité thermique et la température de transition vitreuse, ont été évaluées, ainsi que le comportement viscoélastique par le biais d'une analyse mécanique dynamique. Des essais de traction ont été réalisés à différentes températures et vitesses de déformation pour déterminer le module d'élasticité, les limites de contrainte, les contraintes maximales et l'allongement à la rupture. Des essais d'impact Charpy ont été effectués pour évaluer la résistance à l'impact du matériau, suivis d'une analyse fractographique pour examiner les interactions entre les couches, identifier les caractéristiques des défauts structurels et de rupture, et expliquer les caractéristiques de rupture observées à la suite des essais de traction et d'impact. Des évaluations de la résistance à la flexion ont été réalisées pour comparer la bicouche ABS/PMMA à l'ABS et au PMMA purs. En outre, la dureté et les propriétés tribologiques, y compris le coefficient de frottement et le taux d'usure spécifique, ont été étudiées. Les résultats indiquent que la bicouche ABS/PMMA présente une stabilité thermique notable. La température de transition vitreuse de la bicouche est de 111 °C. Le comportement viscoélastique a été décrit en déterminant le module de stockage et de perte. En outre, les résultats montrent que l'influence des paramètres de température et de vitesse de déformation sur le comportement à la traction de la bicouche ABS/PMMA a également été déterminée, ce qui indique une forte dépendance du comportement mécanique à l'égard de ces deux paramètres. La structure bicouche présentait une bonne adhérence entre les deux couches, et la dureté et le taux d'usure ont été déterminés.

Mots-clés : ABS ; PMMA ; Polymère bicouche ; Propriétés thermiques et mécaniques ; Tribologie ; Fractographie.

ملخص

الهدف من هذه الدراسة هو فحص تأثير درجة الحرارة ومعدل الإجهاد على التوصيف الهيكلي للبوليمر ثنائي الطبقةABS/PMMA. تتكون الطبقة الثنائية من 85% من أكريلونيتريل بيوتادين ستايرين (ABS) و15% من بولي (ميثيل ميثاكريلات الميثيل) (PMMA). يقدم القسم النظري لمحة عامة عن تطبيقات هذا البوليمر ويستكشف إمكانات التشكيل الحراري كتقنية تصنيع لأحواض الاستحمام. ومن الأهمية الكبيرة للتقنية المستخدمة في هذه العملية اكتساب نظرة عامة على العلاقة بين عمليات التشكيل الحراري والخصائص الحرارية والميكانيكية والترايبولوجية للطبقة الثنائية ABS/ PMMA. اشتملت المرحلة التجريبية على سلسلة من الاختبارات المصممة بشكل منهجي على هذه الطبقة الثنائية. تم تقييم الخواص الحرارية، بما في ذلك الثبات الحراري ودرجة حرارة التحول الزجاجي، وكذلك السلوك اللزج، من خلال التحليل الديناميكي الميكانيكي. تم إجراء اختبار الشد في درجات حرارة ومعدلات تشوه متفاوتة للتأكد من معامل المرونة وحدود الإجهاد والإجهادات القصوى والاستطالة عند الكسر. تم إجراء اختبار تشاربي للصدمات لتقييم مقاومة الصدمات للمادة، تلاه تحليل تخطيطي للكسر لفحص التفاعلات بين الطبقات، وتحديد خصائص العيوب الهيكلية والعيوب الناتجة عن الكسر، وتوضيح أنماط الكسر الملحوظة بعد اختبار الشد والصدمات. تم إجراء تقييمات قوة الانحناء لمقارنة الطبقة الثنائية ABS/PMMA مع ABS وPMMA النقي. وعلاوة على ذلك، تم فحص الصلابة والخصائص الترايبولوجية، بما في ذلك معامل الاحتكاك ومعدل التآكل النوعي. أشارت النتائج إلى أن الطبقة الثنائية ABS/PMMA أظهرت ثباتًا حراريًا ملحوظًا. وُجد أن درجة حرارة التحول الزجاجي للطبقة الثنائية 111 درجة مئوية. تم وصف سلوك اللزوجة المرنة من خلال تحديد معامل التخزين والفقد. بالإضافة إلى ذلك، أظهرت النتائج أنه تم أيضًا تحديد تأثير معاملات درجة الحرارة ومعدل الإجهاد على سلوك الشد للطبقة الثنائية ABS/PMMA، مما يشير إلى اعتماد كبير للسلوك الميكانيكي على هذين العاملين. أظهر هيكل الطبقة الثنائية التصاقًا جيدًا بين الطبقتين، وتم تحديد الصلابة ومعدل التآكل.

كلمات البحث: ABS؛ PMMA ؛ بوليمر ثنائي الطبقة؛ الخصائص الحرارية والميكانيكية؛ علم الاحتكاك؛ التحليل الفراغي.

Table of contents

List of Figures

List of Tables

List of abbreviations and nomenclatures

A	Amorphous	
ABS	Acrylonitrile butadiene styrene	
ATG	thermogravimetric analysis	
COF	Coefficient of friction	
DMA	Dynamic mechanical analysis	
DSC	Differential scanning calorimetry	
EIMS	Industrial sanitary materials company	
HIPS	High-impact polystyrene	
HDT	Heat deflection temperature	
HDPE	High density polyethylene	
HV	Vickers hardness	
ISO	International organization standardization	
Pa	Polyamide	
PC	Polycarbonate	
PEI	Polyetherimide	
PET	Polyethylene terephthalate	
PETG	Polyethylene-terephthalate-glycol	
PLA	Poly-lactide	
PMMA	Poly (methyl methacrylate)	
PMMAe	Poly (methyl methacrylate) copolymer	
PMMAh	Poly (methyl methacrylate) homopolymer	
PP	Polypropylene	
PPO	P-phenylene oxide	
PS	Polystyrene	
PVC	Poly (chlorite of vinyl)	
SAN	Styrene acrylonitrile	
SC	Semi-crystalline	
SEM	scanning electron microscopy	
TPE	Thermoplastic elastomer	
TPU	Thermoplastic polyurethane	
b	Width of specimen	[mm]
d	Mean diagonal width (hardness)	[mm]

d	Deflection at mid-span (bending)	[mm]
E	Tensile modulus (Elastic modulus)	[MPa]
E'	Storage modulus	[MPa]
E''	Loss modulus	[MPa]
E_a	Impact strength	[KJ/m^2]
E_c	Energy absorbed	[J]
E_f	Flexural modulus	[MPa]
F	Force	[N]
F_N	Normal force	[N]
h	Thickness	[mm]
HV	Vickers Hardness	[MPa]
L	Beam span in bending	[mm]
L	Sliding distance in tribology	[mm]
Shore D	Shore D Hardness	[-]
T	Temperature	[°C]
Tg	Glass Transition Temp	[°C]
Td	Degradation temperature	[°C]
Tm	melting temperature	[°C]
V	Volume	[mm^3]
W_r	Wear rate	[mm^3/m.N]

Greek symbols

Tan δ	Damping factor	[-]
σ_{eng}	Engineering stress	[MPa]
σ_f	Flexural stress (bending stress)	[MPa]
σ_v	True stress	[MPa]
σ_y	Yield stress	[MPa]
σ_{ult}	Ultimate stress	[MPa]
ε_{eng}	Engineering strain	[-]
$\acute{\varepsilon}$	Strain rate	[s^{-1}]
ε_f	Flexural strain (bending strain)	[-]
ε_v	True strain	[-]
ε_{ult}	Ultimate strain (Elongation at break)	[-]
ρ	Density	[g/cm^3]
μ	Coefficient of friction	[-]

General Introduction

In the contemporary technological environment, the investigation of advanced materials is of paramount importance. Thermoplastic amorphous polymers, with their distinctive properties and applications, represent a significant area of focus in this regard. Understanding these materials' mechanical behavior at the macroscopic level is paramount, as it reveals novel characteristics and behaviors essential for advancing the frontiers of material science and enhancing industrial applications.

The thermoforming process is a widely used method in polymer processing, known for its efficiency, simplicity, and cost-effectiveness. Its versatility allows for producing intricate, large-scale, and custom-shaped products. Thermoforming is regarded as a "secondary" plastic manufacturing process, where a heated thermoplastic sheet is shaped using a vacuum, pressure, or mold. The key aspect of this process is transforming a flat polymer sheet, secured at its edges, into a three-dimensional form [1]. In other words, thermoforming is a process that encompasses all shaping techniques where a material, typically in the form of a sheet or film, is molded after being softened. It involves various methods to transform the material from a flat state into a desired shape once it reaches a pliable condition [2].

The thermoforming process involves subjecting the polymer to various conditions, including applied forces, pressures, temperature changes, deformation rates, impacts, and contact with the mold. These factors are instrumental in determining the material's performance and final properties. Our research is focused on investigating the behavior of an ABS/PMMA bilayer sheet under these conditions, specifically within an industrial sanitary materials company (EIMS of Miliana), where these sheets are used to produce bathtubs. The thesis objective is to optimize the process to enhance material performance and identify potential improvements for producing high-quality shape complex components. A more profound comprehension of these thermoforming conditions could pave the way for the advancement of more efficient and dependable thermoforming techniques for multilayer polymer systems.

Further researches are required to develop advanced analytical techniques that provide a more comprehensive understanding of polymer behavior under the

thermoforming process, thus enabling this material to avoid the posed challenges by new industry developments and products. These researches will contribute to:

- Firstly, a comprehensive understanding of the thermoforming process for polymers is of paramount importance. This study will provide a detailed account of the thermoforming process as it pertains to the production of ABS/PMMA bilayer sheets utilized in bathtub manufacturing at the Miliana industrial facility. It will examine the challenges encountered and the key parameters that influence the thermoforming performance of these sheets.

- Secondly, the study will analyze the thermal and mechanical performance of the ABS/PMMA bilayer sheet. While extensive research has been conducted on the thermal and mechanical behavior of pure polymers and their blends, there is a notable lack of studies that specifically address the impact of temperature and deformation rate on the mechanical properties of ABS/PMMA bilayers. Our analysis will include comparisons with pure ABS and pure PMMA, with a particular focus on aspects such as bending and hardness, as well as a tribological behavior test on ABS and PMMA sides.

Additionally, to the two sections of the general introduction and general conclusion with perspectives, this thesis is divided into four chapters:

The initial chapter presents a comprehensive overview of the current state of the art in thermoforming thermoplastic polymers. The chapter begins with a bibliographic review of the fundamental mechanisms of thermoforming, including an overview of its various types, steps, and polymers utilized in the process. This is followed by an in-depth examination of the thermoforming process employed in bathtub manufacturing at the Miliana sanitary materials industrial company. Additionally, the chapter addresses critical factors influencing the process, such as temperature effects, thickness distribution, and frictional contact with the mold, all of which impact the final product.

The second chapter offers a comprehensive literature review of amorphous polymers, with a particular investigation of the characteristics and structures of ABS and PMMA, as well as the production of ABS/PMMA bilayer sheets through coextrusion. The objective is to provide a comprehensive understanding of the properties, production

methods, and previous research findings to support the experimental work conducted in this study.

The third chapter presents a comprehensive account of the polymer studies (ABS/PMMA), followed by an analysis of the experimental procedures employed to assess the behavior of bilayer sheets. The focus is on their thermal, mechanical, tribological, and hardness properties, together with a fractographic analysis. This comprehensive analysis provides an in-depth understanding of the performance and characteristics of the bilayer structure, thereby offering valuable insights into its suitability for industrial applications.

The fourth chapter presents the results of a series of experiments conducted on the thermal and mechanical properties of the ABS/PMMA bilayer polymer. Additionally, it includes a fracture analysis of the ABS/PMMA bilayer structure following tensile and Charpy impact tests, as well as an investigation into the hardness and tribological behavior of the polymer layers.

Chapter 1.   Thermoforming of thermoplastic polymers

_____

1.1. **Introduction**

Thermoforming is a shaping process that uses heat to form polymer materials. This process permits the manufacturing of products with complex geometry. In the first part of this chapter, it focuses on the thermoforming processes for thermoplastic polymers. It provides a general overview of the different types of thermoforming as well as the materials that can be used in this process. Subsequently, the manufacturing steps of polymer bathtubs at the Miliana Sanitary Materials Industrial Company are discussed, including the different zones of thermoforming, reinforcement, finishing by trimming the edges, and some common defects caused by this process, along with the relationship between bathtub thermoforming to the process parameters of temperature, sheet thickness distribution, and frictional contact.

1.2. **Introduction to thermoforming process**

Thermoforming is a manufacturing process that transforms polymer sheets into plastic products with desired shapes. For the finely chopped walls [3], a sheet of polymer is first heated to a soft, formable state. It is then stretched against the surface of a mold to retain a hollow geometry after cooling. Due to the inherent characteristics of this forming process, contact between the mold and the polymer occurs at different times and in different places, causing non-uniform stretching of the polymer and consequent thickness variations in the manufactured part [4].

Today the production and use of polymers have spread considerably in various fields such as the automotive, sanitary, household appliance, and even decoration industries. This is due to the ease with which raw materials (granules) can be converted by the very modern and advanced technological methods mentioned above (extrusion, molding, etc.). Some produce a finished Product; others are semi-finished and require another process such as thermoforming.

Thermoforming is used to manufacture polymers into complex-shaped objects with surfaces that are difficult to measure, for short-term use in the packaging parts industry [5], [6] and, to a greater extent, in refrigerators [7] and bathtubs.

The principle of the thermoforming process passes through several steps. Firstly, the polymer sheet is clamped mechanically with a clamping frame that applies a load to the end of the sheet. It is then heated by a furnace with a distributed temperature difference

to soften it. When the sheet is sufficiently hot, the initial shape is obtained by pre-forming, with air compression, or by available mechanical means. In most cases, the mold has only one side, meaning that only one side of the sheet is in contact with the forming surface, while the other side is open to the elements. When the sheet undergoes cooling to maintain the shape of the mold, it is retracted. The product is then separated from the excess paper that surrounds it, and the off-cuts are transformed into a new sheet [8].

During thermoforming, it can be said that there is a very interesting problem with the stress-strain of the sheet. Then, the polymer is heated, and the mechanical properties of the material change due to the deformation of the part. As a result, the stress-strain curve varies strongly with temperature [9]. It depends on how to manufacture the product, considering its shape and size. The surface of contact with the mold must be smooth and flawless. Different techniques can be used for forming the extruded plate into the final shape [10], On the other hand, thermoforming includes a variety of techniques, including plug thermoforming, vacuum forming, and positive or negative blow forming, which differ according to the type of pressure applied (vacuum or positive air) and the use of pre-stretching. This versatile process is widely used in the manufacture of food packaging, blister packs, and many consumer goods. Beyond packaging, thermoforming is also used in a variety of industries, such as automotive and toy production [6]. During the thermoforming process, thermoplastic sheets undergo significant deformation both inside and outside the sheet plane to achieve the final product without sheet failure, whether negative or positive thermoforming is used (Figure 1-1).
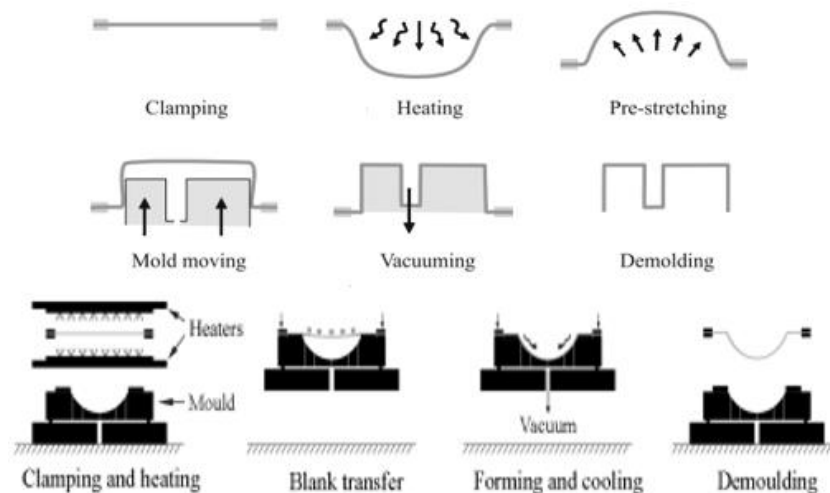
Figure 1-1 : Thermoforming steps: top positive thermoforming [7]**, and bottom negative thermoforming** [4]**.**

1.2.1. Production of semi-finished polymer sheets used for thermoforming

Extrusion of polymeric materials generally involves the continuous shaping of a polymeric fluid through a suitable die, followed by the solidification of the fluid into a solid product [11]. The extrusion process begins by feeding the powder or pellet (Figure 1-2) into the hopper in the solids conveying zone. It is then melted along the cylinder by heating it in the transition zone to a controlled temperature as it travels from the screw to the tip. Finally, it is discharged from the die at the extruder tip via the auger, which presses the extruded die [12]–[14]. It comes in the form of sheets [15] , pipes, and profiles of different thicknesses.
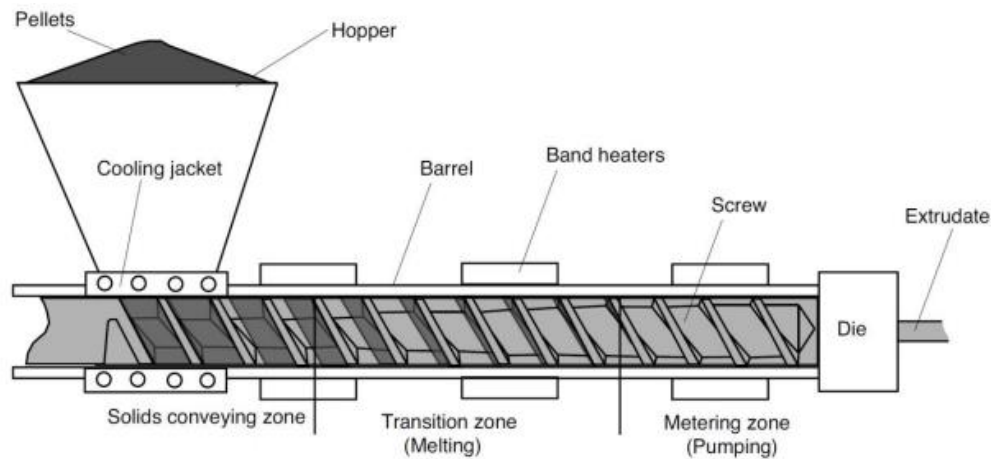
Figure 1-2: Schematics of a single-screw extruder [5]**.**

1.2.2. The materials used in thermoforming

A comprehensive overview of the thermoforming properties of the various polymers used in the thermoforming process is given in Table 1-1. It contains essential information on their specific applications and forming performance. In addition, the table indicates the glass transition temperature (Tg) and melting temperatures (Tm) of each material, which are critical parameters influencing their behavior during thermoforming. These comprehensive data help to select the right thermoplastic for specific applications, ensuring optimum performance and efficiency in the manufacturing process.

Table 1-1: Temperature range for forming polymers used in thermoforming, with additional information about the polymer states (A: amorphous, SC: semi-crystalline) and references [16], [17]**.**

Polymer	Type	Tg (°C)	Tm (°C)	Range forming temperature (°C)
Acrylonitrile butadiene styrene (ABS)	A	90-120	175-235	130-180
Polystyrene (PS)	A	90	175-260	130-182
Poly (methyl methacrylate) (PMMA)	A	100	225	150-190
Poly (chlorite of vinyl) (PVC)	A	90	160	100-155
Polycarbonate (PC)	A	150	230	170-200
Polypropylene (PP)	SC	5	165	150-165
Polyethylene terephthalate (PET)	SC	70	255	120-180
High density polyethylene (HDPE)	SC	-110	134	130-185

1.2.3. Advantages and disadvantages of thermoforming process

Thermoforming offers several competitive advantages. Most notably, tooling and equipment costs are quite low compared to other processes. Specifically, the molds used in thermoforming are relatively simple and thus not overly expensive. Additionally, thermoforming can handle multilayer materials, foams, and printed, and coated materials, which reduces post-forming processing time. Moreover, thermoforming allows for the production of much larger parts than many other processes. However, thermoforming also has distinct disadvantages. Primarily, the complexity of thermoformed parts is limited. Additionally, the process generates a significant amount of waste, leading to higher material costs, although some of this waste can be recycled. Finally, a major drawback is that only certain materials are compatible with the thermoforming process [18].

1.3. Thermoformability

Efforts have been made to define the concept of "thermoformability" of sheet materials clearly and comprehensively, both quantitatively and qualitatively. This term encompasses various factors such as resistance to deformation, flowability, replication accuracy of molds, the ability for deep drawing, consistency in thickness distribution post-thermoforming, shrinkage after forming, and dimensional stability. Typically, evaluating the thermoforming performance and processing range of material involves conducting trials on standard molds like cups or rectangular boxes. However, some studies have sought to correlate inherent material properties with thermoforming behavior. Certain findings suggest that a material, particularly non-reinforced types, is deemed thermoformable when its shear modulus is approximately 1 MPa [19], [20] and

exhibits an elongational viscosity ranging from 10^5 to 10^8 Pa.s during stretching [20]–[22]. When a uniform wall thickness distribution is required, materials showing strain-hardening behavior are highly advantageous [21]. In 1991 Hylton [20] discussed various methods including uniaxial hot tensile tests, viscosity measurements, and biaxial inflation techniques to forecast material "thermoformability." Alongside traditional thermoforming trials and rheological assessments, these techniques continue to be widely employed. Moreover, researchers have delved into alternative definitions of "thermoformability" and material characterization methods. Error! Reference source not found. offers a summary of specific techniques deemed pertinent for thermoforming. Some of these methods [23]–[28] have been designed to establish material parameters for thermoforming simulation (by reverse engineering) or processing windows (including temperature ranges). However, the author suggests that these techniques can also be used to determine a material's "thermoformability".

Table 1-2: An overview of terms and techniques used to define thermoformability.

Term or technique	Description	Reference
Melting resistance tester	The melt strength is assessed using a Gottfert "Rheotens" melt strength tester and then compared to its resistance to sagging.	[29]
Thermoformability index (TFI)	The TFI is determined by multiplying the viscosity by the compliance (also known as creep recovery time) and is evaluated using a rheometer.	[30]
Bubble inflation / Bulging	A biaxial extension test involves bulging a circular-shaped specimen that is clamped at its perimeter.	[31]–[33]
Biaxial extension	A specialized biaxial extension machine is used for this purpose, conducting tensile tests at various speeds and temperatures.	[26], [34], [35]
Plug testing (Thermoforming material characterization apparatus)	A sheet is secured within an oven, and plugging tests are conducted at varying temperatures and speeds.	[27], [28], [36], [37]
Small deformation rheological tests	A combination of dynamic mechanical tests (DMA) conducted at various temperatures and frequencies across the thermoforming range, along with creep (recovery) tests and sag measurements, are performed using a heat deflection temperature (HDT) device.	[24], [25], [38]

1.4.   Characteristics and classification of flexible polymers

A polymer that is flexible because it melts or softens in response to temperature changes. They are made up of small, branched, or linear macromolecules. Physical interactions (van der Wall forces, hydrogen, etc.) give this type of polymer a certain amount of cohesion. These polymers can be inferred to be sensitive to solvents and temperatures because they include solvents and transition from a plastic phase to a liquid phase when heated (breaking the physical type). Thermoplastics can typically be recycled and are simple to turn into liquid [39]–[41]. At room temperature, thermoplastic polymers are almost at their softening temperature (Tg, Tf), and the temperature has a significant impact on their mechanical properties [39]. They can also be found in semi-crystalline and amorphous polymers.

Amorphous polymers, like ABS, PMMA, and PC, which are frequently used in engineering (Figure 1-3), have a homogenous and disordered structure, and other amorphous polymers are used. Zones where the structure is crystallized define semi-crystalline polymers. Examples of this category include (HDPE, PP, and Pa) [12]. It is possible to distinguish between two different methods of polymerizing monomers by changing or combining them: homopolymers are chains of monomers of the same kind, and copolymers are polymerizations of two monomers, also known as co-monomers [42].
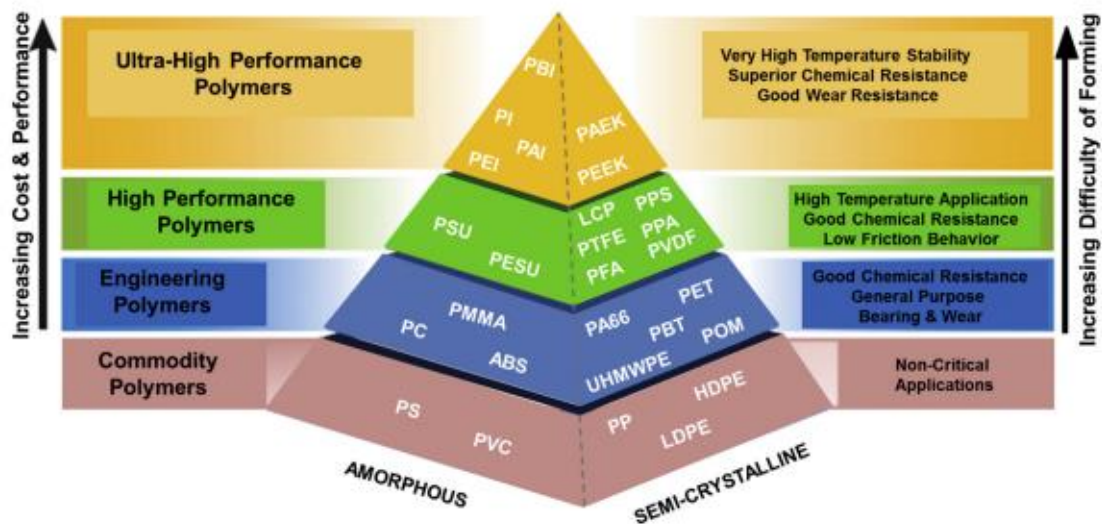
Figure 1-3: polymer pyramids of amorphous and semi-crystalline [43]**.**

1.5.   Manufacture of bathtubs using the thermoforming process at the industrial company of sanitary materials

Algerian company (EIMS) manufactures a wide range of products, such as bathtubs, sinks, and heaters, using various methods, including stamping and thermoforming. Stamping is employed for metal materials (steel sheets) to produce items like bathtubs and sinks, while thermoforming is utilized for plastic materials (polymer sheets). The company's thermoforming business is a crucial aspect of its industrial production due to the high market demand for its products, characterized by their light weight, strength, quality, and appealing appearance. Plastics have found extensive applications across various fields, and their flexibility continues to expand with modern technology, facilitating ease of use and rapid development and production. Thermoforming specifically involves the use of thermoplastic materials, which undergo a softening process that alters specific properties such as density, viscosity, and mechanical properties. Subsequently, the softened sheet is deformed by air pressure to create a pre-stretching (bubble), then pulled to assume the shape of the mold. The final step involves cooling to maintain the molded shape, as illustrated below:
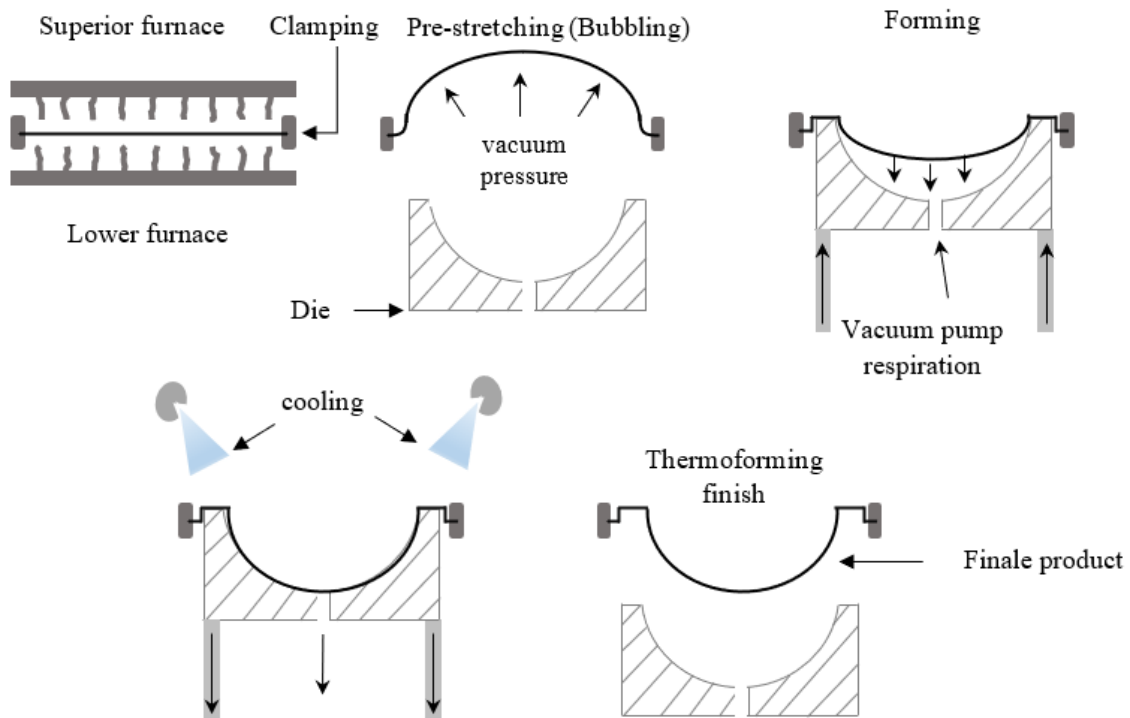
Figure 1-4: bathtub forming cycle at the Sanitary Materials Industrial Company

1.6. *Steps in Bathtub Production at EIMS*

The bathtub is manufactured through several distinct steps. The first fundamental step is thermoforming. The second step involves reinforcing the bathtub to enhance its hardness and strength. Finally, unnecessary appendages are removed, as illustrated in the following diagram:
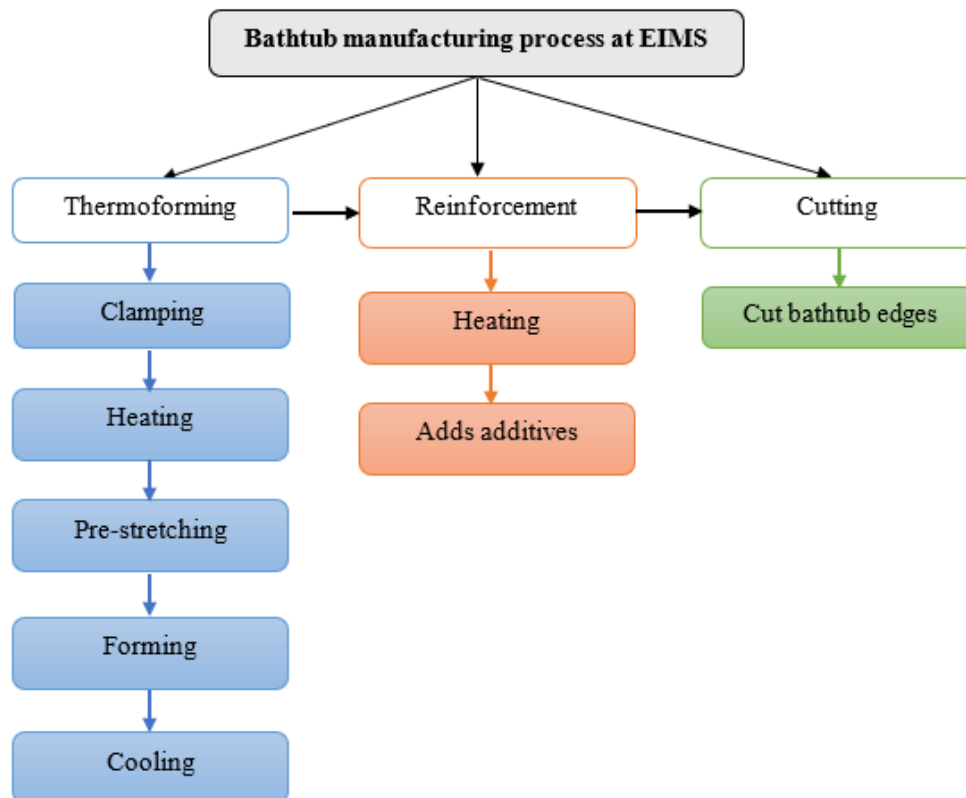
Figure 1-5: Cycle of manufacture of bathtub product at EIMS

1.6.1. Thermoforming zone

At EIMS, bathtub production primarily relies on vacuum thermoforming, facilitated by the LABOFORMA, an Italian-made thermoforming machine (Figure 1-6). This machine, which features straightforward operation via a control panel, boasts an automatic stop function triggered by the proximity of a technician, ensuring enhanced safety with infrared technology. The process utilizes various thermoplastic materials such as ABS, PMMA, PP, and HIPS in sheet form, each with a maximum thickness of 8 mm. With a maximum plate size of 2,050x1,050 mm and a minimum size of 1,050x550 mm, it accommodates diverse production needs, reaching a maximum printed height of 700

mm. Powering the machine are electric motors, compressed air (through a vacuum pump and pneumatic pressure operation), and water for mold heating.

This machine does not accept any materials other than those specified by the supplier, and it does not accommodate different thicknesses than what is requested. Any discrepancies in dimensions between the material and the mold, especially in the setting of the forming reduction codes, result in errors that lead to the production of incorrect and unacceptable products.

Figure 1-6 : Thermoforming machine used at EIMS Miliana.

1.6.1.1. Clamping the sheet

To ensure a successful thermoforming process, all thermoplastic sheet materials must be securely held on all four sides (Figure 1-7). This four-sided grip must be maintained throughout all steps of the thermoforming process. The securing of the sheet materials is crucial for both thin, flexible sheets as well as heavier, more rigid materials.

All thermoplastic sheet materials tend to soften and sag when heated. During the heating cycle, the thermoplastic sheet undergoes thermal expansion, loss of crystallinity,

and relief of molecular orientation, which can lead to sheet movement and distortion. If the thermoplastic sheet is not fully supported on all four sides during the heating cycle, the unsupported side will typically distort and pull away from the clamping area. This can result in a shift in material thickness, with thickening towards the center of the sheet.

Figure 1-7 : Sheet clamping system.

1.6.1.2. Heating the sheet

The polymer sheet used in our study, ABS-15%PMMA, is fed into the conveyor, with dimensions suitable for 1400 mm tubs (1480x785x4 mm). On entering the forming zone, the upper frame descends to hold the sheet firmly in place, enabling the heating process to begin until the polymer sheet softens. For amorphous thermoplastics, this temperature is theoretically higher than the glass transition temperature (Tg). The two upper and lower-temperature furnaces work in parallel to evenly heat the sides of the sheet (Figure 1-8). The sheet is heated primarily by ceramic elements positioned in a heating coil located at the top and/or bottom, each carefully calibrated to maintain specific degrees of temperature. During the heating cycle, there are two modes of thermal energy transfer: conduction and convection. Convection involves the distribution of hot air that heats the polymer sheet. When the surface area, volume, and thickness of the sheet are large, a longer time is needed to heat the sheet. Heat diffusion by conduction is the transfer of energy within the solid (the polymer sheet). This method is preferred for sheets with low thickness because thick sheets have low thermal conductivity, requiring more time for the conduction method, the foil remains free until it reaches a temperature of 100°C. At this point, supports are deployed to secure the ends of the foil. The temperature then continues to rise, precisely controlled by an optical pyrometer immersed in the external heating medium, reaching between 140°C and 160°C. The entire heating process lasts

170 seconds, ending with the retraction of the two resistors to their initial positions. During the heating phase, the sheet's rigidity decreases, and it begins to bend under the effect of gravity.
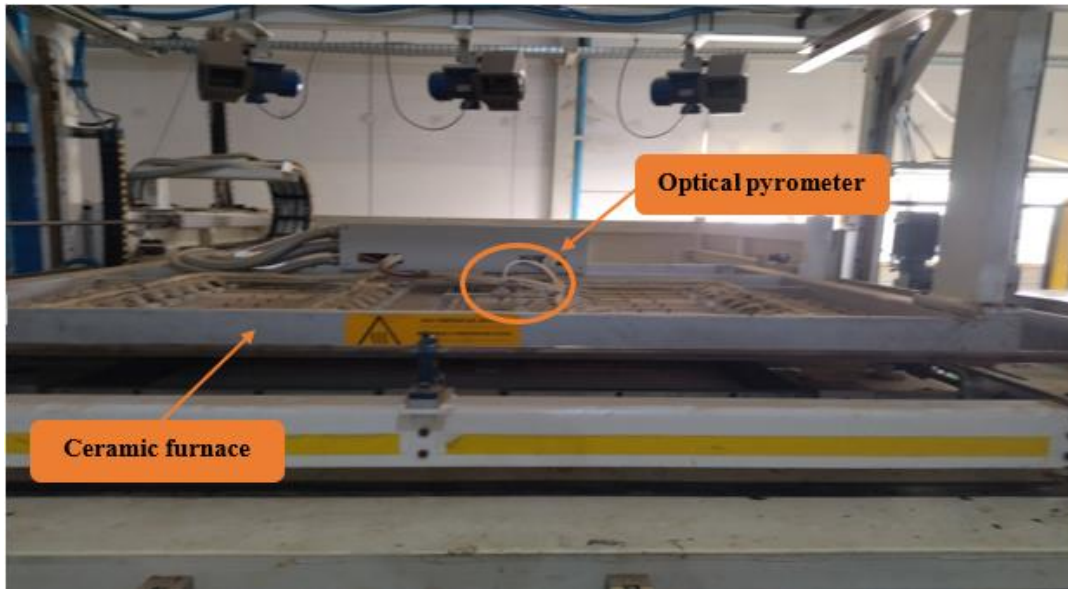
Figure 1-8 : Heating the thermoforming sheet.

1.6.1.3. *Pre-stretching the sheet*

After heating, the sheet is pre-stretched with air to elongate and expand the sheet and facilitate the forming step, which is a rapid deformation under high air pressure, an essential step in the production process. This simultaneous action not only deforms the material but also precisely controls the thickness distribution of the inflated sheet. To maintain precision, the machine is equipped with a 15% inflation control sensor that regulates the bubble formation process. This sensor ensures that the inflation rate does not exceed the specified limit, preventing potential defects and ensuring consistent product quality (see Figure 1-9). Such inflation control is essential to achieve optimum structural integrity and aesthetics of the final product.

Figure 1-9 : Sheet bubbling (pre-stretching).

1.6.1.4. Forming the sheet

Following the pre-stretching step, the mold is elevated using an auger system to enable deep-drawing of the softened sheet. Vacuum pumps play a crucial role in this phase, delicately drawing the sheet through the mold's aeration holes at a precisely controlled rate of deformation until it seamlessly conforms to the mold's contours. To optimize the forming operation and minimize friction (Figure 1-10.a), the mold is equipped with a water hot system, which helps regulate temperature and reduce resistance during shaping (Figure 1-10.b). Subsequently, the polymer sheet undergoes plastic deformation, seamlessly transitioning into its final bathtub shape. This intricate process ensures not only structural integrity but also meticulous attention to detail, resulting in a high-quality end product that meets stringent standards of durability and aesthetics.
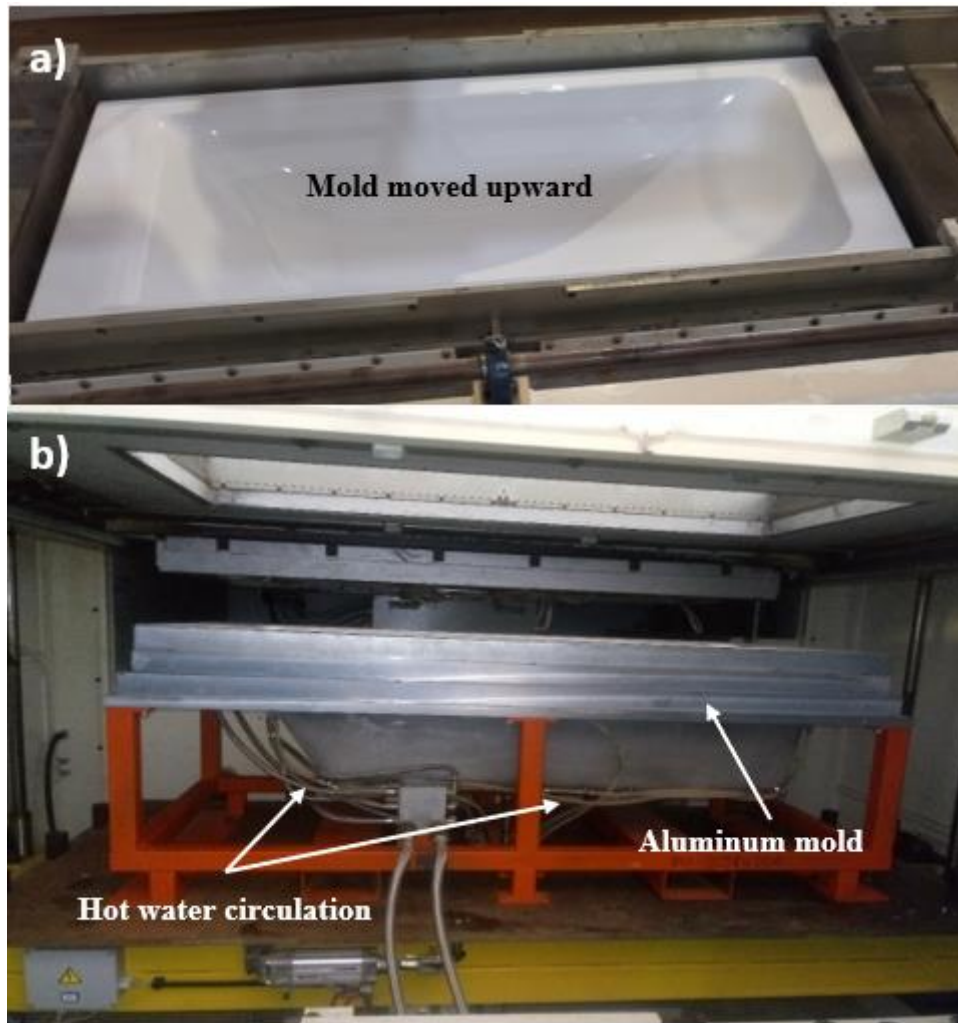
Figure 1-10 : Bathtub-shaped sheet forming: a) forming and b) the mold.

1.6.1.5. Cooling the part

The thermoformed polymer sheet is precisely positioned to meet the heated mold, a critical step in shaping the tub's final contours. After this molding process, the bath temperature is carefully regulated by activating fans to facilitate controlled cooling. As the cooling process begins (Figure 1-11), the mold sinks to the bottom, adding the final touch to the bathtub's formation. This sequential operation ensures not only the precise definition of the tub's shape (see the Annex 1), but also the gradual stabilization of its structural integrity. Thanks to thorough temperature control and mechanical processes, this manufacturing steps guarantees the production of high-quality bathtubs that meet both functional and design demands.

Figure 1-11 : Fans opened for bath cooling.

1.6.2. Reinforcement zone
1.6.2.1. Heating and adding additives to the bathtub

The bathtub obtained from the thermoforming process is not yet considered a finished product, and needs to be reinforced to increase the strength and durability of the material. To achieve this, the company applies a protective material to the outside of the tub, in the form of a foam. This foam not only strengthens the structure, but also acts as a protective layer, protecting the tub from potential damage and extending its lifespan. By incorporating this extra layer, the company ensures that its bathtubs meet rigorous quality standards, offering customers a product that not only prides itself on superior strength, but also long-lasting performance and reliability.

Figure 1-12 : bathtub reinforcement chamber [44]**.**

To strengthen the bond with the foam, the thermoformed bathtub undergoes a second heating process at 60°C in a separate oven. This additional heating step ensures optimum adhesion between the tub and the reinforcing foam. Once heated, the tub is quickly introduced into the reinforcement cabin (Figure 1-12), where the foam application process takes place. The foam, a liquid composite, is composed of crushed thermoformed embossed scrap mixed with an MC+ISO type liquid (Figure 1-13), meticulously designed to provide both structural reinforcement and protective qualities. Thanks to these improvements, the final weight of the bathtub is 6 kg, ensuring a balanced combination of strength, durability and functionality. This comprehensive reinforcement process not only strengthens the tub's structural integrity, but also improves its resilience, guaranteeing a superior product with great durability.

Figure 1-13: Additives for bathtub reinforcement.

1.6.3. Finishing chain

After the reinforcement process, the bathtub enters its final manufacturing step, which involves precision machining using a state-of-the-art CNC machine with 5-axis capabilities (Figure 1-14.a). This machine meticulously cuts the bathtub along its contour and drills holes according to specifications. This phase ensures precise shaping and finishing of the piece. Once completed, the finished products are carefully stored and prepared for delivery to the market, maintaining quality standards and meeting customer demands (Figure 1-14.b).

Figure 1-14: a) Bathtub cutting, and b) bathtub storage.

1.6.4. The bathtub's failure forms are manufactured by thermoforming

The most important objectives for any industrial company are costs and deadlines. In thermoforming processes, acceptance criteria can vary significantly. Acknowledging these challenges is crucial for improving production quality and efficiency. Firstly, holes on the edges of the bowl can occur due to insufficient temperature for the sheet to soften, causing poor friction with the mold (Figure 1-15.a). Secondly, surface defects such as wrinkles are common (Figure 1-15.b). When a part is subjected to very high temperatures, this affects the mechanical properties of the polymer used, such as ABS/PMMA. Thirdly, as seen in Figure 1-15.c, the mold can bend under the effect of temperature, necessitating cuts at all ends to align it. Additionally, high roughness on the product surface due to elevated temperatures is typically referred to as "orange peel" or "surface roughness" (Figure 1-15.d), This phenomenon occurs when the thermoplastic sheet is overheated, causing the surface to develop a textured, uneven appearance similar to the skin of an

orange. High temperatures can lead to differential shrinkage, inconsistent cooling, or degradation of the material, all of which contribute to the rough surface texture. Sometimes, the thermoformed sheet requires a long heating time, consuming a lot of energy. This is often due to the extrusion conditions not being properly implemented. Recognizing and addressing these issues is essential for optimizing the thermoforming process and achieving better results.
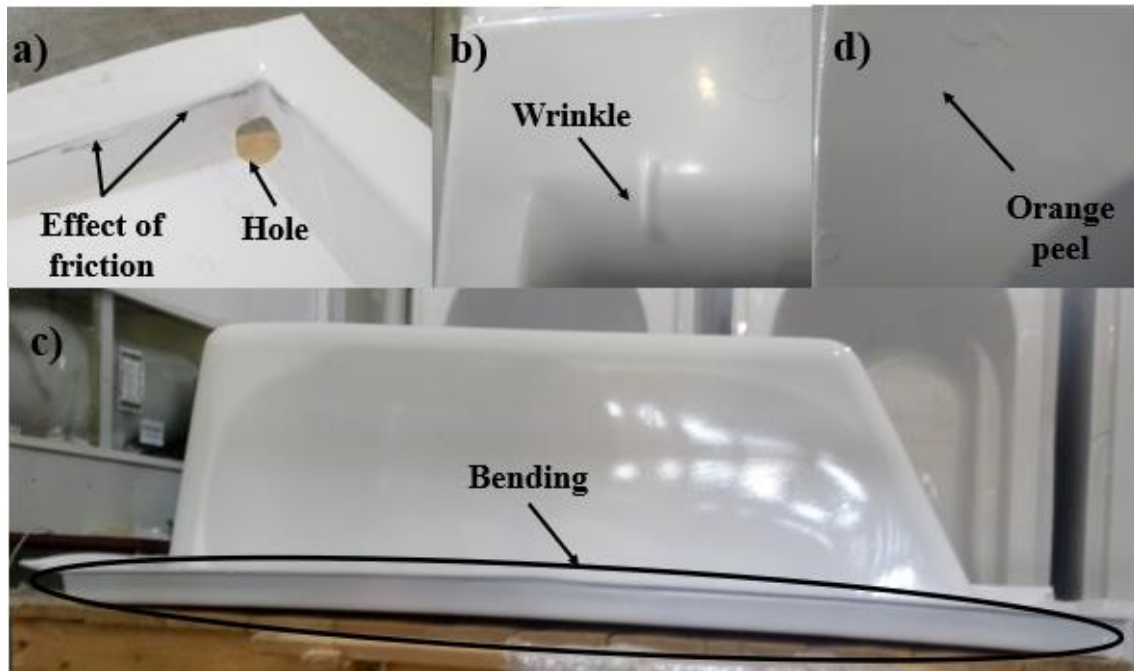
Figure 1-15: bathtub manufacturing failure modes.

Amorphous polymers are inherently easier to shape because they lack intricate meltable crystalline structures, making them the preferred choice for thermoforming applications. At forming temperatures, some amorphous polymers can be stretched up to ten times their original length [4]. In the 1970s, Schmidt et al. [45] Found that high-impact polystyrene (HIPS), which remains a widely used material in thin gauge thermoforming, can achieve polar extension ratios up to 11 during inflation tests. They also noted that other amorphous materials, such as polycarbonate (PC) and polymethyl methacrylate (PMMA), cannot be stretched beyond a hemispherical shape without bursting.

To develop materials that meet specific stretching requirements, researchers have explored various methods of modifying polymers. Over the past 20 years, significant published advancements in polymer modification for thermoforming applications aside from the largely undisclosed chemical developments by material suppliers include [4]. It

is of the utmost importance to select PMMA grades that are particularly well-suited for coextrusion and for maintaining the optimal layer thickness of the PMMA. For a variety of reasons, PMMA is currently the only option available for coextrusion with ABS or PC/ABS. Furthermore, PMMA is readily amenable to polishing, thereby facilitating the attainment of a smooth surface finish. Additionally, it can be colored in a multitude of ways, thus offering considerable versatility in design. Furthermore, PMMA displays remarkable ultraviolet stability and noteworthy chemical resistance, rendering it highly durable in diverse environmental circumstances [46].

1.7.   Temperature influences on Initial Boundary Conditions

For large-drape forming (covering a significant area of the sheet), increasing the temperature of the clamped sheet can lead to thermal deformations due to the relaxation of residual stresses from its thermo-mechanical history. The sheet is mechanically constrained on all sides and sags due to the force of gravity [47]. Sagging (as shown in Figure 1-16) changes the distance between the sheet and the infrared heaters, thereby altering the efficiency of radiative heat transfer [48]. Temperature homogeneity might not always be guaranteed due to the radiative heating technique used and the resulting sagging of the sheet. The radiative energy absorbed by a surface from a radiative source depends on the solid angle that the absorbing surface subtends with the source, which influences the radiation view factor [49]. As the sheet sags, the deformation of the absorbing surface causes the angle subtended by a material point on the sheet to vary depending on its location. Consequently, this unbalanced heating from the ceramic radiators leads to a difference in stretching between the hotter zones on the sheet (T > Tg) and the relatively cooler ones [50].
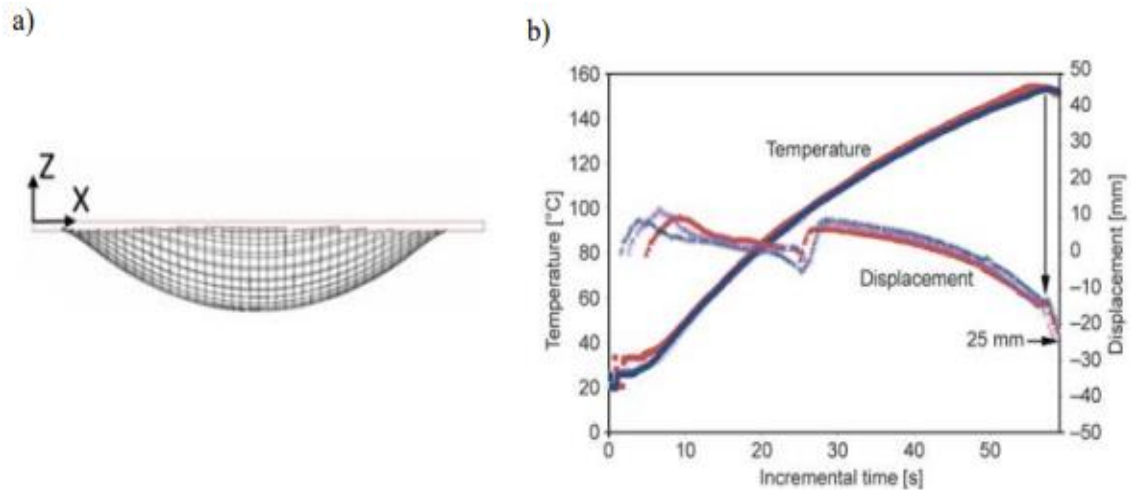
Figure 1-16: (a) Recording displaying the sagging of the sheet followed by heating [45], (b) Vertical displacement and temperature of the sheet over time during the heating step [43]**.**

1.8.   Relation between contact friction and temperature

The final thickness of the product is influenced by the temperature difference between the thermoplastic sheet and the mold. This temperature difference dictates whether the mechanical behavior during the forming phase stays within the forming window or shifts into the glassy range [51]. The friction coefficient, characterizing the contact surface between the sheet and the mold or blug, can also affect the final thickness [5], [47], [52], [53]. Figure 7 illustrates the variation of the friction coefficient between a HIPS sheet and an aluminum plug, as observed by Marathe et al. [52]. Figure 1-17 shows that the COF appears to increase from 0.25 at Tg to values exceedingly almost 0.5 at 130°C in the HIPS formation window.
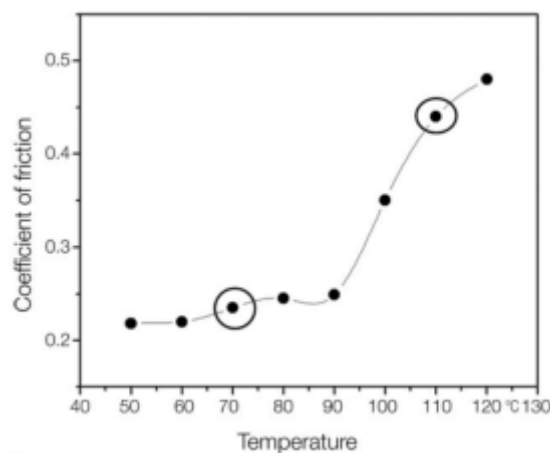
Figure 1-17: Evolution of the coefficient of friction between HIPS and an aluminum plug as a function of temperature increase [52]**.**

1.9.   Sheet thickness not uniform

One of the main limitations of the thermoforming process is the non-homogenous thickness distribution of the parts produced [54]. Thin thermoplastic sheets are essentially incompressible materials. According to the principle of volume conservation, as the sheet expands along a principal axis, its thickness decreases. The ability of a thermoplastic to stretch is influenced by its local properties, which are determined by the temperature distribution after infrared heating. Consequently, achieving a uniform thickness during the stretching phase of thermoforming depends on the homogeneity of heating throughout the sheet. For example, in the case of vacuum-assisted thermoforming, it is well known that the finished parts show significant variations in thickness. Sheet walls are thinner in zones subject to intense stretching, such as mold corners and near bottom edges, as shown in Figure 1-18 [55], [56].
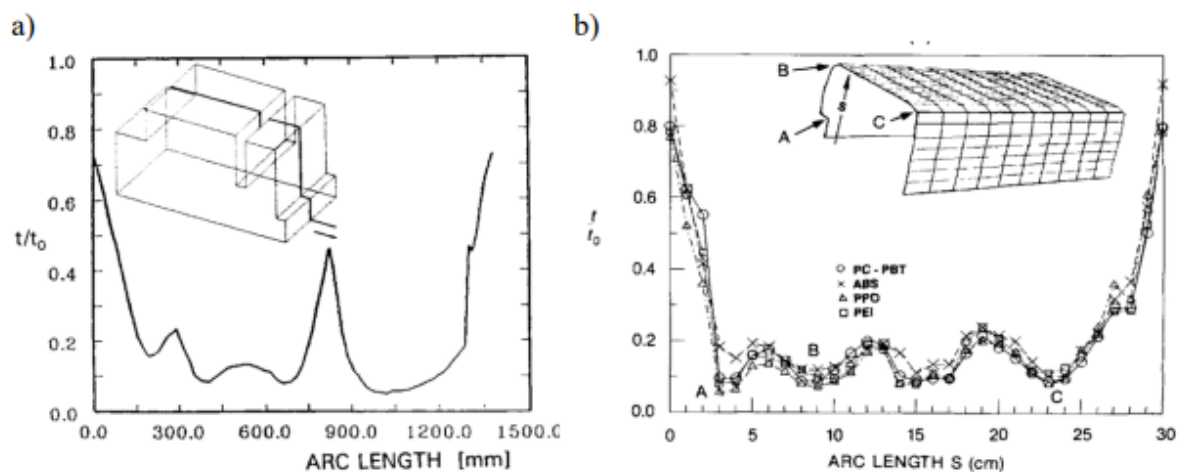
Figure 1-18: Variation of the thickness-to-length ratio in a part with complex geometry using (a) PMMA [55], (b) PC, ABS, PPO, PEI [56].

Figure 1-19 illustrates the variation in thickness measurements of a thermoformed yogurt tub made from HIPS material under the influence of forming temperature. The 135 mm pot shows significant reductions in thickness, reaching values as low as 150 µm and 500 µm, as the temperature increases from 120°C to 140°C.
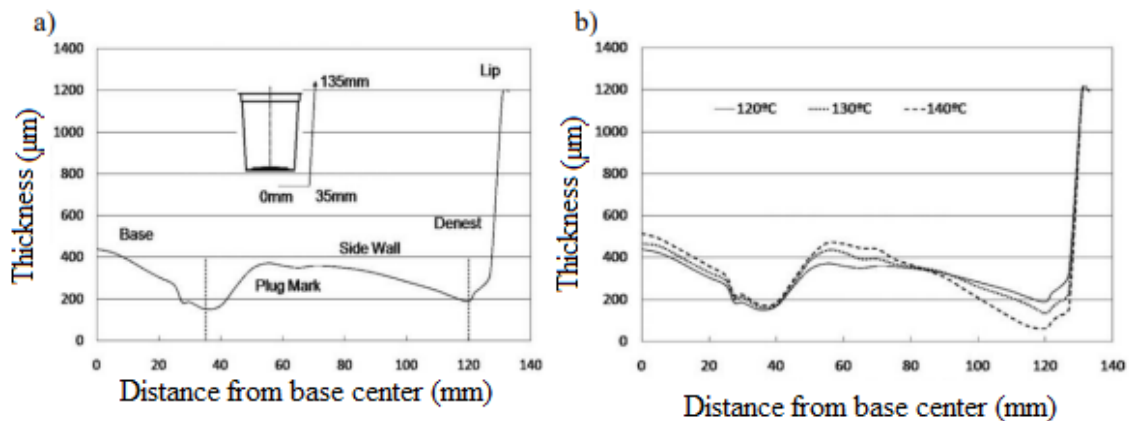
Figure 1-19: (a) Thickness section of a part thermoformed with a HIPS sheet plug at a temperature of 120°C, (b) evolution of thickness distribution for different sheet temperatures [51]**.**

As a result, mechanical stretching can lead to a non-uniform thickness distribution, potentially below the minimum critical thickness specified in the product design [51], [57].

1.10. Conclusion

The bibliographic study has provided us with a deeper understanding of the general principles of the thermoforming process for thermoplastic polymers, particularly in the context of the manufacture of industrial bathtubs at EIMS. From this study, it is observed that the material properties are closely related to various parameters such as temperature, process speed, material selection, and the contact dynamics between the bath and the mold. These insights are essential for refining the thermoforming process and improving the quality of the final products.

Chapter 2.   Literature review on the thermal, viscoelastic, and mechanical performance of amorphous polymers

2.1.   Introduction

In this chapter, it focused on the thermal and mechanical characterization of amorphous polymers, with particular emphasis on ABS and PMMA. A detailed investigation of the individual properties of these materials was conducted to provide a comprehensive understanding of their behavior. This analysis serves as a foundation for exploring the performance of the ABS/PMMA bilayer structure, facilitating insights into how each component contributes to the overall material performance.

2.2.   Amorphous polymers

The use of polymers has become increasingly common across various fields. Today, a wide range of polymer types and processing options are available for selection. Polymers are popular due to their lightweight and low cost, with each field leveraging specific properties to meet their requirements. The stability of these properties over time is crucial for industrial applications. Polymers are generally categorized into three major families based on their properties: elastomers, thermoplastics (non-cross-linked chains), and thermosets (cross-linked chains). Thermoplastic polymers are further classified into amorphous and semi-crystalline polymers [58]

Amorphous polymers are characterized by a large molecular weight and an irregular structure, generally exhibit the properties of amorphous solids. The atoms inside these polymers are arranged randomly [59], although a specific short-range order can be observed due to the physical packing of neighboring atomic spheres. Amorphous thermoplastics are remarkable for their softening behavior and their structural changes during the glass transition [60]. In this temperature range, the polymer is brittle at room temperature but becomes superplastic as the temperature increases [61].

2.3.   Molecular structures and thermal properties of polymers

2.3.1. Structures of macromolecules

Polymers, composed of various monomers, can form carbon-based macromolecular structures that take different shapes. These structures include a nondimensional linear type, a branched type with short lengths, and a cross-linked type that features a tangled configuration, as shown in Figure 2-1.
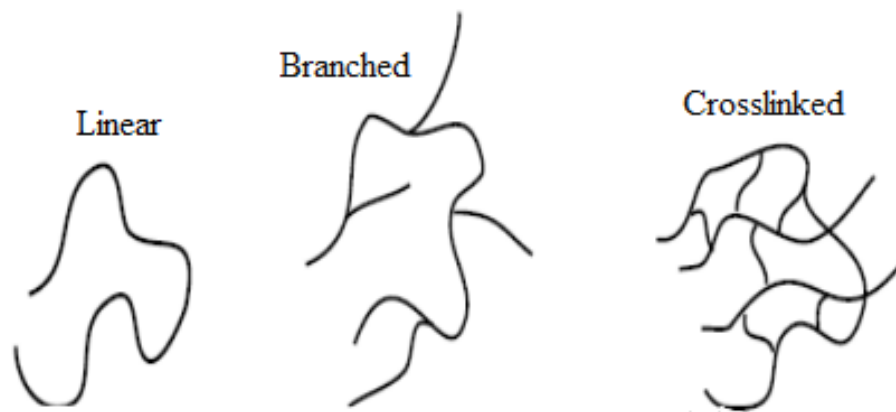
Figure 2-1: Main polymer chain structures [62]**.**

A polymer with side chains attached is considered branched, whereas a polymer with a single main chain is described as linear. When a monomer possesses multiple polymerization sites, forming covalent bonds between individual chains results in a three-dimensional network. Both branched and linear polymers are encompassed within thermoplastic polymers [62]. When the temperature surpasses the glass transition point, these materials display a viscosity level higher than that of linear polymers (Figure 2-1) [63]. Conversely, cross-linked polymers typically manifest as elastomers or thermosets. While cross-linking is appealing due to its impact on specific properties, such as elasticity, shaped polymers generally remain amorphous, albeit with the possibility of being partially crystallized [64].

2.3.2. Thermal behavior of amorphous polymers

For most polymers, there is a critical temperature that permits two distinct states to be distinguished: the rubbery state (at higher temperatures) and the glassy state (at lower temperatures). As a rule, polymers have a rigid glassy state. As the temperature rises, the polymer's macromolecular chains begin to slide relative to one another, softening the material. This transition occurs within a temperature range known as the glass transition temperature (Tg). At this point, the behavior of polymers becomes viscoelastic and they enter the rubbery state, The latter behavior is used to shape plastics [62].

2.3.3. Glass transition temperature

The glass transition temperature (Tg) marks the change from a glassy to a rubbery state. This transition corresponds to the shift from low-amplitude local molecular motion (when T < Tg) to significant motion along the entire macromolecular chain (when T > Tg). The glass transition is a kinetic phenomenon, representing the shift from an equilibrium state to a non-equilibrium state [62]. Gibbs and Di Marzio [65] predicted a second-order phase transition at a temperature T_2, which is lower than Tg. They demonstrated that T_2 and Tg share similar properties and consistently respond in the same way to various factors affecting the glass transition. Therefore, the glass transition behaves similarly to a second-order transition [66]–[68]. The glass transition is detected experimentally using several techniques, such as differential scanning calorimetry (DSC), dynamic mechanical analysis (DMA), and various other methods for analyzing the glass transition.

To determine the glass transition temperature (Tg) from a DSC graph using the midpoint method, identify the midpoint where there is a gradual change in heat flux by drawing tangents to the steepest parts of the curve before and after the transition. The point where these tangents intersect gives an estimate of the Tg value. For a completely amorphous polymer, illustrated in Figure 2-2, an ABS/PMMA blend (50/50) exhibits a distinct change in slope. In contrast, in a fully crystalline polymer, the slope of the curve remains unchanged until the melting point is reached.
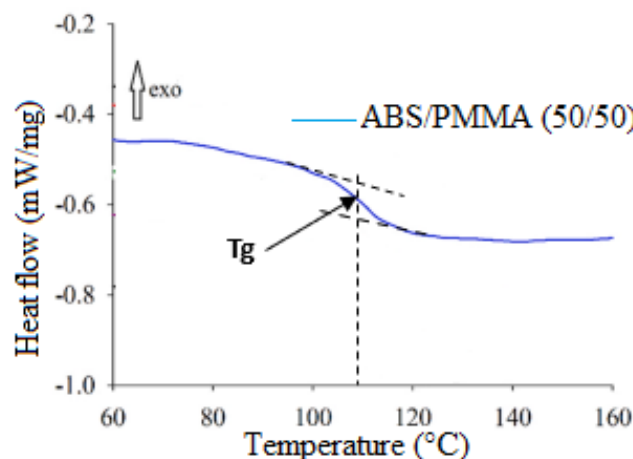
Figure 2-2: DSC curve of amorphous polymer [12].

The glass transition temperature (Tg) is significant from the point of view of industrial processes, as it marks the point at which materials begin to soften for further

processing. It also has an impact on material properties and product performance, and guides material selection for optimum application performance and durability.

2.3.4. Thermal stability of thermoplastics polymer

The thermal stability of amorphous thermoplastic materials refers to their ability to maintain their structural integrity and mechanical characteristics when exposed to elevated temperatures. This stability is essential in determining their suitability for various industrial applications, particularly those involving high-temperature processing or long-term use at elevated temperatures. Amorphous polymers have a glass transition temperature (Tg) instead of a melting point because of their non-crystalline structure. Thermal stability control often involves understanding how Tg influences the material's mechanical strength, dimensional stability, and resistance to heat-induced deformation or degradation.

Figure 2-3 shows the ATG of different polymers, demonstrating that the SAN copolymer and ABS exhibit high levels of thermal degradation at lower temperatures compared to the other polymers, such as PMMA homopolymer and copolymer, PS [69].
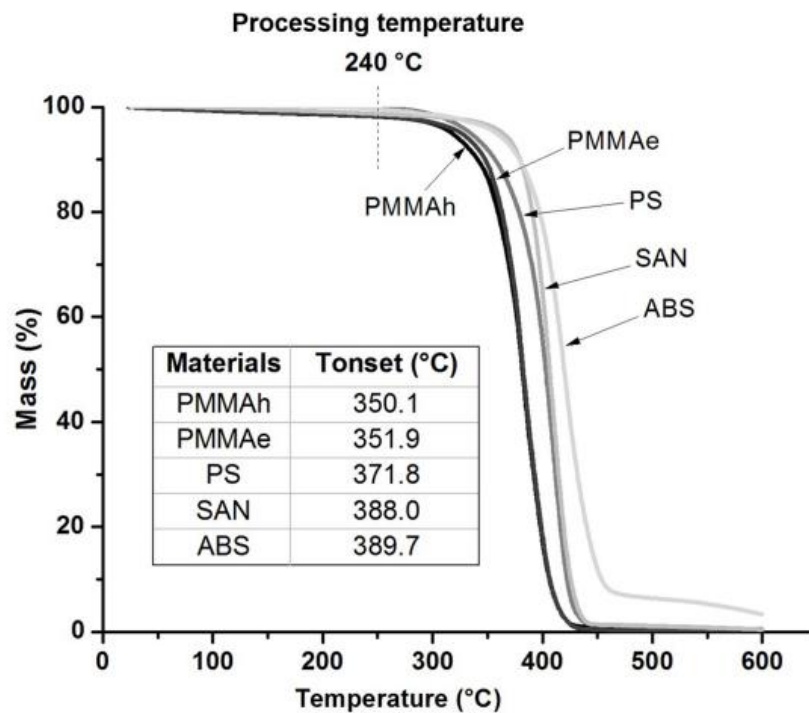
Figure 2-3: thermogravimetric analysis curves of pure thermoplastics [69]**.**

2.4. *Mechanical behavior of polymers*

The behavior of polymers varies widely, with each type exhibiting different characteristics such as brittleness, ductility, and rubberiness. In general, the constitutive laws governing these polymers are influenced by temperature and strain rate, which in turn affect their viscoelasticity and mechanical properties, including Young's modulus, maximum stress, and strain at break. For example, an increase in temperature can make a polymer more ductile Figure 2-4, while higher strain rates can increase its strength. These factors can either increase or decrease these properties, depending on the specific conditions and polymer type.
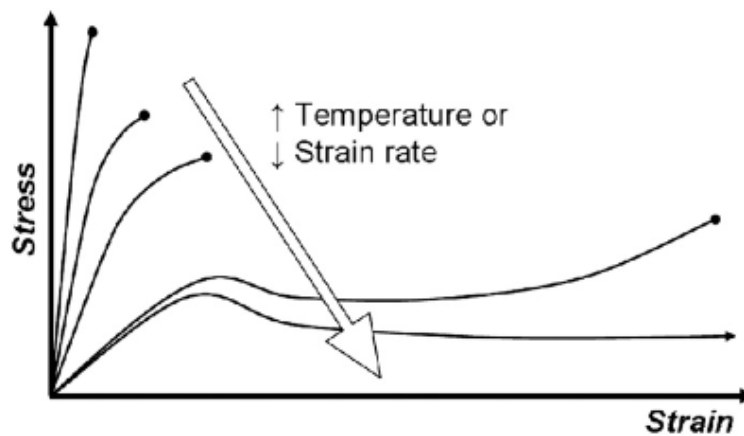
Figure 2-4: Higher temperatures and slower strain rates in polymers [70]**.**

2.4.1. The effect of temperature on the mechanical properties of polymers

The effect of temperature on the mechanical behavior of amorphous polymers is significant. At ambient temperature, these polymers exhibit high tensile strength and elastic modulus, resulting in brittle behavior with minimal elongation at break. As the temperature rises until the glass transition (Tg), the tensile strength and elastic modulus decrease, causing the polymer to become less stiff and more prone to deformation. This results in a significant increase in elongation at break as the polymer becomes more ductile. This behavior is due to the weakening and extension of molecular interaction forces within the polymer as shown in Figure 2-5.a, allowing for greater molecular mobility and reorganization. Consequently, the polymer transitions from a rigid, brittle state to a more flexible, ductile state as the temperature increases.

2.4.2. The effect of strain rate on the mechanical properties of polymers

The effect of strain rate on the mechanical behavior of amorphous polymers is significant. At higher strain rates, these polymers exhibit higher tensile strength and modulus of elasticity, resulting in stiffer, more brittle behavior, with minimal elongation at break. As the rate of deformation increases, tensile strength and modulus of elasticity continue to rise, making the polymer even more resistant to deformation. As a result, the elastic modulus and tensile strength of the polymer increase considerably, while the elongation at break decreases, highlighting the effective relationship between strength and flexibility at varying strain rates as shown in Figure 2-5.b.
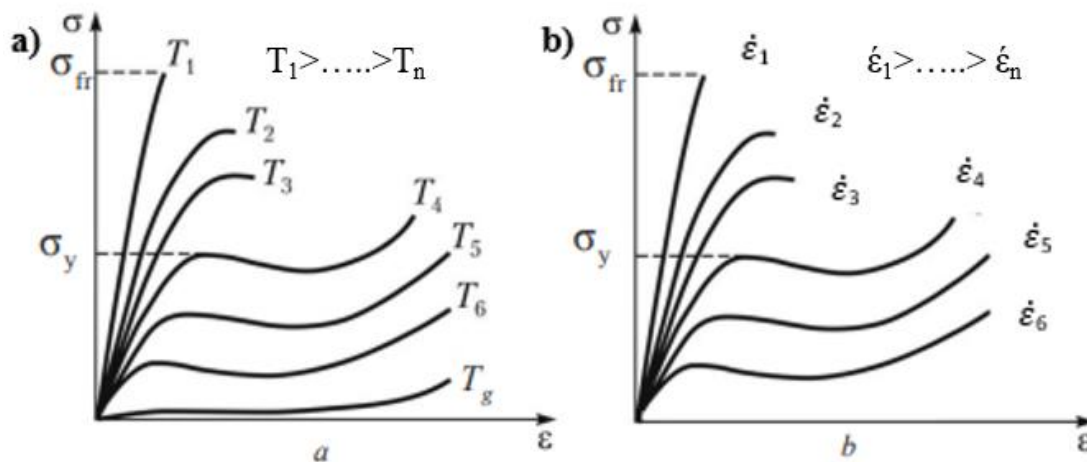
Figure 2-5: typical stress-strain curves: a) constant strain rates vs different temperature, b) constant temperature vs different strain rates [71]**.**

2.4.3. Impact strength

The transition between the behavior of "resistant 'and' brittle" materials, characterized by the energy required to form a fracture surface, is emphasized. The impact strength has been determined by measuring the energy absorbed in relation to the fracture surface, using older impact testing techniques that do not allow the tracking of load and time. This method complicates the distinction between materials that fracture under low load but absorb more energy during propagation and those that fracture under high load but absorb little additional energy. Differences in the balance between fracture initiation and propagation cause variations in impact strength results depending on the specimen geometry. In addition, the small amount of energy absorbed by the fracture surface in

polymers can be overshadowed by other energy losses. During testing, the rate of displacement varies unpredictably, altering the kinetic energy. Variations in sample size and geometry also affect results [72].

The main factors influencing impact resistance are temperature, notch thickness, and notch radius [73]. Temperature is an intrinsic property, while notch thickness and notch radius are geometric factors. A smaller notch radius increases the rate of deformation at the bottom of the notch, which affects the material's yield strength and its ability to blunt cracks, thus influencing the tendency to brittle fracture. Increasing temperature generally raises impact resistance by lowering yield strength and tensile modulus, thus reducing loading rates. Thermoplastics show a plateau in impact resistance at low temperatures, with a sharp increase at higher temperatures indicating a transition to harder behavior. Notch sensitivity varies considerably from polymer to polymer, with hard, crystalline polymers being the most affected, although modifications such as rubber hardening or fiber reinforcement can improve impact resistance [72].

2.5. Tribology and hardness of polymers

2.5.1. Tribology of polymer

The study of polymer tribology is highly complex, having been extensively explored since the mid-20th century. Polymers are valued for their unique mechanical properties, such as elasticity, shock absorption, low friction, and high wear resistance, along with their ability to be modified [74]. Unlike other materials, polymers can readily absorb external liquid lubricants, a property that can be influenced by operating conditions and environmental factors, making traditional metal-based experimental methods less applicable [75], [76]. Additionally, distinguishing between different types of polymer wear is challenging because wear mechanisms are interrelated and rarely occur in isolation. Wear resistance depends on material properties such as elastic modulus, tensile strength, and elongation at failure. Generally, polymers with high tensile strength and elongation at failure exhibit better wear resistance. Linear thermoplastic polymers with a semi-crystalline structure typically perform better in wear resistance compared to thermosets or amorphous thermoplastics under consistent conditions [74].

2.5.2. Hardness of polymer

Hardness tests are valued for their simplicity and are widely used for rubbers and metals, though less so for plastics, where their significance has been less clear. Among the hardness testing methods, Shore durometers (Shore A and Shore D) are particularly popular for plastics, using handheld devices with indenters to measure hardness based on penetration depth [77]. In contrast, Vickers hardness testing employs a pyramidal indenter with a load-on, load-off approach, creating geometrically consistent impressions irrespective of penetration depth. The process involves measuring two diagonal lengths on the indent, averaging them to determine the impression area, and calculating the Vickers hardness number by dividing the load by this area. Vickers microhardness testing, which produces small indents (less than 150 µm), is effective for polymers. Additionally, micro-Vickers hardness testing involves using a load below 2 kg and typically measures diagonals with an optical microscope due to the small scales. This method is preferred in scientific research for its precision in assessing hardness at specific locations [78].

2.6.   Morphology of amorphous polymers

Fractography is a crucial technique in the advancement of technology and optimization of materials. It serves to identify significant shortcomings and ensure that materials possess the requisite mechanical properties. The field of fracture mechanics is concerned with the study of the mechanisms of crack propagation, both prior to and following the formation of critical crack size, as well as the locations of crack initiation. As illustrated in the attached diagram, the actual fracture surfaces are shown in Figure 2-6, where the centers of fracture initiation are clearly identifiable. Regardless of whether the initiation center is a defect within the volume or on the surface, macro fractography (focused on examining larger fracture regions at lower magnifications or by the naked eye) reveals several distinctive features surrounding it.

- Mirror: a flat area surrounding the defect;
- Mist: a slightly rugged area surrounding the mirror;
- Hackle: a highly rugged area exhibiting a network of rivers in the radial direction, centered at the initiation point;
- Terminal zone of fracture: the region of material observed on both the tensile and pressure surfaces of the sample [79].
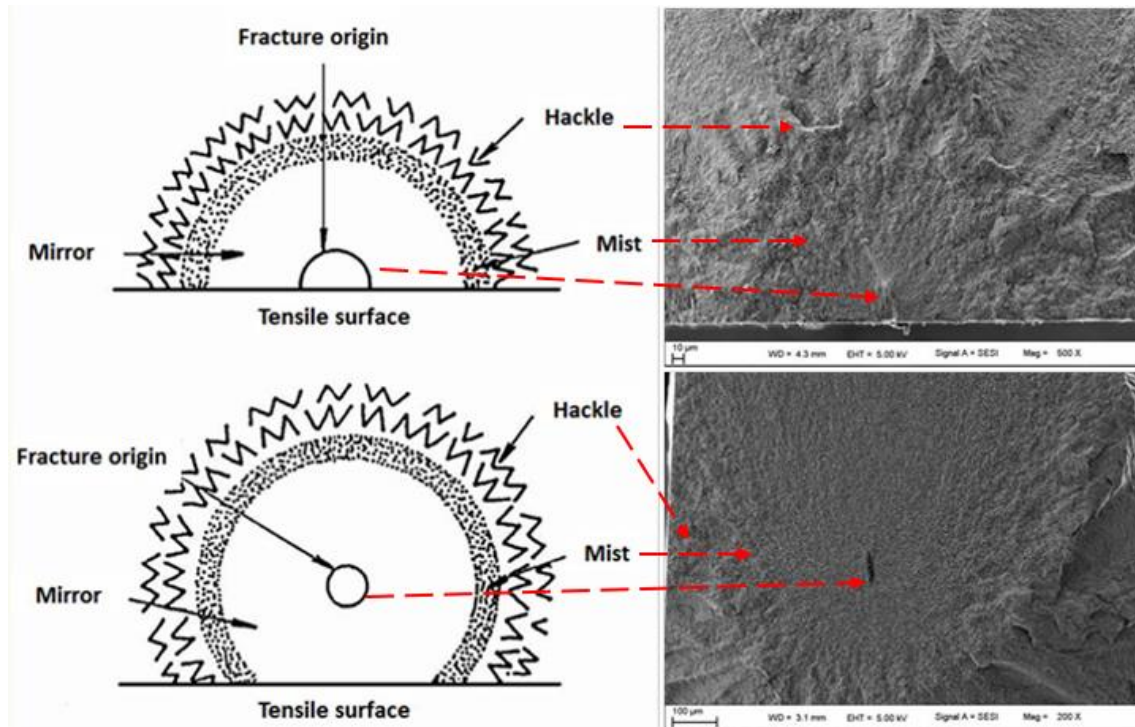
Figure 2-6: A schematic representation of surface and volume defects with examples in brittle materials [79]**.**

The investigation of polymer fracture surfaces allows scientists to understand the behavior of these materials under external loads, considering factors such as material defects and environmental influences like humidity or weathering. Several researchers have studied the fractography of polymers, focusing on factors such as tensile strength at different temperatures, strain rates, and impact strength. By examining these surfaces, scientists gain invaluable insights into the mechanisms of fracture, which are essential for improving material performance and preventing future failures. Unlike crystalline polymers, amorphous polymers lack a regular internal structure, which influences their fracture behavior. Fractography helps identify the nature of cracks and surface morphology, revealing whether failures result from brittleness, stress concentration, or environmental factors. For example, the mirror zone and ribs disappear from the PMMA polymer as the deformation speed increases, indicating a transition from a ductile to a more brittle fracture behavior (Figure 2-7.A). Additionally, in Figure 2-7.B, a brittle fracture of the ABS polymer occurs at a deformation speed of around 60 mm/min, accompanied by smaller voids. This suggests that the material's toughness decreases under higher strain rates, leading to a more brittle failure mode. Fibrils can be observed

on the fracture surface of several polymers, such as ABS, indicating the presence of plastic deformation mechanisms (Figure 2-8.a). However, defect-induced fractures can also be observed, characterized by features like parabolic shapes and cracks (Figure 2-8.b and Figure 2-8.c), which suggest higher stress absorptions and potential points of failure within the material.
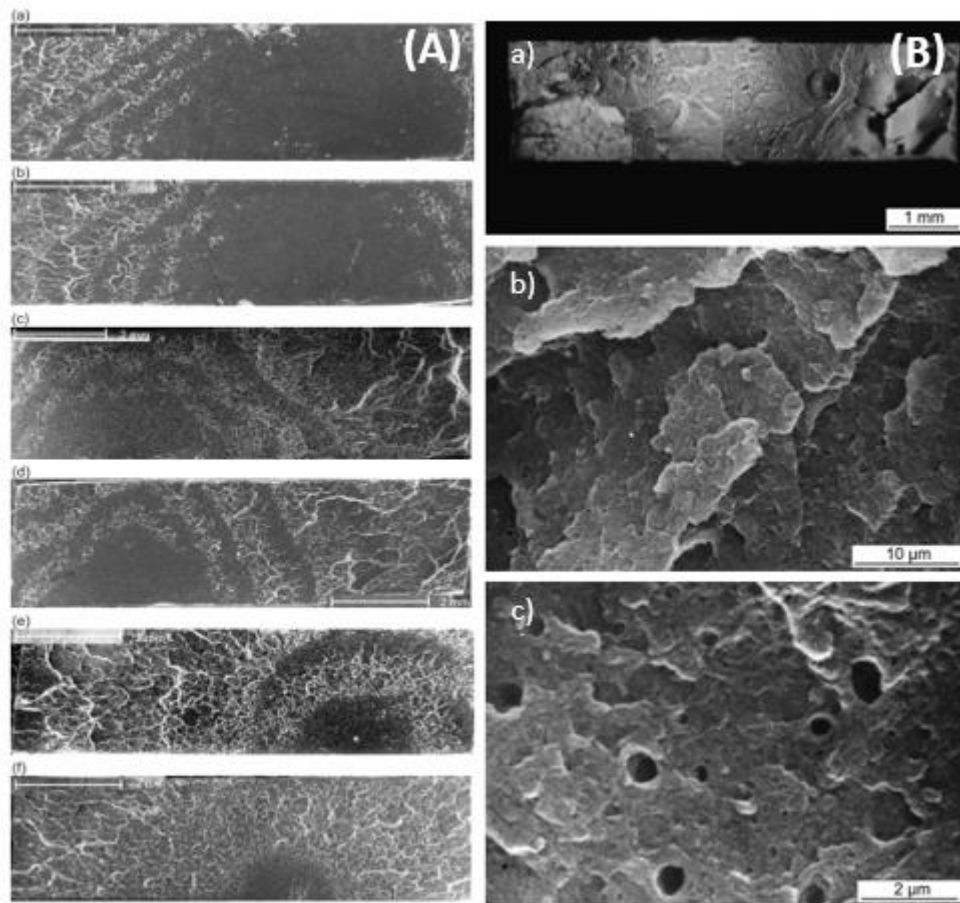
Figure 2-7: The morphologies of fracture surfaces (A) different strain rate of PMMA polymer: (a) 2.31x10 $^{-5}$ s^{-1}, 2.38x10 $^{-4}$ s^{-1}, 2.01x10 $^{-3}$ s^{-1}, 0.292x10 $^{-1}$ s^{-1}, 2.81x10 $^{-1}$ s^{-1} [80], (B) Brittle fracture of ABS polymer at loading rate of 60 mm/min [81]**.**
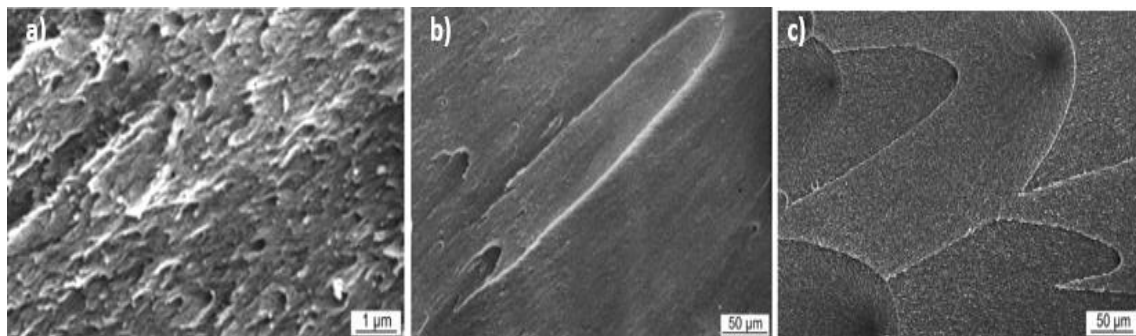
Figure 2-8: Observations of a fracture surface: a) fibrils, b) cracks and c) parabolas [81]**.**

2.7.   *Acrylonitrile Butadiene Styrene (ABS)*

Acrylonitrile Butadiene Styrene (ABS) is an important amorphous thermoplastic widely used in the mechanical engineering industry. ABS is utilized in the manufacture of household appliances (refrigerators, washing machines, air conditioners), sports equipment, vehicle parts (bumpers, wheel guards, dashboards), luggage, and packaging parts produced by various processes such as thermoforming and injection molding …etc.

ABS is one of the most important synthetic polymers on the market today. Almost everyone in the modern world owns an ABS product. Finished products made from ABS inherit the properties of its three main components: acrylonitrile, butadiene, and styrene (Figure 2-9). ABS was developed as a replacement for styrene-butadiene rubber (SBR), which styrene had been used to substitute for many years [82]. Acrylonitrile provides hardness, heat resistance, and chemical resistance. Styrene offers rigidity, strength, and ease of processing. Butadiene enhances elasticity, reinforcing the plastic's impact resistance and toughness [83].
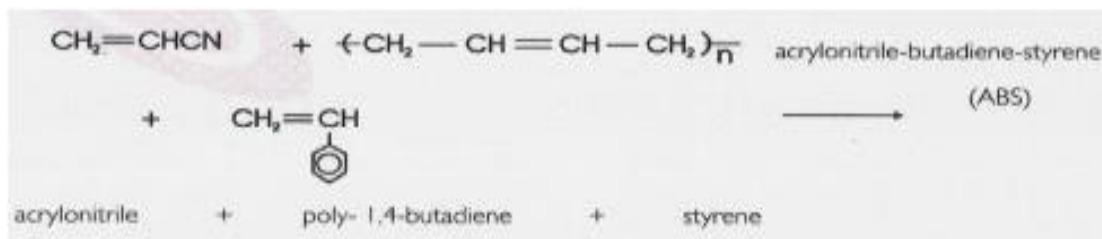
Figure 2-9: Chemical Structure of ABS [84]**.**

The thermos-physical properties of ABS polymer are crucial considerations in various applications. ABS exhibits acceptable thermal stability, making it resistant to deformation or degradation at elevated temperatures. Additionally, its high flammability makes it susceptible to combustion, highlighting the importance of understanding its ignition temperature and heat release rate for safety assessments. Moreover, ABS has a favorable glass transition temperature, indicating the temperature range at which it transitions from a hard, rigid state to a more pliable state. These thermal properties play a significant role in determining the suitability of ABS for diverse applications [85].

Based on the ABS material tests described above and the literature review, Table 2-1 summarizes the main mechanical, electrical, and thermal properties of the ABS material studied.

Table 2-1: Thermal and mechanical properties of ABS polymer.

property		ABS	References
Density (g/cm^3)		1.01 - 1.21	[86], [87]
Hardness	Vickers HV	5.6 – 16	[86], [87]
	Shore D	74 - 76	[88], [89]
Glass Transition Temp. (°C)		88 - 128	[87]
Thermal Expansion Coefficient (10^{-6} /K)		84.6 – 234	[86], [87]
Thermal conductivity (W/m K)		0.188 - 0.335	[86], [87]
Yield stress (MPa)		18.5 - 51	[86], [87]
Tensile Strength (MPa)		27.6 - 55.2	[86], [87]
Tensile modulus (MPa)		1100 - 2900	[86], [87]
Elongation at break (%)		2-10	[86], [87]
Flexural strength (MPa)		73.5	[90]
Flexural modulus (MPa)		2450	[90]
Impact strength (kJ/m^2)		23.6 - 27.82	[91], [92]

2.8. Poly (Methyl Methacrylate) (PMMA)

Poly (methyl methacrylate) (PMMA) is a transparent amorphous polymer known for its excellent optical clarity and weather resistance. It is synthesized from methyl methacrylate (MMA) through radical polymerization, a process that uses peroxides as initiators and occurs at temperatures up to 100°C (see Figure 2-10). PMMA is widely used in applications such as engineering medical fields, packaging parts and transports.
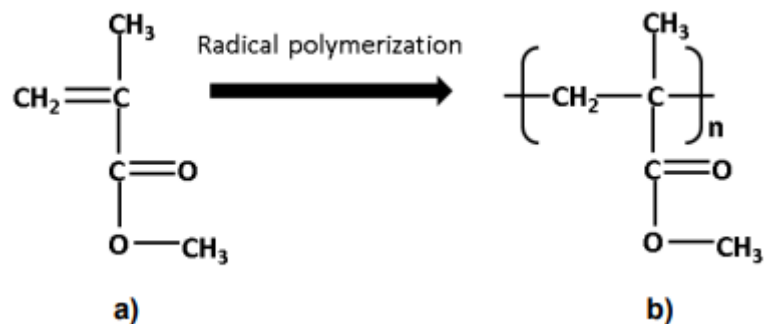
Figure 2-10: a) Methyl methacrylate. b) Poly (methyl methacrylate) [93]**.**

PMMA exhibits several notable properties: it has good mechanical tensile strength, high hardness and scratch resistance, low water absorption, strong thermal and hydrolytic resistance, excellent transparency, effective thermal insulation properties, and outstanding resistance to UV-induced aging. These characteristics have made PMMA a widely used material in various applications [94], [95].

2.8.1. Physical and mechanical properties of PMMA

Table 2-2 presents the characterization of PMMA obtained from various literatures. It shows that PMMA is a glassy polymer with a good glass transition temperature (Tg) and thermal stability. Despite its brittleness, it has a high modulus of elasticity and low elongation at break, making it a rigid and durable material.

Table 2-2: Thermal and mechanical properties of PMMA polymer.

property		PMMA	References
Density (g/cm^3)		1.18-1.19	[96], [97]
Hardness	Vickers HV	16-21	[86]
	Shore D	(78-86)	[98][99]
Glass Transition Temp. (°C)		110 to 120	[96], [100]
Thermal Expansion Coefficient (10^{-6} /K)		72–162	[86]
Water Absorption (%)		0.3	27
Thermal conductivity (W/m K)		0.08–0.25	[86], [96], [101]
Tensile Strength (MPa)		72	[97]
Tensile modulus (MPa)		3100	[97]
Flexural strength (MPa)		110	[100]
Flexural modulus (MPa)		3000	[100]
Elongation at break (%)		5	[97]
Impact strength (kJ/m)		2	[102]

2.9.   Application of the ABS/PMMA bilayer sheets

ABS polymer-based sheets have a matte surface which is usually co-extruded with another polymer such as PMMA protecting it against scratches [103], [104] and chemical attacks [105]. By combining of these performances, many ABS/PMMA multilayer sheets are generally used in the manufacture of parts by thermoforming process [106]. These thermoplastics are well-suited to specific engineering applications requiring excellent mechanical resistance [107] and good thermal stability under severe use conditions [108]. Interesting application domains using these sheets continually grow such as: exterior panels and vans, bumpers, guards and wheel arch for trucks, kitchens [109]–[112], bathroom [46], [113] electronic and medical areas [114], [115].

2.10. Literature review on the mechanical behavior of ABS and PMMA polymers

To enhance the performance of ABS/PMMA bilayer sheets, many experiments were performed to determine the mechanical and thermal properties of several sheets made by combining of polymers, using different processes, in function of temperatures [116] and strain rates [117]–[119] separately or combined [120]–[122]. Among these experiments, Li et al. [123] and Huang et al. [124] have determined the tensile properties of ABS polymer at different temperatures and glass transition temperature using DMA analysis. They showed that the ABS uniaxial tensile behavior exhibited temperature sensitivity, a decrease in Young modulus, yield stress and maximum stress with increase in temperature, while the strain increased significantly [123]. These findings showed a high flexibility of ABS polymer at high temperatures [123], [124]. The glass transition temperature, Tg, of ABS was 110°C [124]. An increase in Young's modulus with an increase in strain rate due to the viscous nature, while a softening behavior was observed when the temperature was increased [125]. In the other hand, Abdel-Wahab et al. [61] analyzed the mechanical behavior of the PMMA polymer via tensile and three-point bending tests in function of different temperatures ranging from 20°C to 80°C.They showed that the PMMA polymer exhibited the same temperature sensitivity as ABS polymer. At 80°C, the PMMA polymer exhibits a 79% drop in Young's modulus and 67% drop in yield strength compared to the ambient temperature, while the maximal strain increased by 110%. The stress evolution of PMMA also exhibits a high sensitivity to the strain rate [80]. Additionally, under compression tests of PMMA [126], [127], a decrease in yield stress with increasing temperature and decreasing strain rate was observed. Comparing the characteristics of these two polymers, it can be deduced that PMMA is more brittle than ABS at low temperature, but becomes more flexible at high temperatures [61], [123].
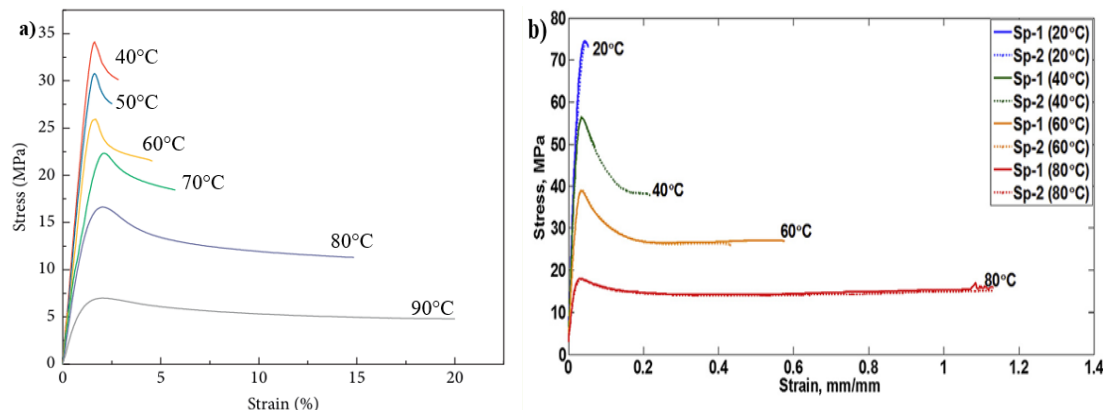
Figure 2-11: Tensile stress-strain curves at different temperatures: a) ABS polymer [123]**, b) PMMA polymer** [61]**.**

2.11. Characterization of the ABS/PMMA blend

The combination of these two polymers, using mixing or co-extrusion processes, permits the obtaining of composite sheets taking advantage of each ABS and PMMA polymer characteristics. Therefore, certain experimental works were conducted on ABS/PMMA blends made by mixing process at only room temperature. Al Haydary et al. [128] found that the PMMA/ABS polymer blend exhibits ABS main bands, while the methyl stretching vibration of the PMMA C-O bands confirms interactions between the PMMA and ABS functional groups. Notably, when the ABS percentage increases up to 70%, the glass transition temperature of PMMA tends be not clear and though it isn't completely miscible. Moreover, they observed that the material's tensile and bending strengths exhibit an upward trend with higher proportions of ABS additive. However, the optimal mechanical properties were achieved with a 55% ABS composition, underscoring the delicate balance needed for achieving peak performance in PMMA/ABS blends. Reinaldo et al. [69] studied PMMAh/ABS and PMMAe/ABS blends. They found that the glass transition temperatures of these blends were similar, with ABS exhibiting more thermal stability than the other polymers. PMMAh/ABS blends behave more brittle than the PMMAe/ABS blends which exhibit ductile behavior, due to that the elastic modulus of PMMAh was higher than of ABS and PMMAe. Kuleyin et al. [129] studied the thermal, chemical and mechanical performance of a range of ABS proportions in PMMA/ABS blends. The results showed increased bond strengths and peak intensities in the interaction between C=O and C≡N, suggesting improving miscibility and structural modifications within the blend system. As well, thermal stability and glass transition

temperature increased up to112.2°C with increasing ABS content, accompanied with decreasing of mechanical properties such as modulus of elasticity and peak stress. Ma [130] investigates blending PMMA/ABS to enhance mechanical and optical properties. Through varied blending processing and conditions, including extrusion cycles and injection parameters, the ABS/PMMA blend properties for electrical enclosure applications were optimized. the findings show that dual extrusion process improves impact strength and tensile properties, while at specific injection conditions of 220°C leads toa yield stress of 70 MPa superior than obtained via extrusion process.

2.12. Mechanical behavior of extruded bilayer polymer structures

With regard to the literature review, there is a notable absence of research examining the thermal and mechanical properties of sheets produced through the co-extrusion process, particularly in the context of ABS/PMMA bilayers. Khledj et al. investigated the mechanical properties of ABS/PMMA bilayer structures under tensile testing. The tests were conducted under varying strain rates and temperatures, and the results demonstrated that the ABS/PMMA bilayer exhibited robust mechanical properties. As the strain rate increased, the bilayer displayed brittle characteristics, while at elevated temperatures, it exhibited ductile and plastic behavior. The fractography analysis revealed that the strain rate affects the fracture surfaces of ABS/PMMA polymers, which present fibrils at low strain rates and large cracks and crazes at high strain rates [131]–[133]. Comparison of the ABS/PMMA bilayer with pure ABS and pure PMMA by three-point bending reveals that pure ABS is ductile, while pure PMMA is brittle and has no plastic zone, giving it high mechanical properties compared with pure ABS. However, the ABS/PMMA bilayer structure has even higher mechanical properties than pure ABS, as well as higher ultimate deformation [134]. Many other bilayer structures have been studied by various researchers. Indeed, Leong et al. [135] studied the molding conditions effect on the mechanical characteristics of the injection molded PP Film/PP Matrix bilayer by modifying pressure and speed of injection. Bending tests showed similar properties with no noticeable effect from the inserted film. Wittmann and Drummer [136] analyzed the melt flow index of an extruded thermoformed and non-thermoformed polypropylene PP sheet with monolayer and multilayer. They found that the Young's modulus of thermoformed parts remained unchanged, with minor reducing

attributed to the forming temperature-induced crystallinity. However, the tensile strength of post-thermoforming PP slightly exceeded the non-thermoformed PP sheet due to molecular chain elongation. Ji et al. [137] investigate the characterization of shape-memory polymeric materials fabricated with TPE/PLA polymers bilayer and blend. The obtained results show that the glass transition of TPU/PLA bilayer has a higher storage modulus than the TPE/PLA blend. Furthermore, the tensile strength of the TPU/PLA bilayer exhibits higher elongation at break strain compared to the TPU/PLA blend. While the TPU/PLA blend presents slightly higher tensile strength than the TPU/PLA bilayer. Chen et al. [138] used 3D extrusion printing of PETG/ABS, varying layer thickness, print speed and fill density. They found that when print speed and fill density increase, the tensile strength and the Young's modulus significantly increased.

2.13. Conclusion

This chapter has provided a comprehensive overview of amorphous polymers, with a particular focus on ABS and PMMA, which are integral to this research project. The distinctive properties of amorphous polymers, including their exceptional thermal and mechanical characteristics, underscore their versatility and suitability for diverse industrial applications. The glass transition temperature (Tg) is a critical parameter that significantly impacts the performance of these materials, influencing their behavior during processing and end-use. Furthermore, the mechanical characteristics, including impact strength, tribology, and hardness, highlight the importance of material selection for specific applications. Understanding the interplay of molecular structure and environmental factors can enhance the performance of ABS/PMMA bilayer systems. This knowledge paves the way for advancing thermoforming applications, ultimately contributing to innovation in polymer engineering. Further research and experimentation will be essential in optimizing these materials for enhanced durability and functionality.

Chapter 3.   Material and experimental procedures

_____

3.1.   Introduction

The development and optimization of polymeric materials, particularly multilayered structures, have attracted considerable attention in recent years due to their enhanced performance and extensive range of industrial applications. The use of coextruded bilayer structures, such as those composed of ABS and PMMA, is becoming more prevalent due to their combined mechanical strength, thermal stability, and aesthetic qualities. In this study, a comprehensive series of experimental tests were conducted to assess the properties and behavior of an ABS/PMMA bilayer structure.

To investigate the thermal properties of the material, thermogravimetric analysis (TGA) and differential scanning calorimetry (DSC) were employed. The viscoelastic and mechanical characteristics were analyzed through dynamic mechanical analysis (DMA), tensile tests, Charpy impact tests at varying temperatures, and three-point bending tests. Following, a fractographic analysis was conducted using scanning electron microscopy (SEM) on fractured surfaces from tensile and Charpy tests. Additionally, the durability of the material was evaluated through the application of Vickers and Shore D hardness tests, while tribological analysis facilitated the acquisition of data on the coefficient of friction (COF) and wear rate.

3.2.   The ABS/15%PMMA coextruded sheet

The sheets were composed of acrylonitrile-butadiene-styrene (ABS) and a 15% poly(methyl methacrylate) (PMMA) bilayer, produced by a coextrusion process. These commercial bilayer polymer sheets are used in the manufacturing industry, in particular by local company EIMS-Miliana in Algeria. Using the thermoforming process, EIMS-Miliana manufactures products with complex geometries from these bilayer sheets, including a variety of bathtub sizes. The company wishes to evaluate the thermoforming capabilities of the ABS/PMMA bilayer material. To this end, experimental studies on the thermal and mechanical behavior of the sheets have been carried out to assess the performance of products obtained by thermoforming. ABS/PMMA bilayer is a high-gloss, amorphous thermoplastic polymer with a density of 1.11 g/cm³. ABS offers high impact resistance, rigidity and thermal stability show in (Table 3-1) from (Annex 1), while PMMA offers transparency, high gloss and excellent scratch and impact resistance. The geometry of the sheet received was also investigated under the optical microscope, as

shown in Figure 3-1. The total thickness of the ABS/PMMA bilayer sheet is 4 mm, with the PMMA layer measuring 0.72 mm (as shown in Figure 3-1). The remaining thickness, around 3.28 mm, is the ABS layer.

Table 3-1: Characterization of ABS/PMMA bilayer sheet (Annex 1).

ABS/15%PMMA sheet	properties
Density (g/cm^3)	1.11
Tensile modulus (MPa)	>1800 (ISO 527- 50 mm/min)
Maximum stress (MPa)	>38 (ISO 527 - 50mm/min)
Charpy unnotched	>20
HDT (°C) (KJ/m^2)	>100
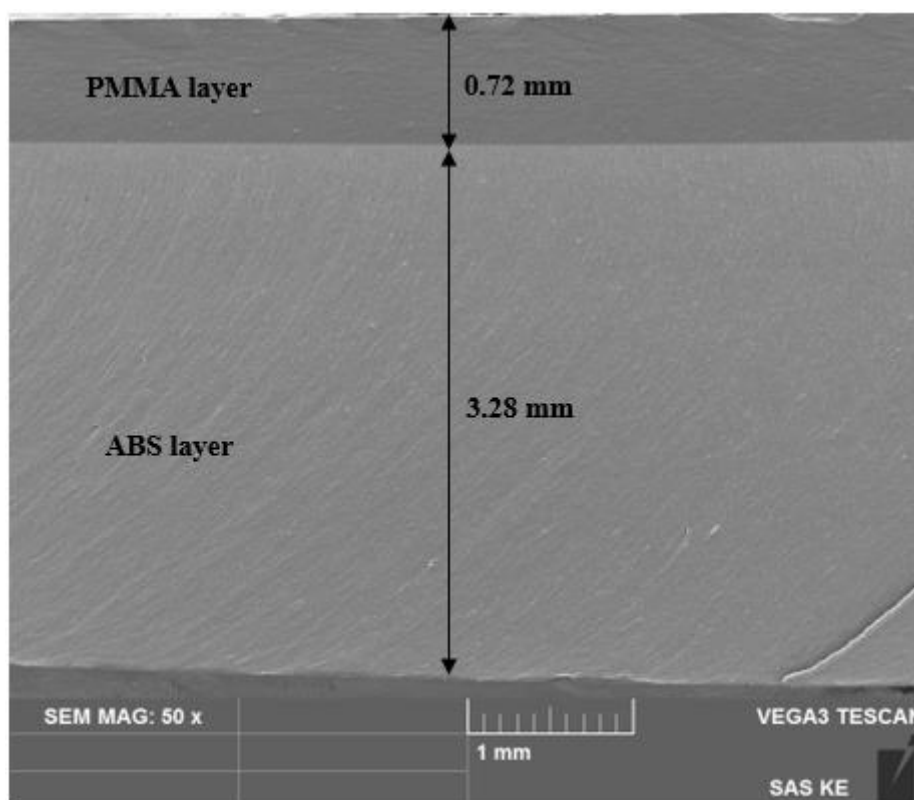
Figure 3-1: SEM of sheet layers thickness of ABS/PMMA.

In Algeria, the production of polymer/polymer-based coextruded sheets involves using co-extrusion, a manufacturing technique where two or more polymers are simultaneously extruded and combined to create a single structure with multiple layers (Figure 3-2). The selection of each layer is designed to impart specific characteristics to the final product, including barrier properties, heat-sealability, strength, and chemical

resistance. This results in an integrated product that exhibits all of these qualities. To guarantee the superior quality of the coextruded product, it is essential that each layer maintains a consistent thickness, that the layers adhere seamlessly to one another, and that the structure remains free from interfacial instabilities [14].
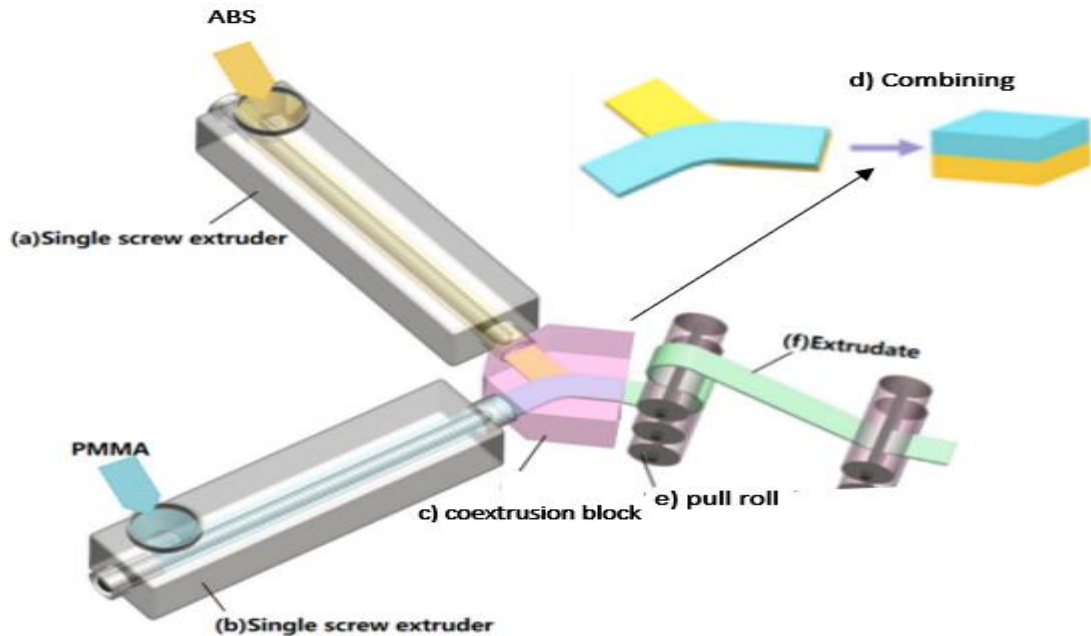
Figure 3-2: Schematic of the bilayer co-extrusion technology [139]**.**

The bilayer polymer sheets used in EIMS come from the Blida *decoplast* industry, which manufactures a range of extruded polymers such as ABS, PMMA, impact PS, SAN, and PP....

The organized ABS/PMMA bilayer materials were produced using a layer coextrusion system at the *Decoplast* industrial facility, as depicted in Figure 3-3. In this process, ABS and PMMA granulates are fed into separate single-screw extruders. The first extruder, dedicated to ABS granulation, achieves a final bilayer composition of 85% ABS and 15% PMMA in the second extruder (Figure 3-3.a). Precise temperature control is crucial throughout the extrusion process, with set points of 180°C for the hopper, 200°C for the cylinder, and 220°C for the die, ensuring optimal melting and uniformity of the materials. The molten ABS and PMMA are combined in a coextrusion block (Figure 3-3.b), forming a cohesive bilayer structure. This composite material is subsequently guided through a pull roller (Figure 3-3.b), which securely bonds the two layers and regulates the thickness of the ABS/PMMA bilayer. The process culminates in

discontinuous sheet extrusion (Figure 3-3.c), followed by precision cutting, resulting in uniform, high-quality sheets of different polymers ready for application (Figure 3-3.d).

Figure 3-3: Fabricated polymer sheets via extrusion and co-extrusion processes; (a) single screw extrudates, (b) co-extrusion block and pull roll, (c) extrudate, and (d) extruded polymer sheets.

This research examines a bilayer polymer composed of ABS and 15% PMMA. In addition to characterizing this composite material, comparative tests were conducted with pure ABS and PMMA polymers. This approach allows for the comparison of the mechanical, thermal, and viscoelastic properties of the bilayer with those of its constituents. By conducting a comprehensive analysis of these materials, the objective is to elucidate the synergistic effects of combining ABS and PMMA, thereby identifying potential applications in various industrial sectors.

3.3. Thermal properties

3.3.1. Thermogravimetric Analysis (TGA) and Differential Scanning Calorimetry (DSC)

Thermogravimetric Analysis (TGA) was conducted using a *PerkinElmer TGA* (Figure 3-4), with a heating rate of 10 °C/min and a nitrogen gas flow of 20 ml/min, starting from ambient temperature up to 700 °C., This analysis allowed us to study the

thermal stability of the material. After that, Differential Scanning Calorimetry (DSC) was performed. The *Perkin Elmer DSC* analyzer was used with a heating rate of 20 °C/min and a nitrogen gas flow of 25 ml/min, starting at room temperature and up to 400 °C (Figure 3-4).
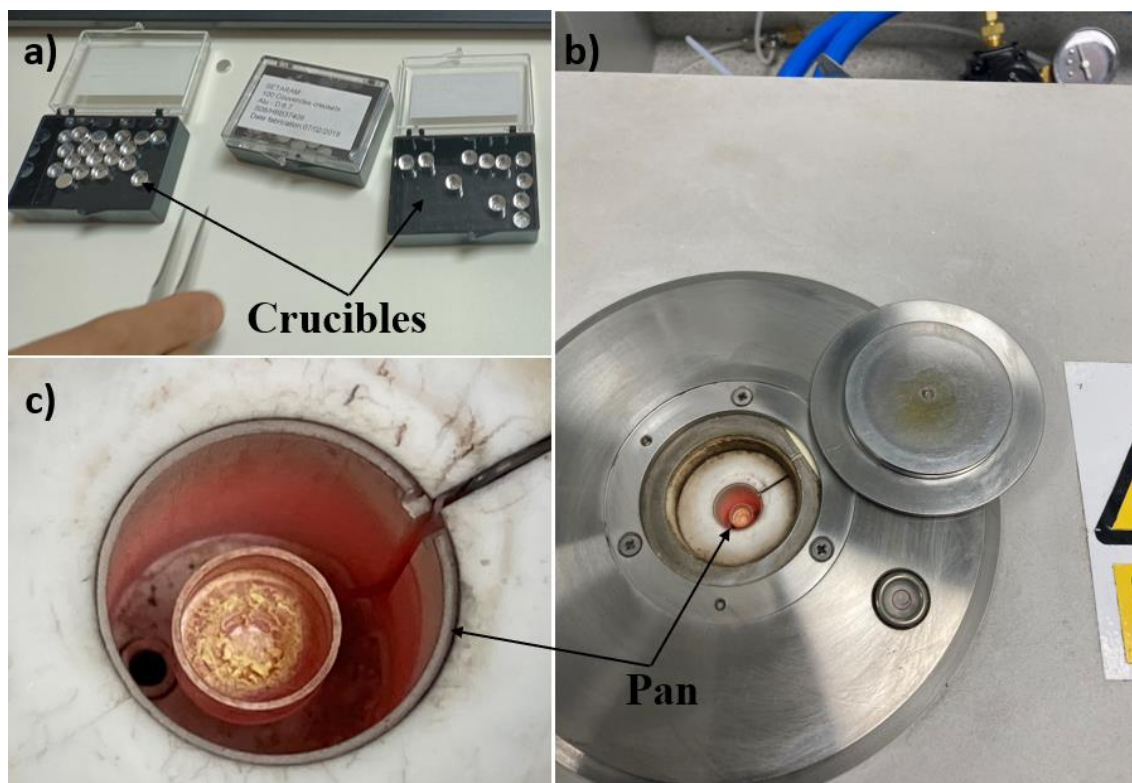
Figure 3-4: The device used to measure the thermal properties of polymers.

3.3.2. DSC and TGA operating principles

The techniques of differential scanning calorimetry (DSC) and thermogravimetric analysis (TGA) are complementary and are used to investigate the thermal behavior and stability of materials. The fundamental principle of differential scanning calorimetry (DSC) is to quantify the differential heat flow required to raise or lower the temperature of a sample in comparison to a reference material, both subjected to a controlled temperature program. This technique is of great importance for the identification of thermal transitions, including melting, crystallization, and glass transitions (Tg), as well as for the assessment of the thermal stability of materials [140].

In a typical DSC experiment, the sample, which may be an ABS/PMMA bilayer, is placed in a crucible (Figure 3-4.a), while the reference material, which is typically an empty pan (Figure 3-4.b) or one containing an inert substance, is placed in a separate,

thermally isolated pan. The rate of heating or cooling applied to both the sample and the reference is identical. During the heating phase, endothermic events, such as melting or glass transition, result in the sample absorbing more heat than the reference, forming a peak on the DSC curve. Conversely, exothermic events, such as crystallization, release heat and appear as downward peaks. The first heating cycle removes any thermal history, while the second heating cycle reveals more intrinsic thermal properties. Additionally, cooling cycles provide valuable data on crystallization behavior and phase transitions.

In contrast, thermogravimetric analysis (TGA) entails the measurement of a material's mass change as it is subjected to heating or cooling under a controlled temperature program, frequently within an inert or oxidative atmosphere. This technique is employed to ascertain the material's thermal stability and decomposition temperature by monitoring mass loss resulting from processes such as volatilization, degradation, or oxidation. In a TGA experiment, the sample is subjected to a controlled heating process, and the resulting weight loss is continuously recorded. This allows for the identification of multiple thermal events, including the loss of moisture, the decomposition of organic components, and oxidation. The derivative thermogravimetric (DTG) curve can be employed to further highlight the rate of mass loss and to identify specific degradation stages [140].

Together, DSC and TGA provide a comprehensive insight into the thermal properties of polymers and other materials. DSC focuses on heat flow, specifically endothermic and exothermic transitions, whereas TGA concentrates on mass changes, such as degradation and thermal stability. This combination of techniques is particularly beneficial for elucidating intricate thermal behavior in both amorphous and crystalline materials [140].

3.3.3. Methods for Separating the Layers of an ABS/PMMA Bilayer Sheet

To compare the thermal properties of the ABS/PMMA bilayer polymer with those of its layers, ABS and PMMA, used a microtome device to separate the bilayer structure (Figure 3-5.a). An *Epredia microtome* is a precision instrument that cuts extremely thin slices of material, down to 3 microns and is often used in microscopy and material

science. This advanced method allows for detailed analysis and characterization of the separated layers and is generally employed in polymer composites. In this instrument, the knife moves vertically against a fixed block, progressing in a straight plane. It was designed to cut thin layers, as shown in Figure 3-5.b and Figure 3-5.c.
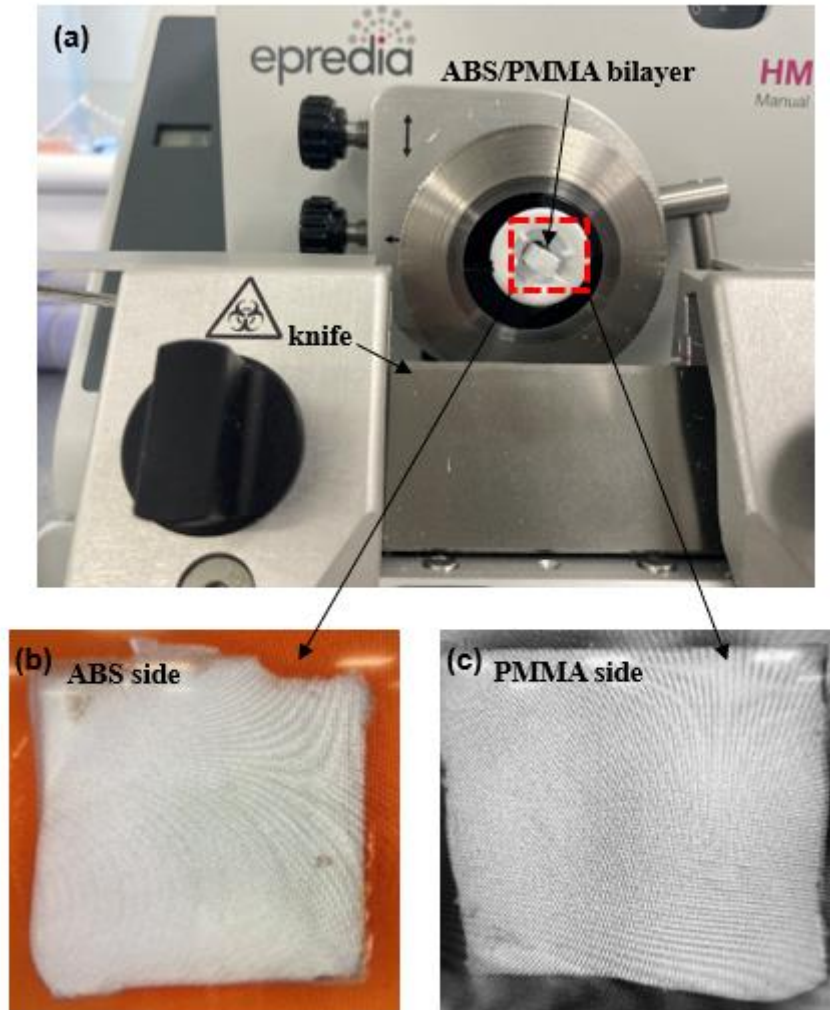
Figure 3-5: Layer separation technique: (a) microtome device, (b) ABS side and (c) PMMA side.

3.4. *Viscoelastic and mechanical properties*

3.4.1. Dynamic Mechanical Analysis (DMA)

During thermal and mechanical characterization, the viscoelastic properties of the material were determined using Dynamic Mechanical Analysis (DMA) under tension strain. These tests were conducted with the *Metravib DMA 50* instrument (Figure 3-6). A sample measuring $23 \times 4 \times 2$ mm was cut from the extruded ABS/PMMA bilayer sheet

and mounted in the grips of the instrument. Testing was carried out over a temperature range of 35 °C to 150 °C, applying frequencies of 1.5 Hz and 10 Hz. This analysis aimed to assess the viscoelastic properties of ABS/PMMA and identify the thermoforming range utilized at EIMS Miliana.

Figure 3-6: Dynamic mechanical analyzer.

3.4.2. Tensile test at different temperatures

In order to ensure accuracy and quality, the tensile specimens are shaped using an Opal waterjet with a high sand flow rate on a *PRO-X 3D* cutting head machine using cutting-edge technology. By using these methods, cut edges are guaranteed to meet strict shape quality criteria and have a polished, smooth finish. The cutting parameters were 3,000 Bars of pressure and 15 mm/s of cutting speed. The tensile samples were prepared according to ISO 527 standards [141], as depicted in Figure 3-7.a. Testing was conducted using a *Zwick-Roell* testing machine with a 25 kN capacity and equipped with an environmental chamber capable of temperatures ranging from -50 to 270°C. Two different tensile strain rates were applied: $3.33 \times 10^{-4} s^{-1}$ and $1.66 \times 10^{-2} s^{-1}$, corresponding to values indicated as mm/min in Refs. [141], [142]. Mechanical properties of the ABS/PMMA bilayer were evaluated through tensile tests performed at room temperature

(23°C) and various elevated temperatures (35°C, 50°C, 70°C, and 90°C). The environmental chamber was monitored and stabilized using a thermocouple attached to the tensile machine. Prior to testing, each specimen was placed in the chamber until the temperature stabilized for 7 minutes, as illustrated in Figure 3-7.b. Five specimens were tested at each temperature condition.
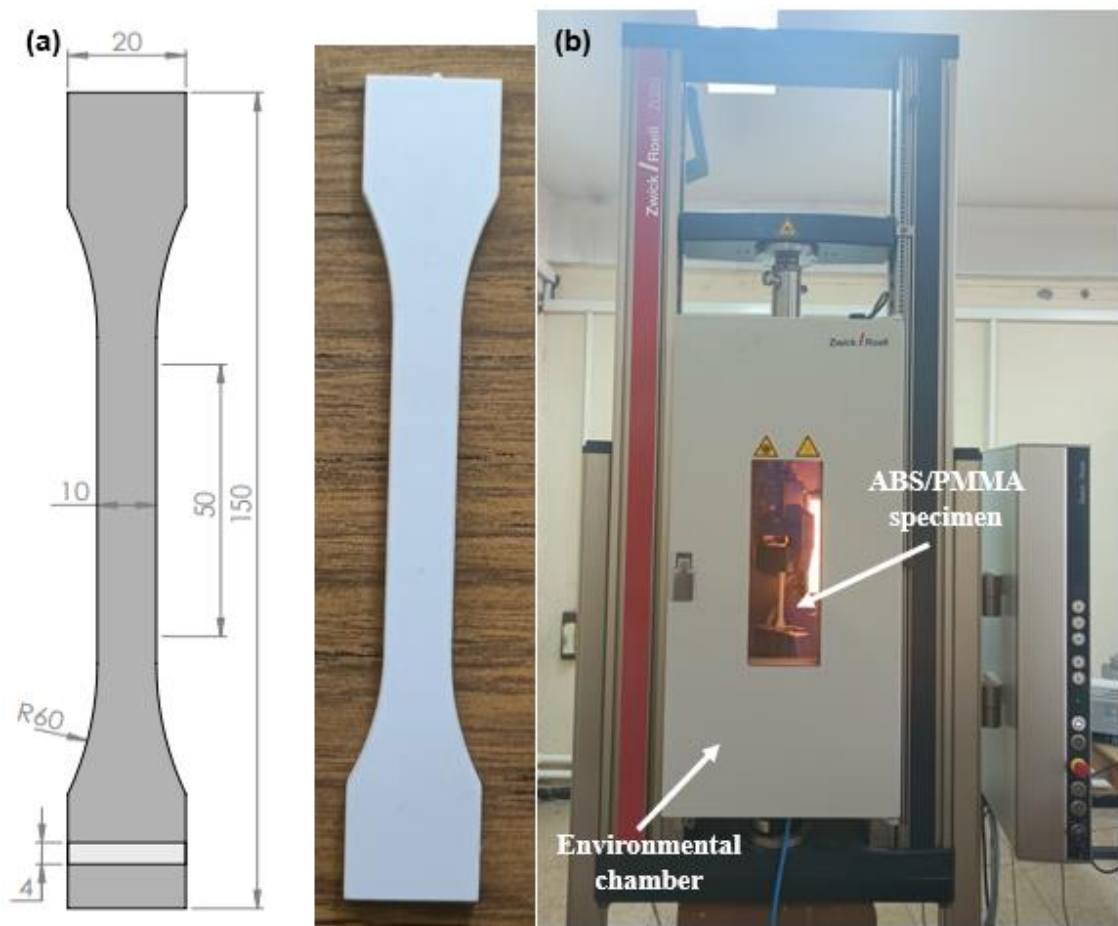
Figure 3-7: (a) Tensile specimen shape and dimensions and (b)specimens into environmental chamber.

Tensile tests were conducted at various temperatures on the ABS/PMMA polymer bilayer to analyze its behavior in terms of stress, strain, and Young's modulus.

3.4.2.1. Elastic modulus

The behavior of an elastic material is characterized by its Young's modulus, which is the ratio between the mechanical stress (σ) and the strain (ε) at 0.02% of the material's deformation. This modulus defines a material's ability to store and release mechanical energy, which is essential for predicting its response to various loads in engineering applications which determination of the modulus is given by the equation as follows:

$$E = \frac{\sigma}{\varepsilon} \quad in \ (MPa) \tag{1}$$

3.4.2.2. True stress

True stress is derived from technical stress and provides a more accurate characterization of the state of a material in a tensile test. Unlike technical stress, which is based on the original cross-sectional area, true stress takes into account the actual cross-sectional area at a given moment of deformation. This adjustment enables more accurate measurement of a material's response under load, particularly when significant plastic deformation occurs. The true stress is determined by the following formula:

$$\sigma_v = \sigma_{eng}(1 + \varepsilon_{eng}) \tag{2}$$

Where σ_{eng}, σ_{eng} are engineering stress and engineering strain.

3.4.2.3. True strain

True strain, offers a more realistic representation of material deformation. True deformation takes into account progressive changes in length, giving a continuous measure of deformation, whereas engineering strain measures the change in length relative to the initial length. The following formula is used to determine actual deformation:

$$\varepsilon_v = ln(1 + \varepsilon_{eng}) \tag{3}$$

3.4.3. Impact strength (notched Charpy)

The impact tests were performed using a Charpy tester, conducted following ISO 180 standards at various temperatures (25 °C, 70 °C, and 100 °C). A V-notch with a depth of 2 mm was utilized for these tests. The dimensions of the impacted specimens were as follows: a length of 80 mm, a width of 10 mm, and a thickness of 4 mm (Figure 3-8.a). To guarantee precision and uniformity, each specimen was meticulously prepared and conditioned before testing. The specimens were heated in an oven (Figure 3-8.b) for an adequate period to reach thermal equilibrium at the required temperature. Once the target temperature was attained, the specimens were swiftly moved to the Charpy tester to minimize any heat loss. The Charpy machine used in this experiment is a resilience tester (Figure 3-8.c). The recorded outcomes were expressed in terms of energy absorbed, measured in joules (J) were used to compute impact strength values, represented in terms of kJ/m², determined using the equation:

$$E_a = \frac{E_c}{h.b} \times 10^3 \qquad\qquad (4)$$

where Ec represents the corrected energy absorbed by the specimen (in Joules), h is the thickness of the specimens (in mm), and b is the width (in mm).
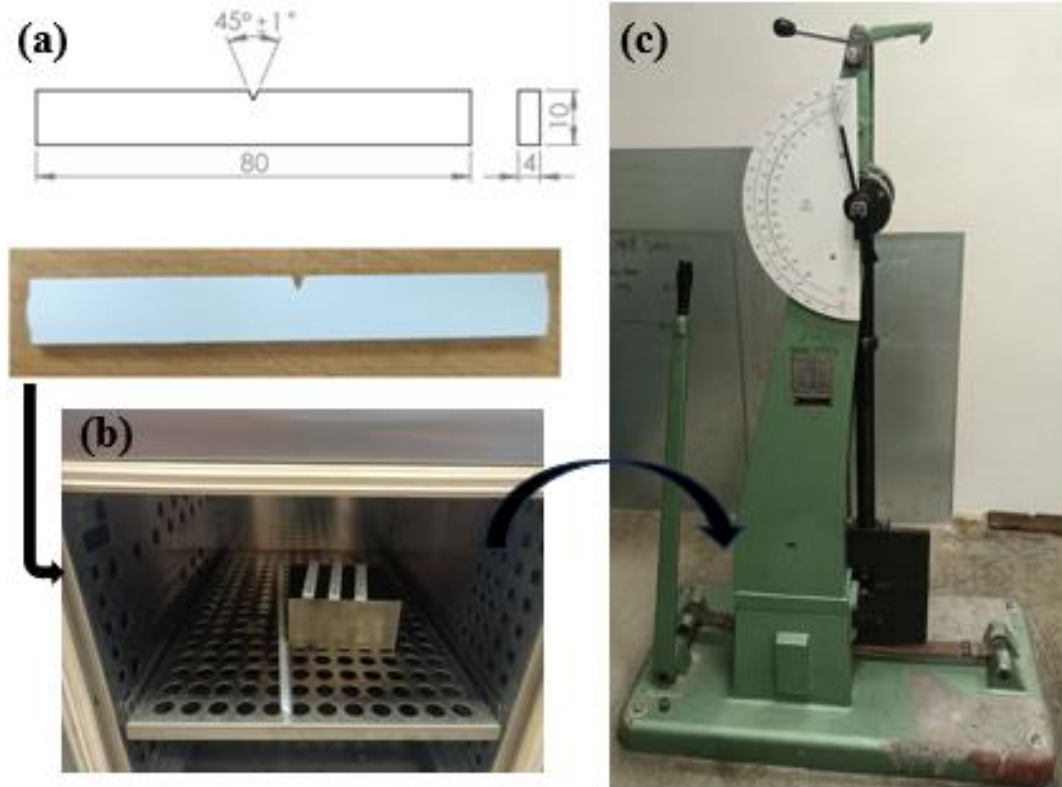
Figure 3-8: Charpy test: (a) shape and specimen dimension, (b) oven, (c) resilience tester.

These tests impact energy measurements and offer important insights into the material's capacity to absorb energy during fracture. This data is essential for evaluating a material's performance under various temperature conditions, especially in applications where temperature fluctuations are anticipated.

3.4.4. Fractography analysis

The study of the morphology of an ABS/PMMA bilayer was carried out using *a Tescan Vega 3 XMU* scanning electron microscope (Figure 3-9), equipped with a variable acceleration voltage, to perform a detailed fractographic analysis of the fracture surfaces of ABS/PMMA bilayer specimens. This study aimed to explore the microstructure and adhesion characteristics between ABS and PMMA layers, particularly after subjecting the

specimens to tensile and Izod impact tests at different temperatures. By studying these fracture surfaces, it sought to understand how temperature variations influence the interfacial properties and overall structural integrity of the bilayer material.

Figure 3-9: Scanning Electronic Microscopy analyzer.

3.4.5. Three-point bending

Three-point bending tests were conducted using a Three-point bending test were conducted using a Zwick universal testing machine equipped with a 15 kN load cell. The supports, crafted from tool steel (Figure 3-10), provided a span of 64 mm between the lower supports. The loading speed was set at 3 mm/min. The specimens for the three-point bending tests were prepared and produced in accordance with ISO 178 standards [143], with dimensions of 80 mm in length, 10 mm in width, and 4 mm in thickness. To evaluate the bending stress and stiffness of our ABS/PMMA bilayer, it compared its performance with that of pure ABS and pure PMMA, both of which are commercial polymers produced by the extrusion process. This comparison allows us to understand the mechanical advantages and limitations of the bilayer structure with its individual components. The data obtained from these tests, including maximum flexural stress and corresponding strain, were carefully recorded and analyzed. This information is essential for assessing the material's behavior under bending forces and for determining its suitability for various applications.
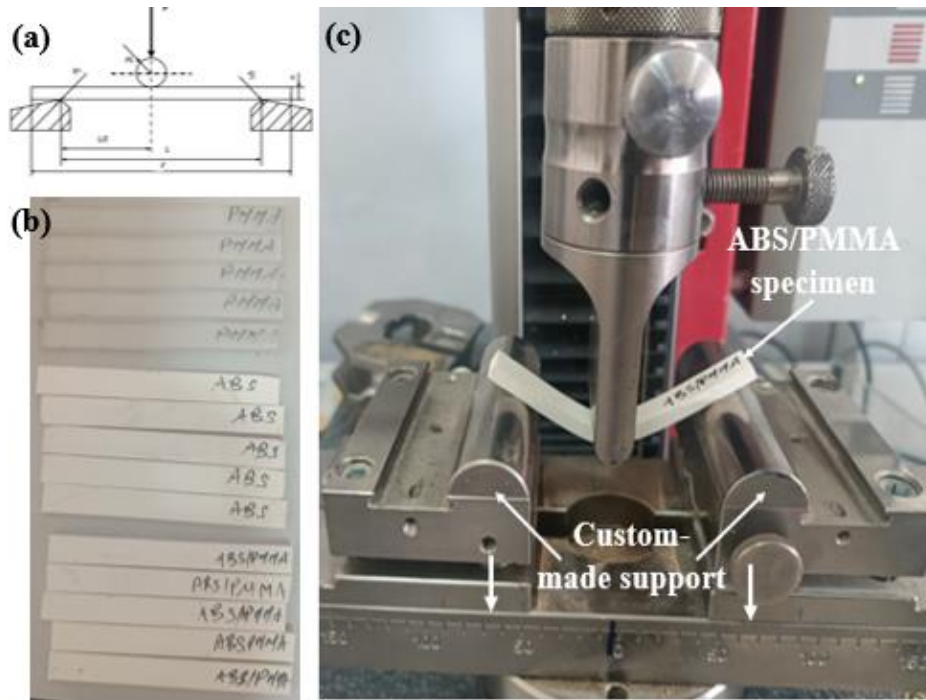
Figure 3-10: Test set-up according to ISO 178 (a), specimens (b), and Three-point bending specimen mounted on custom-made supports during test (c).

The highest bending stress and associated strain, as well as other test results, were meticulously noted and examined. Understanding material behavior in applications where bending forces are common requires knowledge of this information. The overall dependability of the test findings was increased by the employment of tool steel supports and loading rate control, which guaranteed reliable and accurate readings.

The following equations for flexural stress (σ_f) and strain (ε_f) were used to convert the load-displacement (deflection) data acquired during bending into stress-strain curves.

$$\sigma_f = \frac{3Fl}{2bh^2} \tag{5}$$

$$\varepsilon_f = \frac{6hd}{l^2} \tag{6}$$

where h and B are the thickness and width of the specimen, F is the force, d is the displacement (deflection) at midspan.

Equations (1) and (2) were also obtained using the load-deflection approach. Using the following formula [13], the modulus of elasticity (E) for PMMA was computed using the load-deflection responses found in the three-point bending tests:

$$E_f = \frac{\sigma_{f2} - \sigma_{f1}}{\varepsilon_{f1} - \varepsilon_{f2}} \qquad\qquad (7)$$

Where σ_{f1}, σ_{f2} are flexural stress, in megapascals, measured at strain (deflection) ε_{f1}, ε_{f2}.

3.5. Hardness and tribology

3.5.1. Hardness tests

3.5.1.1. Shore D hardness

The most widely recognized hardness measurement scale is the Shore durometer used for polymers, available in two main variants: Shore A and Shore D. These handheld instruments feature specific geometric indenters that are driven into the material surface under a defined spring force. Although originally designed for hand-held use, they are often mounted on stands to improve measurement reproducibility. The depth of indentation produced by the indenter is measured using a scale marked directly in units of hardness. Older models used dial gauges, but modern hardness testers are equipped with a digital display for more accurate measurements [144].

Shore D hardness was determined in accordance with ISO 868/7619 using a Bareiss hardness tester (Figure 3-11), with tests applied to both sides of the ABS/PMMA bilayer polymer, to verified which layer hardened.
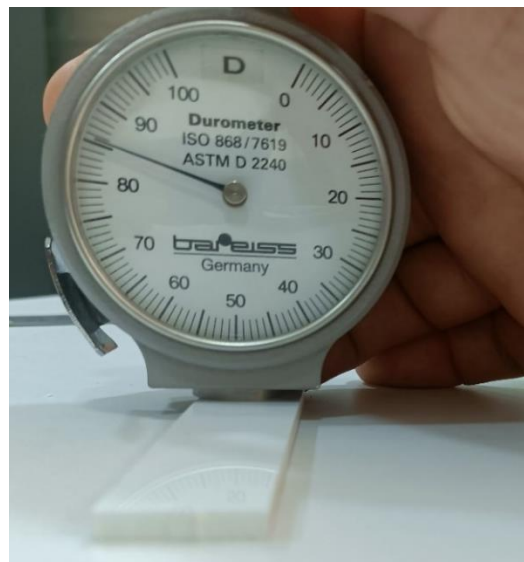
Figure 3-11: Shore D durometer

3.5.1.2. Vickers Hardness

Hardness tests were carried out on ABS/PMMA bilayer sheet using the Vickers method with a Wilson Tukun 1102 micro-durometer (Figure 3-12). This method enabled the hardness of the material to be measured accurately. Loads of 10 g, 25 g, 50 g, 100 g, and 300 g were systematically applied to the ABS and PMMA surfaces. Each indentation was held for 15 seconds for each load, and the process was repeated eight times to ensure reliable, accurate, and consistent results. The Wilson Tukun 1102 micro-durometer enabled the shape and size of the indentations to be studied in detail, giving an insight into the hardness characteristics of the material surface at different load levels. This approach not only enabled us to assess the bilayer's resistance to indentation but also facilitated a comprehensive hardness comparison between the ABS and PMMA layers, contributing to an in-depth understanding of their mechanical properties.

Figure 3-12: Vickers hardness tester

Hardness analysis involved testing and measuring the diagonals on each side of the ABS/PMMA bilayer using a *ZEISS* optical microscope (Figure 3-13). This made it possible to accurately investigate the indentations made during the hardness tests. The Vickers hardness test, carried out with loads ranging from 10 g to 300 g on the ABS and PMMA faces, provided a better understanding of the material's surface hardness characteristics. Each indentation was carefully observed and measured using the optical microscope, enabling hardness values to be accurately determined across the entire

bilayer structure. This approach enabled us not only to assess the material's resistance to indentation, but also to investigate in detail the differences in hardness between the ABS and PMMA layers.

Figure 3-13: ZIESS optical microscope analyzer surface.

The Vickers method measures the average diagonal of the depression made by a pyramid of straight diamonds placed on a square base. This yields the hardness relationship, which can be expressed as follows:

$$HV = \frac{2F\,sin(\theta/2)}{9.81*d^2} \cong 0.1891\frac{F}{d^2} \tag{8}$$

Where's HV is Vickers hardness (MPa), F is the force applied in (g), d the mean diagonal width of the impression (mm) and θ is the angle of the pyramid (= 136°)

3.5.2. Tribology test

Tribological tests were conducted using a Reciprocating Motion Tribometer (*CSM, Slovakia*) with a ball-disc contact configuration (Figure 3-14). The stationary counter body samples were Φ5 mm AL_2O_3 alumina. A polymer-on-steel contact setup was chosen to ensure stable contact conditions, with the use of alumina balls preventing any wear on the stationary sample. The tests were performed at two normal loads, 2 N and 5 N, on both the ABS and PMMA sides at a sliding velocity of 10 mm/s. Each test lasted for 1 hour, corresponding to approximately 250 m of sliding distance, to ensure steady-state conditions. All tests were conducted dry and under laboratory conditions (23 ± 2 °C).

Figure 3-14: Tribometer measurement device.

The measurement of friction can be achieved through the analysis of forces, moments, or energy transmission within the tribological pair illustrated in Figure 3-15. The coefficient of friction, an empirical value, is used to quantify the sliding friction between two bodies. The coefficient of friction is expressed as the ratio of the tangential force (F_S) to the normal force (F_N) acting on the tribological pair. This relationship, known as the first law of friction, states that the force required to initiate sliding motion is directly proportional to the normal force.

$$\mu = \frac{F_S}{F_N} \tag{9}$$
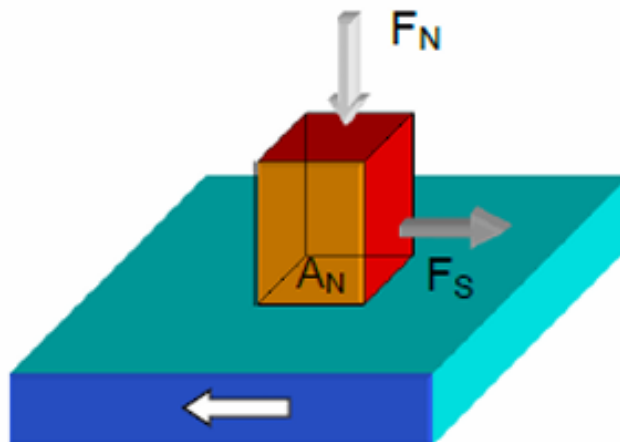
Figure 3-15: The forces applied in friction tests [79].

Following the tribological tests, The friction coefficients were continuously recorded throughout the tests, and the material losses, specifically the volume of wear tracks on each layer of the ABS/PMMA sheet, were precisely measured using a high-resolution microscope *PLu neox 3D* Optical Profiler by SENSOFAR (Figure 3-16). A Nikon 20x objective lens provided detailed magnification for accurate observation, while the *SensoMAP* program was employed to perform advanced surface analysis and calculate the wear metrics.

Figure 3-16: PLu neox 3D confocal microscope profiler [145]**.**

To accurately determine the wear rate, the volume and surface area of the wear scar on the polymer sample were measured using a 3D confocal microscope and using equation following:

$$W_r = \frac{V \ (mm^3)}{F_N(N) \times L(m)} \qquad (10)$$

Where W_r is the wear rate, V is the volume of tribology test, F_N is the normal force, and L is the sliding distance.

3.6.   Conclusion

In this chapter, it successfully fabricated the ABS/PMMA bilayer using various devices adhering to standard testing protocols. The thermal properties of the ABS/PMMA bilayer were evaluated and compared to those of the individual ABS and PMMA layers under controlled temperature conditions. It also investigated the mechanical properties

through tensile tests at different temperatures and two deformation rates, followed by a comprehensive study of viscoelasticity, both in tension and dynamic modes. Additionally, the material's impact resistance was assessed using notched Charpy tests, while durability was evaluated with Shore D and Vickers hardness tests. The three-point bending test was conducted to analyze and compare the structural characteristics of ABS, PMMA, and the ABS/PMMA bilayer. Tribological tests were performed to determine the COF, and finally, fractographic analysis was conducted using scanning electron microscopy (SEM) to further understand the material's behavior under stress.

- 64 -

# Chapter 4.   Results and discussions of ABS/PMMA bilayer polymer

4.1.   Introduction

The previous chapter examined the unique characteristics of polymer materials, with a focus on amorphous thermoplastics such as ABS and PMMA, which are extensively utilized in a range of industrial applications due to their advantageous mechanical and thermal properties. In this study, it conducted experimental tests on an ABS/PMMA bilayer, which was designed to leverage the complementary strengths of these two polymers. The analysis concentrated on assessing the bilayer's thermal stability, mechanical resistance, and tribological behavior. Additionally, a comprehensive fractographic analysis was conducted to examine fracture surfaces, providing valuable insights into the material's failure modes and interfacial bonding between the layers. This chapter presents a detailed analysis of the results obtained from the ABS/PMMA bilayer, offering a deeper understanding of its performance, durability, and potential applications under different operating conditions.

4.2.   Results of Thermal properties

4.2.1. Thermogravimetric analysis (TGA)

Figure 4-1 presents the thermogravimetric analysis (TGA) results showing the ABS layer, ABS/PMMA bilayer, and PMMA layer degradation temperatures. Table 4-1 summarized the obtained degradation temperatures of specimens. These TGA results showed that the thermal degradation of ABS layer was higher than of ABS/PMMA bilayer and PMMA layer, these results are attributed to the increasing PMMA content in the ABS structure [129]. It can be seen from Table 4-1 and Figure 4-1 that the ABS layer has higher decomposition temperature, associated with mass losses of 5% and 50%, than the ABS/PMMA bilayer, indicating that the PMMA layer has low thermal stability. Additionally, as the temperature at which thermal degradation occurs is higher than that of the coextruded polymer bilayer, does not have negative effect on the mechanical properties of the ABS/15%PMMA bilayer structures [129]. Due to acrylonitrile presence in the chemical structure of ABS, which causes the enhancement of thermal stability [69].
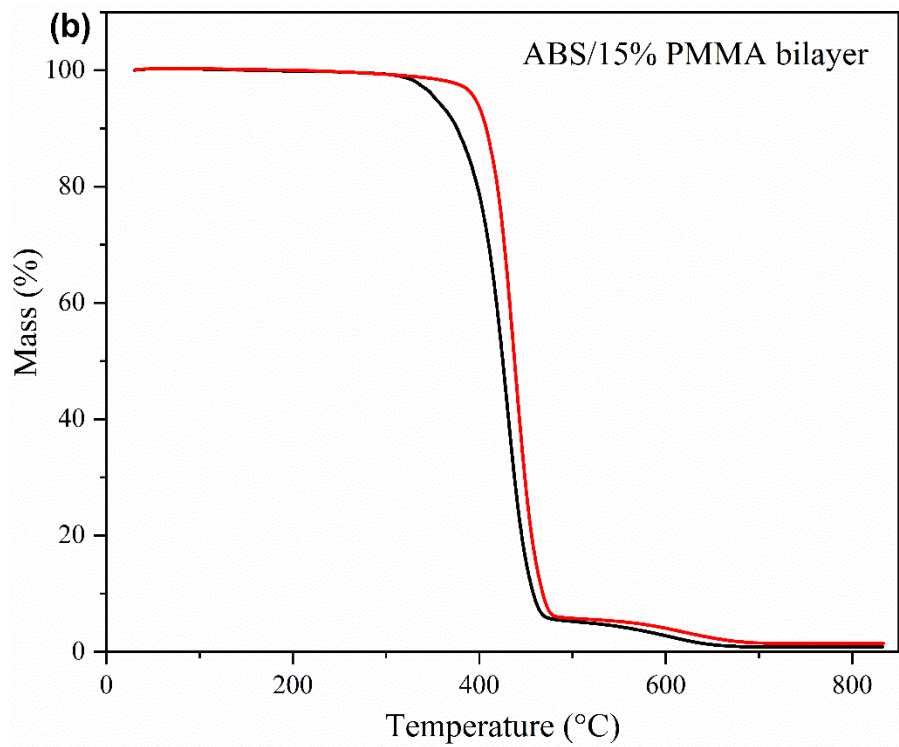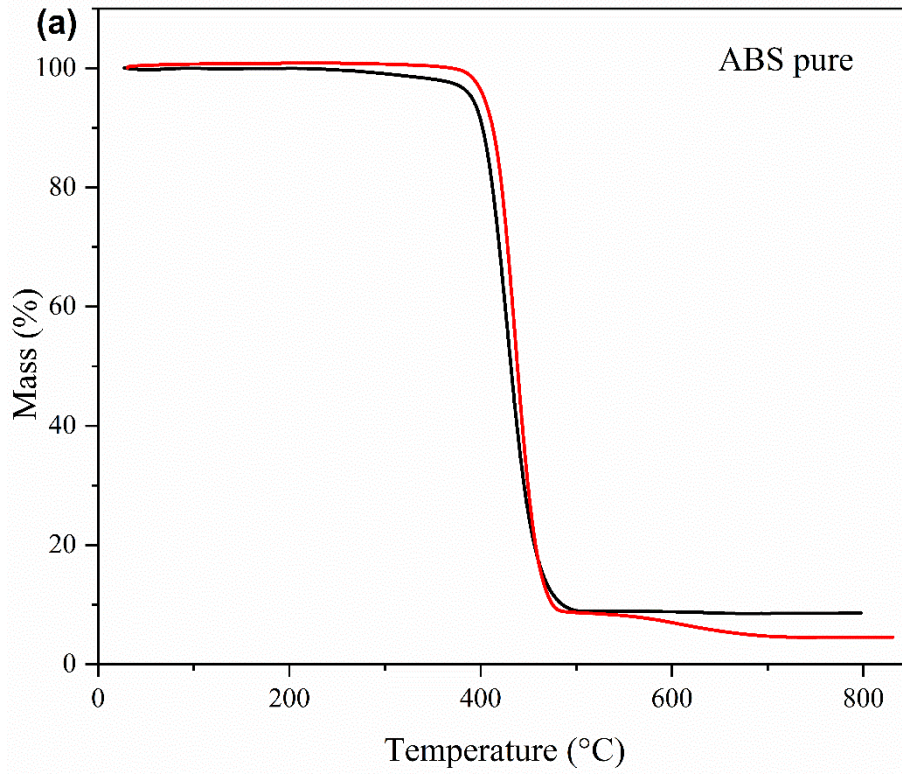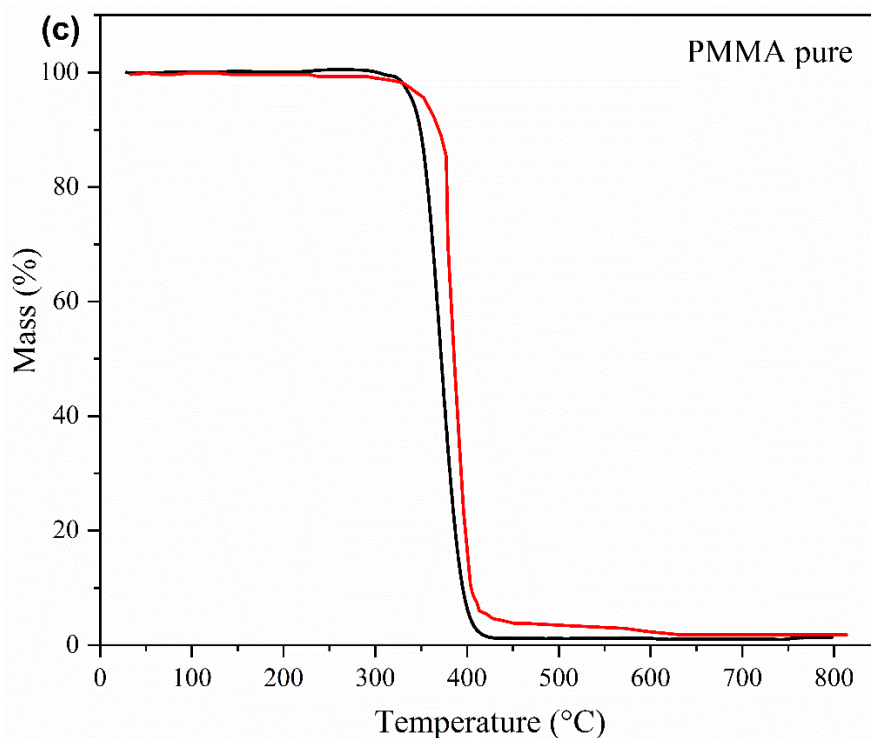
Figure 4-1: Thermogravimetric analysis of amorphous material: (a) ABS pure, (b) ABS/15%PMMA and (c) PMMA pure.

4.2.2. Glass transition temperature (Tg)

The glass transition temperatures of pure PMMA, pure ABS and ABS/PMMA bilayer polymer are shown in Figure 4-2 and Table 4-1. It is clearly shown that the difference between the Tg of the PMMA layer is 112 °C which is slightly higher than that of the ABS layer which is 109 °C. It note that the glass transition temperature Tg of the ABS/PMMA bilayer is 111°C represents the mean of the two glass temperatures of its components. This Tg of the bilayer is close to the Tg of the ABS80 fraction in ABS/PMMA blends, which is 112.2°C [129]. While, the heat flow of the polymer undergoes an endothermic process, whereby it has been observed that ABS melts at approximately 425°C (Figure 4-3 and Table 4-1), while ABS/PMMA melts at 485°C. This indicates that the bilayer exhibits a higher melting temperature. In contrast, PMMA has a lower melting temperature than both ABS and the ABS/PMMA bilayer. It can therefore be concluded that the ABS/PMMA bilayer exhibits a higher melting temperature, potentially due to the combined influence of both ABS and PMMA components.
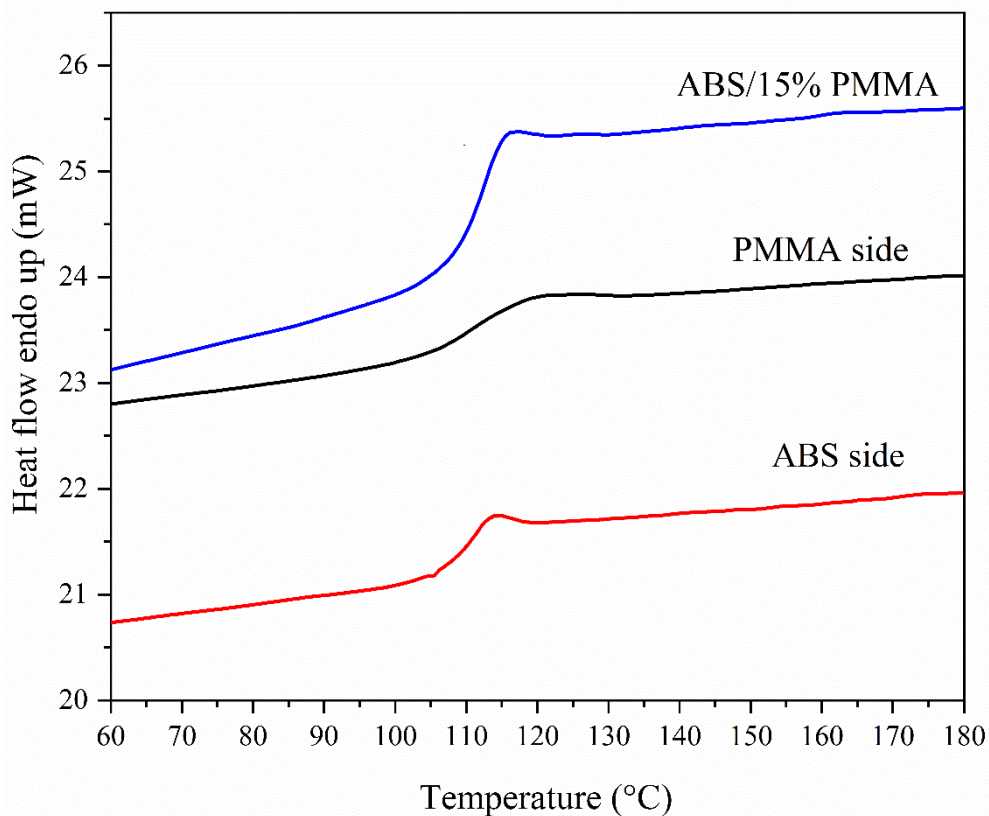
Figure 4-2: DSC of ABS side, PMMA side, and ABS/15%PMMA.
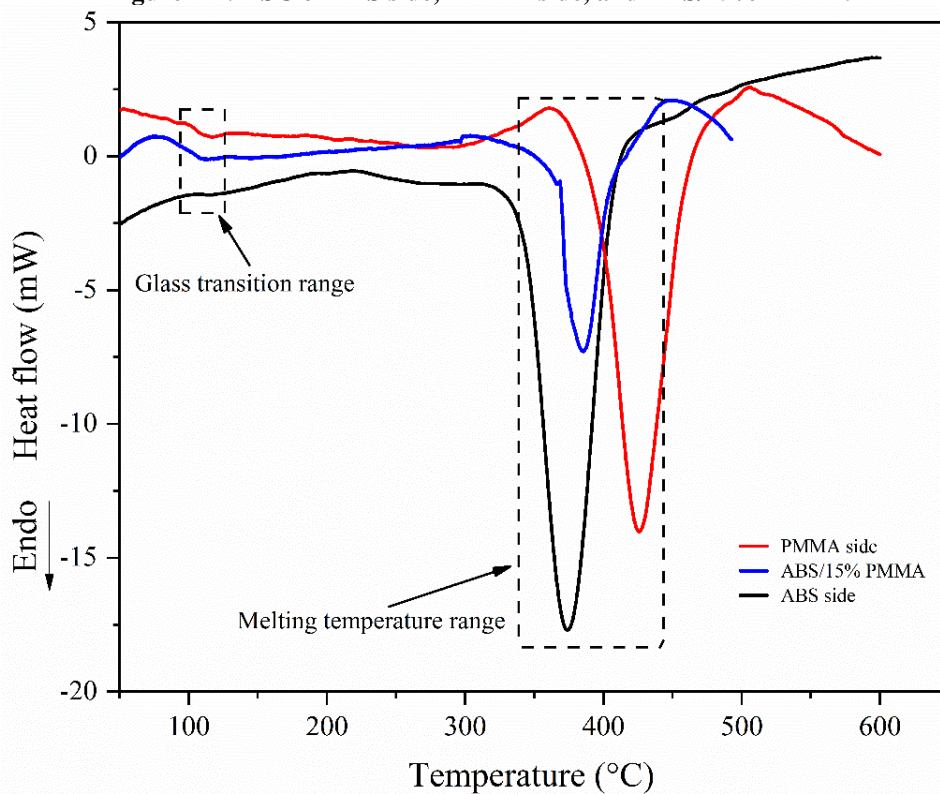
Figure 4-3: Tg range Melting temperature range of ABS/PMMA bilayer, ABS side and PMMA side.

Table 4-1: Obtained thermal properties of ABS layer, ABS/PMMA bilayer and PMMA layer.

Specimen	T_d (˚C) (at 5% mass loss)	T_d (˚C) (at 50% mass loss)	T_g (˚C)	T_m(˚C)
ABS side	403.64	438.43	109.27	425.89
ABS/PMMA bilayer	395.86	437.91	111.09	385.49
PMMA side	353.69	425.28	112.7	375.21

4.3.   Viscoelastic and mechanical behavior results

4.3.1. Dynamic mechanical properties

The mechanical properties, storage, E', and loss modulus, E", obtained via DMA under tension loading in function of temperature are shown in Figure 4-4 and Figure 4-5. For this purpose, these modulus measurements were carried out on a specimen heated at a rate of 3 °C/min and a temperature range of 35–150 °C using two frequencies of 1.5 and 10 Hz. The evolution of the storage modulus versus temperature (Figure 4-4) at the two frequencies is nearly similar and slowly decreases in the glassy state. However, after reaching a certain temperature of 97°C, which is the temperature of glassy state onset, there is a rapid decrease in the storage modulus.
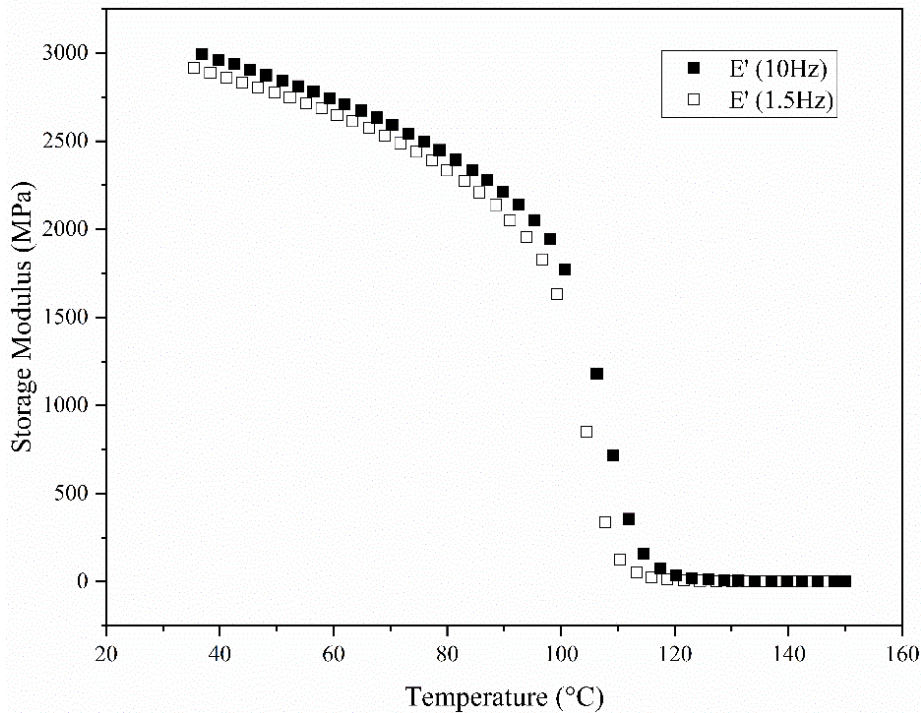
Figure 4-4: Storage modulus of ABS/PMMA bilayer sheet.

As it is presented for the storage modulus, the loss modulus evolution, E'', is shown in Figure 4-5. This loss modulus shows slight variation with temperature before reaching specific peaks within the transition interval. As a function of frequency, there are small differences between the loss modulus values for all used temperatures except in the transition region, where slight differences in modulus peak values and their corresponding temperature were obtained. The loss modulus evolution permits the determination of the glass transition temperature (Tg), which was found included in the range of 100 °C to 110 °C for both used frequencies. The Tg values are similar to those obtained via DSC, which was around of 111°C.
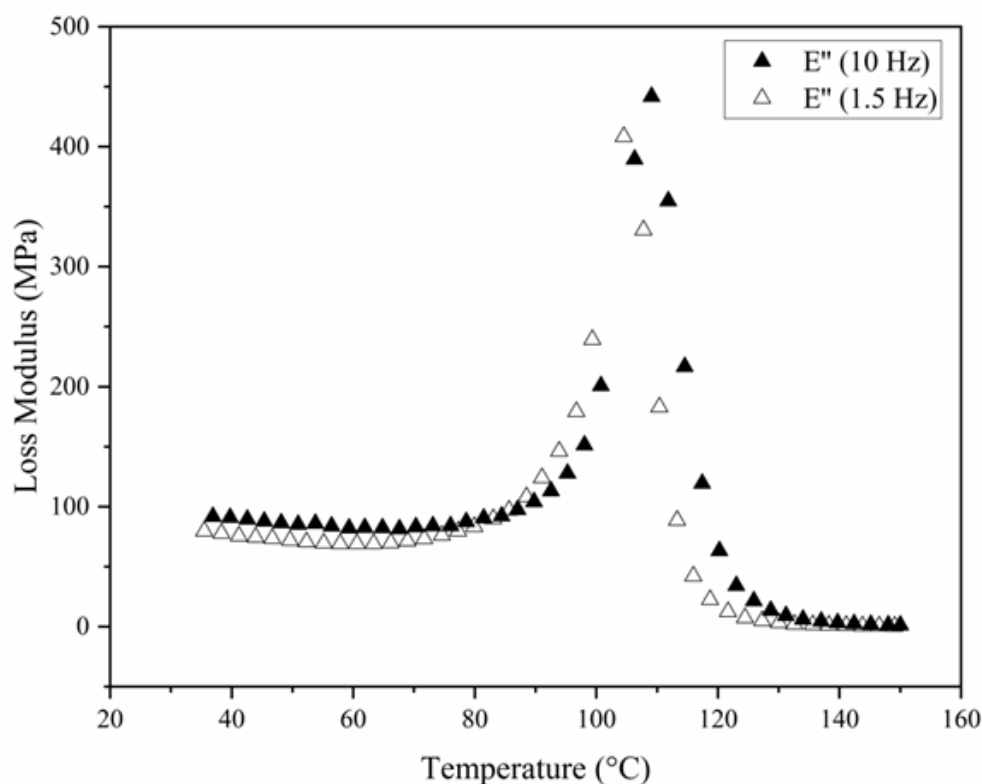
Figure 4-5: Loss modulus of ABS/PMMA bilayer sheet.

However, a slight shift in Tg range variations was observed as a function of frequency (Figure 4-5). As it is well known, the loss modulus, E'', defines the tendency of the material to dissipate mechanical energy as heat dissipation during deformation cycles. This behavior is closely associated with the movement of molecular chains within the material [146].

Figure 4-6 illustrates the evolution of the loss factor, also called damping factor, Tan δ as function of temperature. The loss factor, Tan δ, quantifies the relationship

between the energy dissipated by damping (E'') and the elastic energy retained and then recovered during a sinusoidal deformation cycle (E'), as follow:

$$Tan\ \delta = E''/E' \tag{1}$$

As it is presented in Figure 4-6, this factor evolves constant when the temperature is less than Tg. Beyond this temperature, the damping factor reaches rapidly a peak nearly the same value for both frequencies and equal to 1,7 (60°) for two close temperatures 116 °C and 122 °C for 1,5 Hz and 10 Hz respectively. Comparing the results in Figure 4-4 to Figure 4-6 and in function of the two used frequencies, the material behaves as viscoelastic with an amorphous structure.
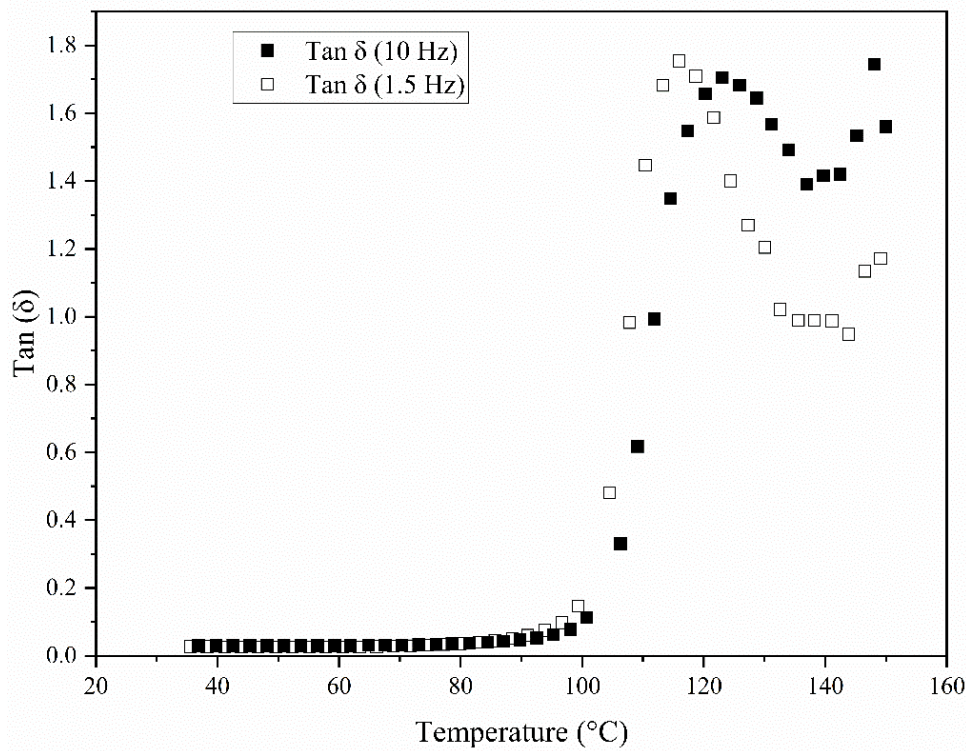
Figure 4-6: Damping factor of ABS/PMMA bilayer sheet.

It is well known that the damping factor determines the viscoelastic ability of materials to dissipate mechanical energy in the form of heat during dynamic loading. A higher tan δ value corresponds to more effective vibration damping, which increases with frequency [147]. High frequencies induce subtle changes in the storage modulus, reflecting the material's ability to store and recover energy and simultaneously intensifying the energy dissipation within the material. Approaching Tg, the increase in

loading frequency slightly reduces the damping factor peak, but an inverse tendency of this factor was obtained with increasing temperature (Figure 4-6).

4.3.2. Tensile tests

Figure 4-7 to Figure 4-10 present the determined mechanical properties using uniaxial tensile tests. Amorphous polymers are known to be sensitive to temperature changes due to the weak intermolecular forces that hold their molecular chains together. In these experimental tests, the tensile strength of ABS/PMMA bilayer was measured at ambient and different temperatures ranging from 23°C to 90°C under glass transition temperature with two different strain rates of $3.33 \times 10^{-4} s^{-1}$ (Figure 4-7.a) and $1.66 \times 10^{-2} s^{-1}$ (Figure 4-7.b). These figures show similar tensile behavior of material in function of temperature. However, a small influence of strain rate on the plastic domain and an increase in yield stress were obtained. The maximal stresses, at 23 °C, were 31 MPa and 41 MPa for strains of $3.33 \times 10^{-4} s^{-1}$ and $1.66 \times 10^{-2} s^{-1}$ respectively. Comparing the two tensile results (Figure 4-7.a and Figure 4-7.b), it is shown that the yield stress decreases with the increasing of temperature, but with the different maximum stress interval between the two limit temperatures 23 °C and 90°C, 11 MPa at $3.33 \times 10^{-4} s^{-1}$ and 19 MPa at $1.66 \times 10^{-2} s^{-1}$.

The tensile properties of ABS/PMMA bilayer are highly affected by temperature due to the viscoelastic nature of this polymer. The nonlinear part of the elastic domain of the stress-strain curve is most affected. Also, strain rate has a major role in mechanical properties. At the higher test rate, the more significant the mechanical properties of the ABS/PMMA bilayer rise. In other words, temperature affects strongly the mechanical behavior.

Figure 4-7 shows the ABS/PMMA samples after fracture. It observe that for the two strain rates, the sheet material exhibits a similar behavior and the same maximal strain, when the temperature of the specimens varies from 23°C to 50°C. While this increases significantly at temperatures of 70°C and 90°C. It can be seen that samples subjected to a strain rate of $1.66 \times 10^{-2} s^{-1}$ break more quickly than those strained at $3.33 \times 10^{-4} s^{-1}$. The fracture of the specimen tested at 90°C does not occur at a rate of $3.33 \times 10^{-4} s^{-1}$. In addition, a curve at the two ends of the fracture section of the specimen when the rate is $1.66 \times 10^{-2} s^{-1}$ for the temperatures: 50°C, 70°C, 90°C (Figure 4-7.b) is observed. While

it does not exist when the rate is $3.33 \times 10^{-4} s^{-1}$ (Figure 4-7.a). This was due to the difference in thermal expansion coefficients.
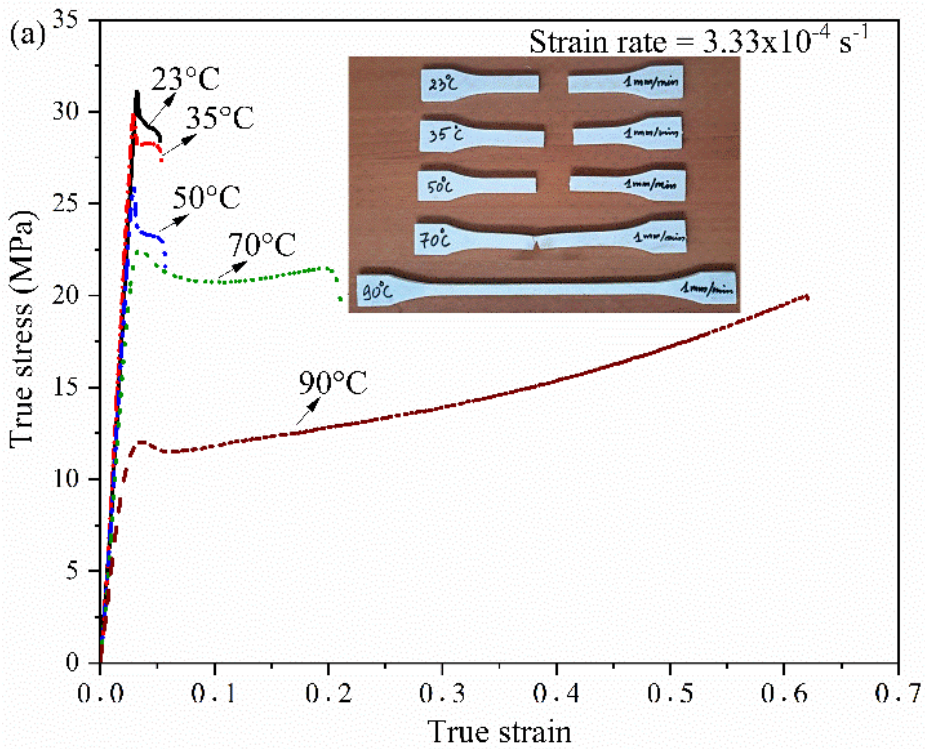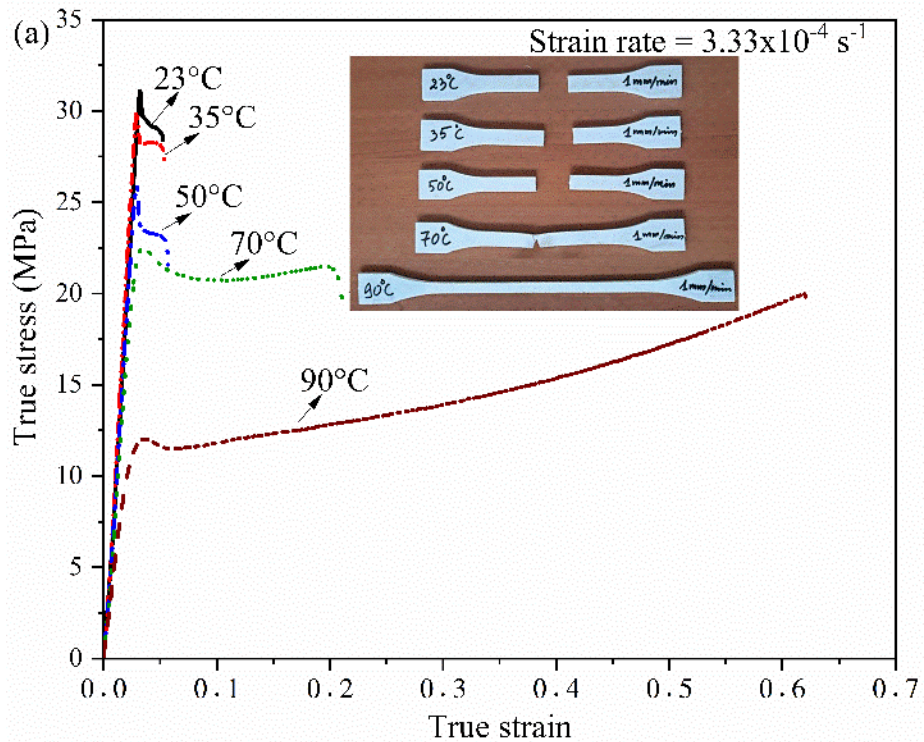
Figure 4-7:True stress–true strain at different temperatures.

For the two rates used, the elastic limit and the ultimate stress decrease with increasing temperature (Figure 4-8). The viscoelastic behavior of the tested material is remarkably observed for the two determined stresses.
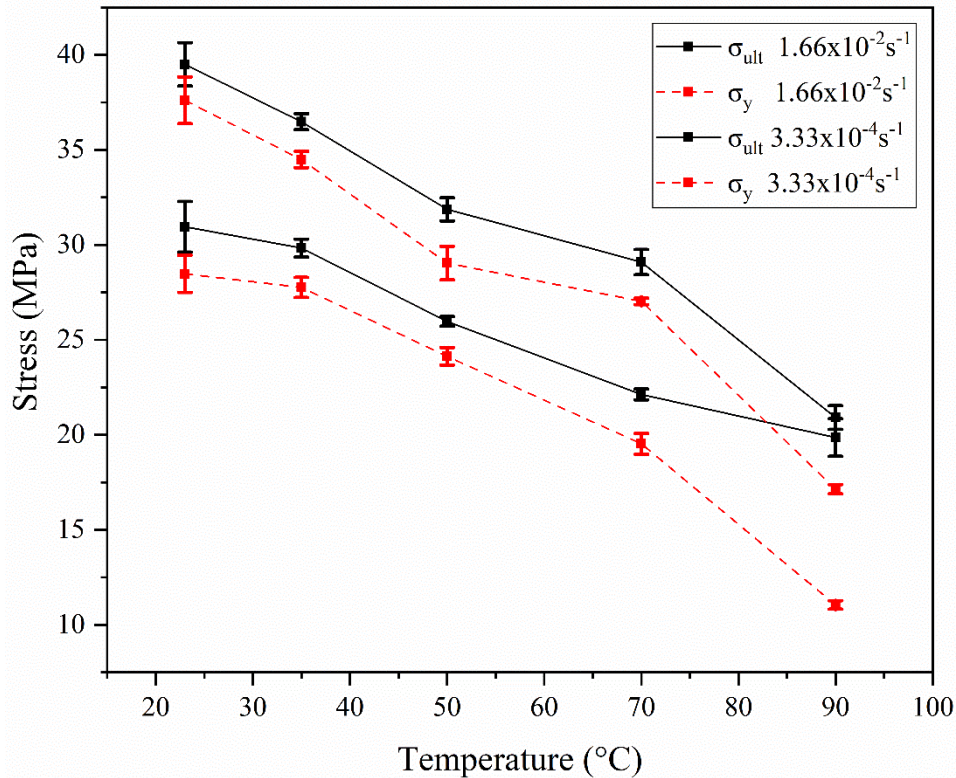
Figure 4-8: Yield stress (σy) and ultimate stress (σult) of ABS/PMMA bilayer vs. temperature and strain rates.

A difference in yield strength between room temperature and maximum temperature, from 23°C to 90°C, was 67%, at a rate of $3.33 \times 10^{-4} s^{-1}$. However, at $1.66 \times 10^{-2} s^{-1}$, this difference was 46%. In addition, the yield strength and ultimate stress obtained at $1.66 \times 10^{-2} s^{-1}$ are higher than those at a rate of $3.33 \times 10^{-4} s^{-1}$. Thus, this viscoelastic behavior is sensitive to the increase in temperature and also to the strain rate.

It observe the progressive degradation of the elastic modulus of the ABS/PMMA bilayer with the increase in test temperatures (Figure 4-9). A drop in the elastic modulus is observed when going from 23°C to 90°C. This is around 74%. Indeed, values of 1872 MPa at 23°C and 579 MPa at 90°C were recorded. This transition from a solid state to a soft state of the ABS/PMMA bilayer with increasing temperature is due to the weakening of intermolecular forces.
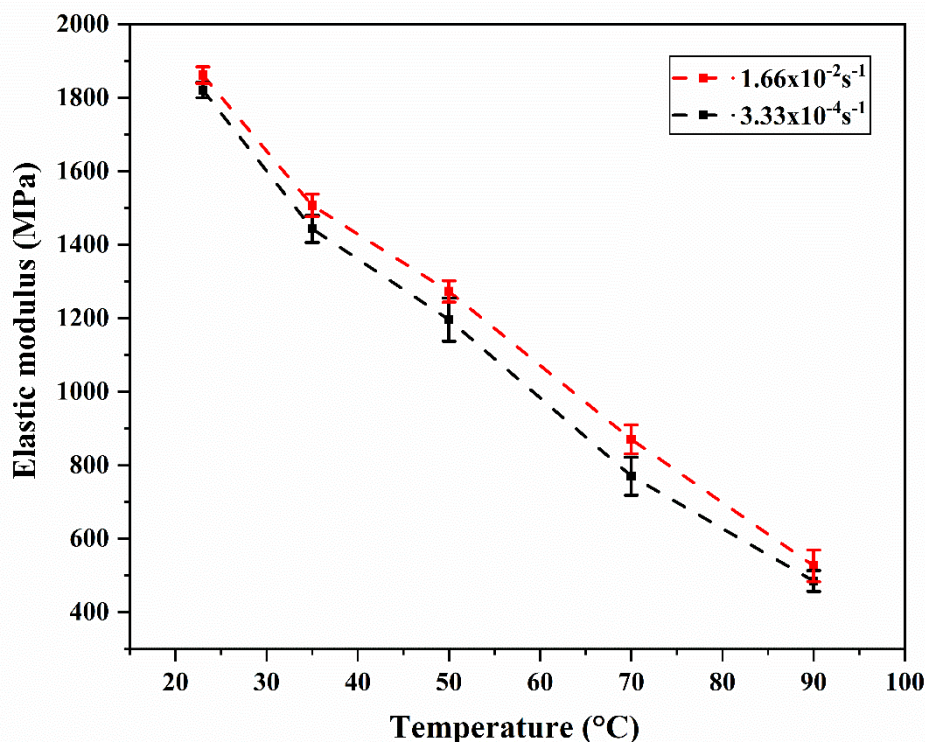
Figure 4-9: Evolution of elastic modulus ABS/PMMA bilayer vs. temperature and strain rates.

However, the elastic modulus of the ABS/PMMA bilayer presents a small variation depending on the two strain rates used at all temperatures. The same observation was made for the two components, PMMA and ABS studied separately [147]–[149]. The bilayer sheet studied contained 15% PMMA and ABS made up the rest. Thus, this invariance and this evolution of the elastic modulus with the strain rate and the temperature can be attributed to the specific mechanical properties of each layer.

The behavior of ABS/PMMA bilayer exhibits a softening response (Figure 4-7) when subjected to varying strain rates and high temperatures. At low strain rate of $3.33 \times 10^{-4} s^{-1}$, this bilayer displays a pronounced softening effect across the used temperature range. With these latter conditions, the softening has a high deformation at break point compared to the one obtained with high strain rate of $1.66 \times 10^{-2} s^{-1}$. Specifically, and under the two strain rates, the studied bilayer shows minimal softening at temperatures ranging from 23°C, to 50°C (Figure 4-10). Beyond 50 °C, a softening behavior with temperatures till 90°C was noticed. Consequently, the temperature plays a dominate parameter influencing the mechanical properties of the ABS/PMMA bilayer. Temperatures beyond 50 °C significantly increase the bilayer ductility, allowing the

material to undergo great plastic deformation without fracturing, especially with low strain rate of $3.33 \times 10^{-4} s^{-1}$.
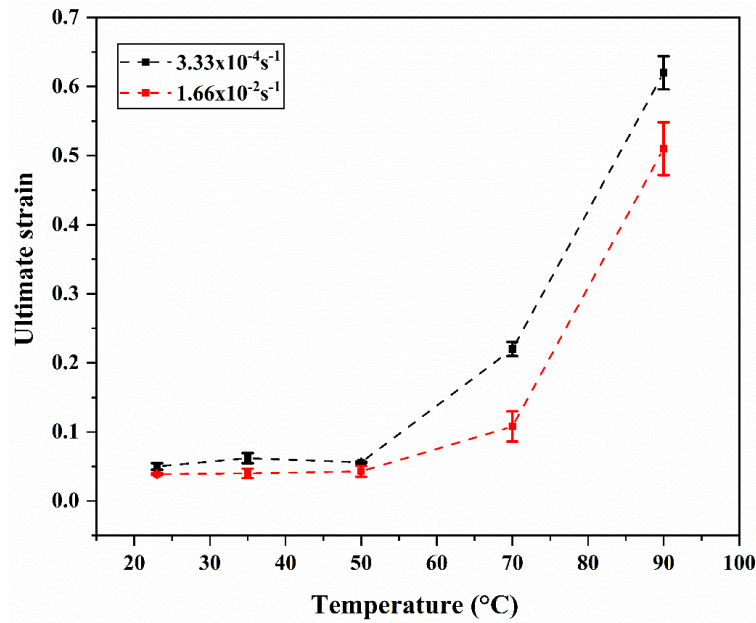
Figure 4-10: Ultimate strain of ABS/PMMA bilayer vs. temperature and strain rate.

The mechanical properties obtained from the experiments are presented in (Figure 4-8 to Figure 4-10), which show the average results as means with corresponding standard deviations, giving a comprehensive overview of the material's performance in different situations (Annex 2). Statistical analyses were carried out using MS Excel (Microsoft), ensuring the accuracy and reliability of our results. A detailed summary of these analyses can be found in Table 4-2 below, which presents key statistical parameters such as p-values and confidence intervals:

Table 4-2: Mechanical properties of ABS/PMMA bilayer at different temperature and strain rate.

Mechanical properties	Yield stress (MPa)		Ultimate stress (MPa)		Elastic modulus (MPa)		Elongation at break	
Strain rate (s⁻¹) Temperature	3.33×10^{-4}	1.66×10^{-2}	3.33×10^{-4}	1.66×10^{-2}	3.33×10^{-4}	1.66×10^{-2}	3.33×10^{-4}	1.66×10^{-2}
23°C	28.48±0.98	37.61±1.23	30.95±1.33	39.50±1.14	1820.79±21	1861.56±22	0.050±0.004	0.039±0.001
35°C	27.76±0.53	34.49±0.43	29.83±0.47	36.48±0.42	1443.41±35	1507.13±30	0.062±0.007	0.041±0.006
50°C	24.13±0.46	29.04±0.88	25.97±0.26	31.87±0.61	1196.25±58	1273.04±29	0.056±0.001	0.043±0.007
70°C	19.53±0.55	27.02±0.17	22.13±0.29	29.09±0.66	775.37±51	870.65±39	0.22±0.010	0.10±0.022
90°C	11.05±0.22	17.14±0.24	19.86±0.99	20.91±0.62	485.33±28	526.40±42	0.62±0.024	0.51±0.038

4.3.2.1. Temperature and strain rates effect on tensile properties of the ABS/PMMA bilayer

The mechanical response of ABS/PMMA bilayer sheet via tensile tests showed an initial elastic reaction, then yielding behavior, followed by strain softening, and ultimately, nonlinear strain hardening as it is also shown in [122]. As noted in this previous article, when polymer glasses were subjected to deformation beyond their yield stress, there was a decrease in stress level referred to as strain softening or yield-drop [119], [150]. Strain softening marks the initiation of strain localization and holds significant importance in regulating the ultimate mechanical characteristics of polymers [61].

At the low strain rate of $3.33 \times 10^{-4} s^{-1}$, the polymer molecules have more time to adjust and reorient, leading to slower molecular expansion and longer fracture times causing more mobility and arrangement of molecule [151], increasing softening behavior of the material. These parameters of strain rate and elevated temperature accelerate the material creep phenomenon. On the other hand, the high strain rate, of $1.66 \times 10^{-2} s^{-1}$, limits molecular reorientation and adjustment processes. This may lead to a more brittle behavior and/or to rapid material fracture, indicating less material flexibility and adaptability under high strain rates (Figure 4-7 and Figure 4-10).

The viscoelastic behavior of ABS/PMMA (Figure 4-11), known as sensitive to the temperature and to the strain rate, is closely linked to its mechanical characteristics. Changes in temperature and strain rate does not only affect the material's viscoelastic properties but also influence its mechanical behavior, leading to variations in stress strength, yield stress, and overall material performance [80].

4.3.2.2. Viscoelastic domain analysis

Figure 4-11 shows the behavior of the ABS/PMMA bilayer at different temperatures at two strain rates ($3.33 \times 10^{-4} s^{-1}$ and $1.66 \times 10^{-2} s^{-1}$) in the elastic zone. At the low rate of $3.33 \times 10^{-4} s^{-1}$ (Figure 4-11.a), the elastic domain of the true stress-true strain curve is linear at temperatures (23°C, 35°C, and 50°C) and weakly linear with increasing temperature (70°C and 90°C).However, at the high strain rate of $1.66 \times 10^{-2} s^{-1}$ (Figure

4-11.b), the true stress-true strain curve presents an elastic domain made up of two parts: one strictly linear and the other non-linear except at temperature ambient (23°C) where the linear part is predominant. At temperatures (35°C, 50°C, 70°C and 90°C), the behavior remains linear from the beginning until the deformation reaches 2% indicated by the inflection point in Figure 4-11.b, and immediately after it becomes nonlinear. Which indicates that the distinct behaviors of the two layers (ABS layer and PMMA layer) are influenced by strain rate ($1.66 \times 10^{-2} s^{-1}$) and temperature. This point of inflection is explained by the fact that the ABS layer deforms more quickly than the PMMA layer under the effect of temperature. As a result, it can remark (Figure 4-11.b) that at temperatures superior to room temperature, there is a linear elastic behavior up to a strain of 2%, beyond which it changes to a viscoelastic response. This behavior becomes more noticeable at high temperatures. This difference in sheets elastic behavior is obtained by the combined action of strain rate and temperature. It is affected by the influence of the ABS-PMMA interface.
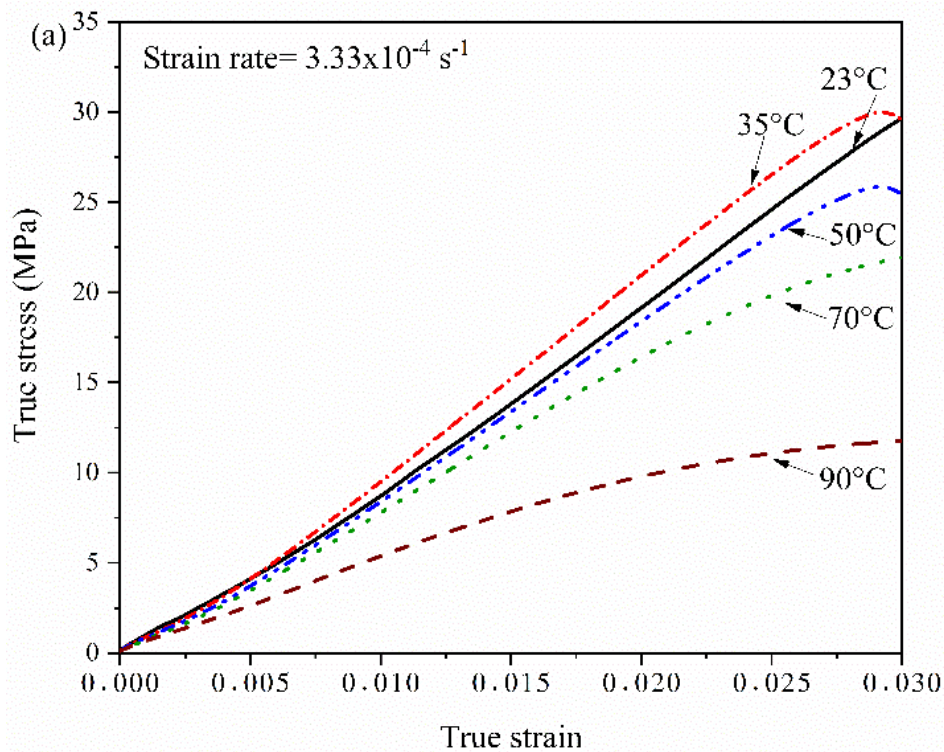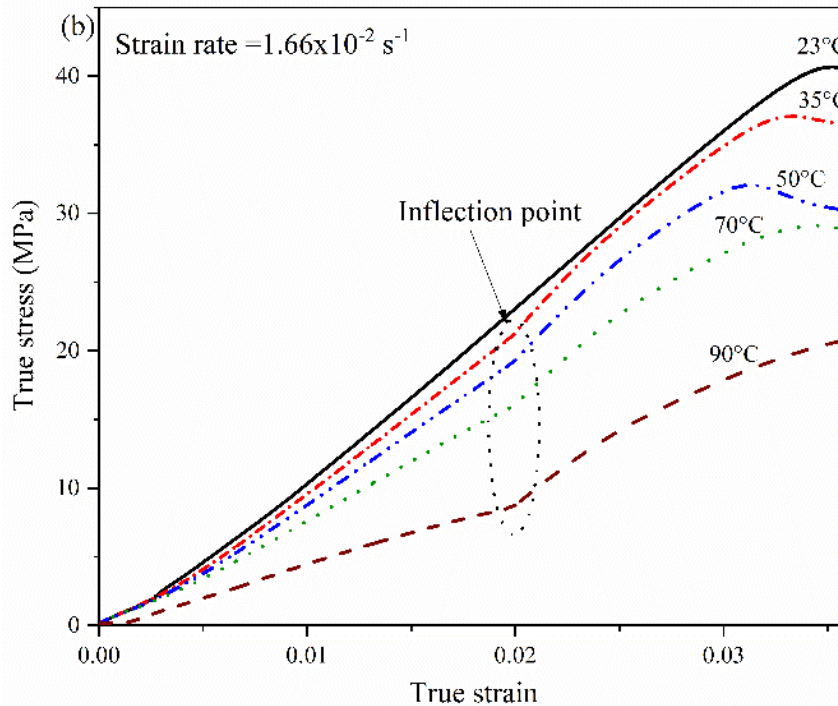
Figure 4-11: Tensile tests of ABS/ PMMA bilayer in the elastic zone with two strain rates: (a) 3.33×10^{-4} s $^{-1}$ and (b) 1.66×10^{-2} s $^{-1}$.

4.3.3. Fractography analysis of ABS/PMMA bilayer polymer
4.3.3.1. SEM images of tensile test

The scanning electron microscopy (SEM) images of the fracture surfaces of the PMMA/ABS bilayer structure after tensile tests, conducted at various temperatures and two strain rates ($3.33x10^{-4}s^{-1}$ and $1.66x10^{-2}s^{-1}$), are presented in Figure 4-12. At 23°C, mirror zones appear on the PMMA layer for both applied strain rates. They are then slightly observed at 35°C for the $3.33x10^{-4}s^{-1}$ strain rate. These mirrors are followed by ribs and spaces between them, extending to the starting line of the ABS layer and fine cracks are visible at the ends of the ABS and PMMA layers. However, at a strain rate of $1.66x10^{-2}s^{-1}$ (for 35°C), mirrors and ribs disappear, and large cracks and crevices appear in the ABS/PMMA structure. In addition, semi-circular blunt zones begin to appear with a limiting radius of 72 µm, propagating towards the edge of the PMMA layer.

At 50°C and a strain rate of $3.33x10^{-4}s^{-1}$, the PMMA layer develops numerous fine cracks that terminate at the interface with the ABS layer. Conversely, at a rate of $1.66x10^{-2}s^{-1}$, there is an increase in blunt zones observed in dark gray on the extreme edge of the

PMMA side. Additionally, significant large cracks and a few fibrils appear in both the ABS and PMMA layers.

At temperatures of 70°C and 90°C, the structural shape of the ABS/PMMA sheet differs from that observed at lower temperatures. The color of the PMMA layer is a darker gray compared to the light gray appearance of ABS. The material becomes softer and more flexible at higher temperatures (70°C and 90°C), resulting in weaker and broader molecular chains. External microcracks ranging from 14 µm to 28 µm appear on the sample, followed by the emergence of blunt zones on the PMMA side. Additionally, fibrils develop along the direction of the molecular chains in the ABS/PMMA structure.

The ABS/PMMA polymer structure changes from a less ductile to a more ductile state due to the ABS content in the ABS/PMMA bilayer. The weight of the polybutadiene phase of the rubber in the ABS content (i.e. the PB of ABS) [130]. It is observed that the mirror zone, the ribs, and the spaces between them appear in a brittle state at low temperatures. These results are consistent with similar findings reported in other studies of PMMA polymers in the literature [80]. The blunt region and fibrils are more visible in the ductile state than in the brittle state, which is consistent with the results obtained at room temperature in the literature [129]. It can be concluded that the blunt area is increased with temperature, resulting in surface microcracks during tensile testing of the ABS/PMMA polymer. These cracks penetrate deeper into the sample, hence the appearance of the blunt region.
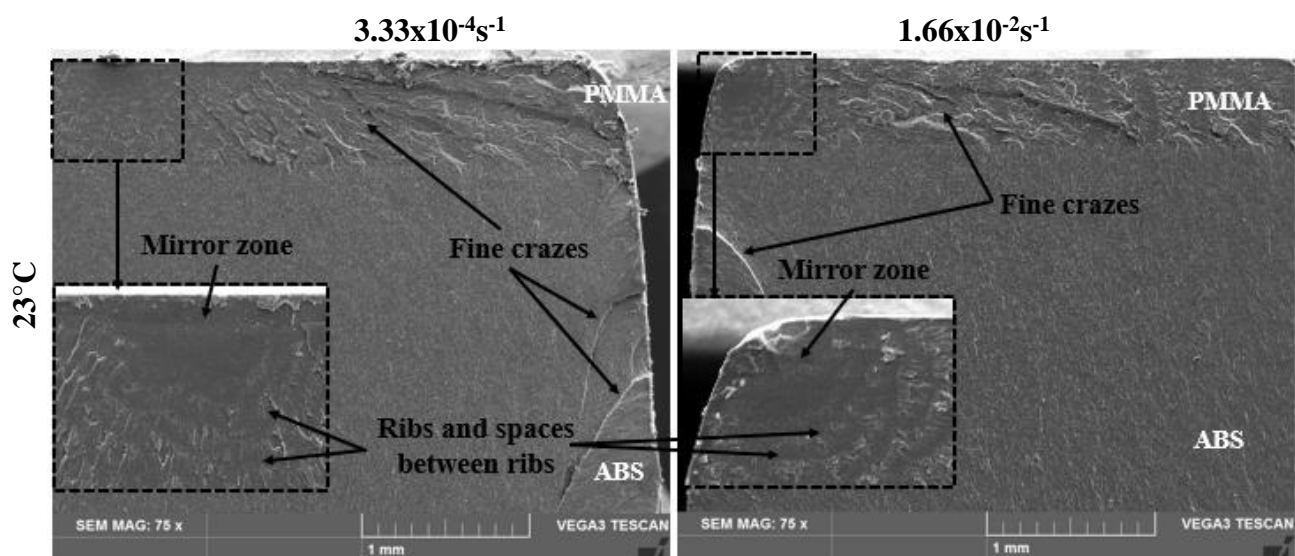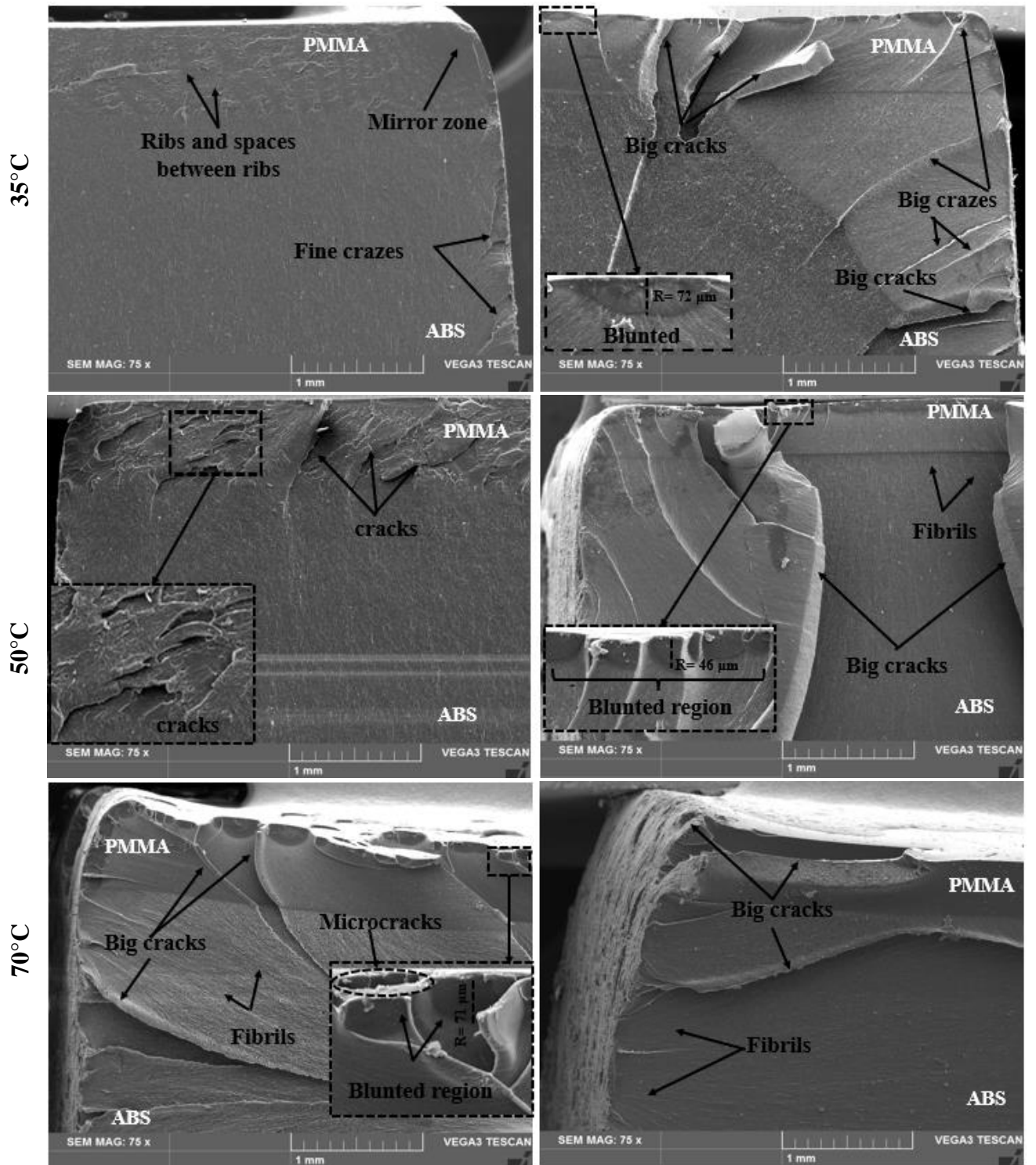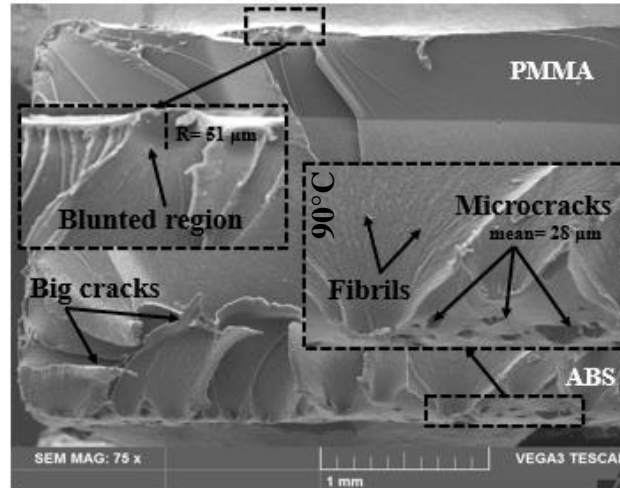
Figure 4-12: SEM image of fractured specimens after tensile test.

4.3.3.2. The effect of strain rate and temperature on ABS/PMMA polymer structure

The fractured surfaces of ABS/PMMA structure specimens are shown at two loading speeds and at different temperatures (23°C, 35°C, 50°C, 70°C and 90°C) (see Figure 4-13 and Figure 4-14). At a strain rate of $3.33 \times 10^{-4} s^{-1}$ (Figure 4-13), a characteristic ductile fracture appearance is clearly displayed. Conversely, at a strain rate of $1.66 \times 10^{-2} s^{-1}$ (Figure 4-14), brittle fracture is apparent, resulting in the initiation of large cracks and extensive fracture propagation across the specimens. However, an increase in temperature induces softening of the ABS/PMMA bilayer structure and elongation of the molecular chain, prolonging the fracture time during the tensile test and making it particularly flexible and thickness-reducing. therefore, it can be said that the ABS/PMMA bilayer structure exhibits an inverse relationship between temperature and strain rate. Higher strain rates lead to brittle fracture, whereas elevated temperatures result in ductile fracture, rendering the polymer more flexible and superplastic.
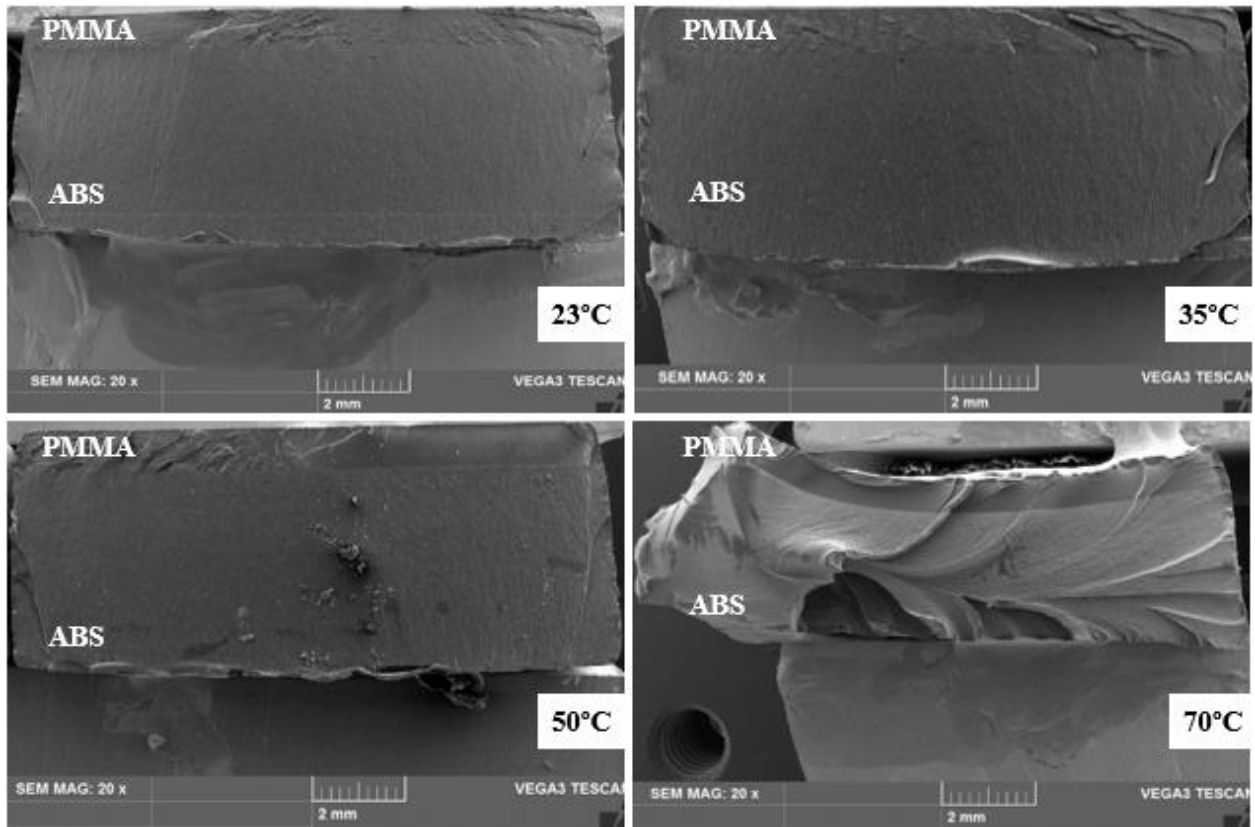
Figure 4-13: SEM image of ABS/PMMA structure after tensile test at a strain rate of 3.33×10^{-4} s^{-1}.
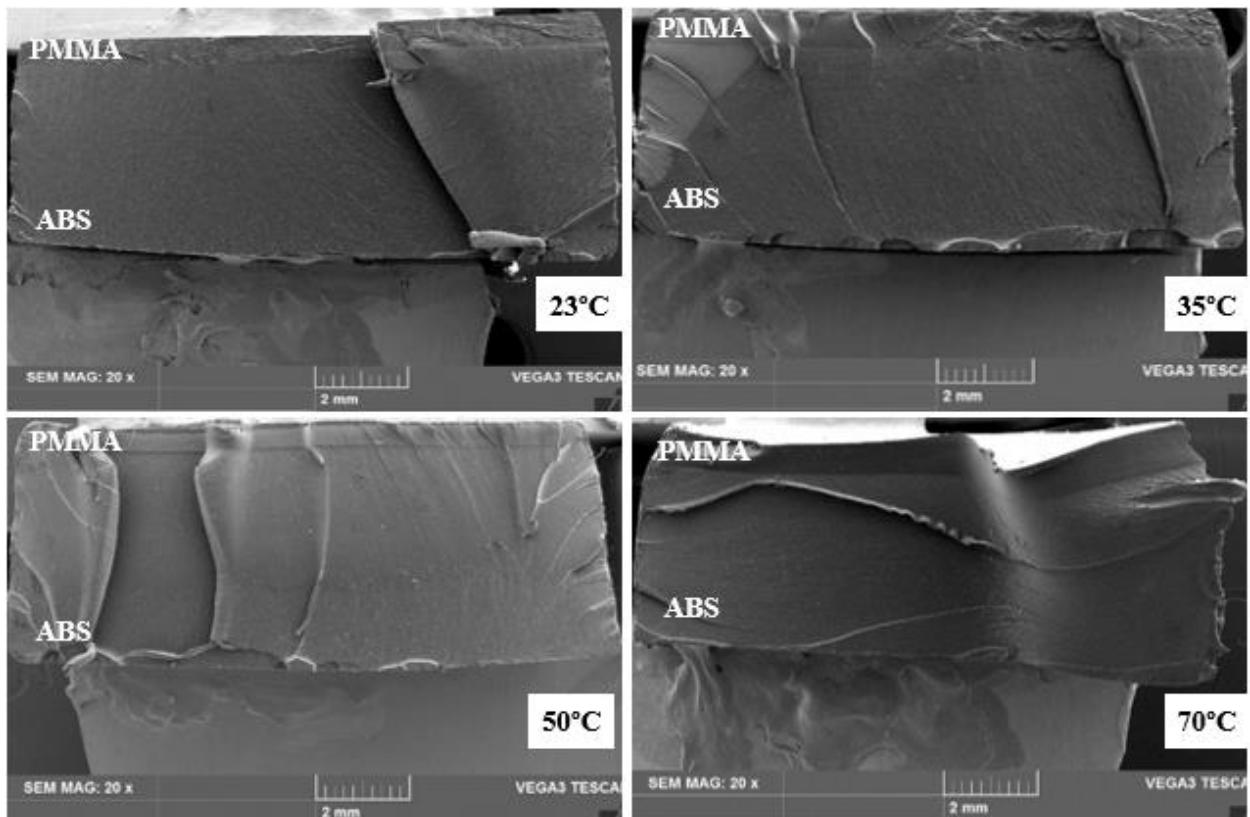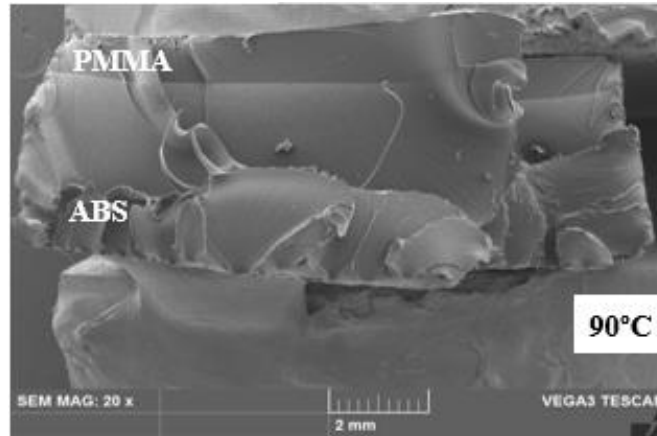
Figure 4-14: SEM image of ABS/PMMA structure after tensile test at a strain rate of 1.66x10^{-2}s^{-1}.

Figure 4-15 presents an enlarged view of the contact line between the PMMA and ABS layers at varying temperatures. This indicates that the molecular chains of PMMA (resembling scarp formation) are marginally larger than those of the ABS layer. These molecules remain stable at temperatures below 23°C and above 35°C. As the temperature increases from 50°C to 90°C, the molecular chain structure of ABS and PMMA transforms, taking on a resemblance to molecular fibrils with micro-voids. The layer cohesion, resulting from the coextrusion manufacturing method, permits the two polymers to fuse intimately, thereby creating molecular chains that combine and become tightly bonded. This results in enhanced molecular compatibility at the interface during coextrusion, which can be of significant importance in maintaining adhesion between ABS and PMMA layers. Despite exposure to elevated temperatures and high loading speeds on the polymer sheet, the adhesion is maintained due to the convergence of their thermal properties. This serves to reinforce the necessity of considering the specific material properties and manufacturing techniques involved when designing composite materials.
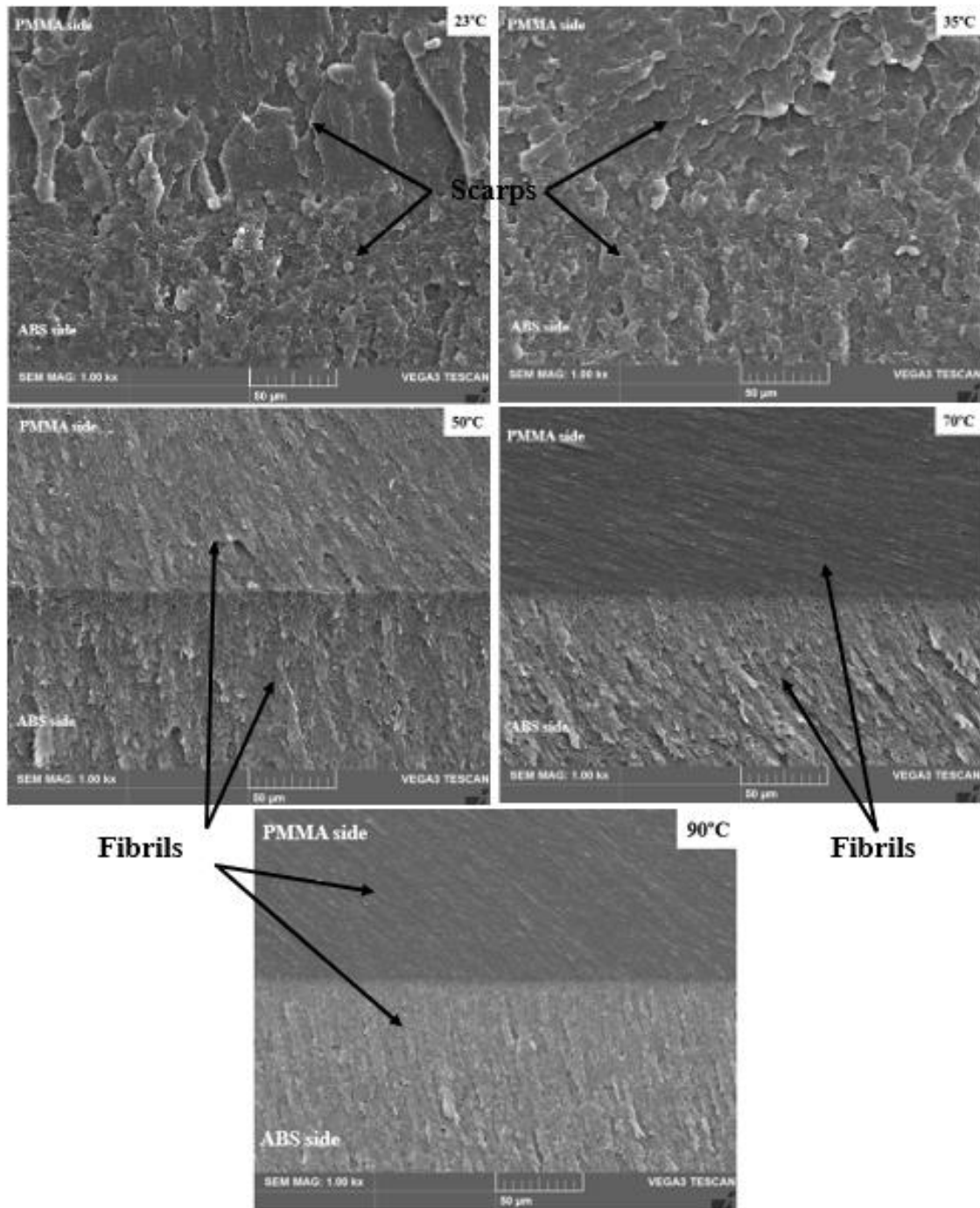
Figure 4-15: SEM image of ABS/PMMA bilayer structure polymer at different temperatures.

4.3.4. Three-point bending tests

Figure 4-16 illustrates the stress-strain curves depicting the three-point bending behavior of various polymers, including PMMA, ABS, and the ABS/PMMA bilayer. PMMA demonstrates high strength and exhibits brittle fracture behavior at room temperature, characterized by minimal deformation after yielding (Figure 4-16.a). In

contrast, ABS displays a weaker performance compared to PMMA but shows a significantly higher elongation at break (Figure 4-16.b), indicative of its ductile nature.

The ABS/PMMA bilayer combines the properties of its constituent polymers, exhibiting stress levels close to those of PMMA while maintaining strain levels similar to those of ABS. This unique combination results in a material that balances strength and flexibility (Figure 4-16.c). The enhanced ductility observed in ABS and the ABS/PMMA bilayer is attributed to the presence of butadiene in the ABS polymer matrix. Butadiene acts as a rubbery component, imparting significant flexibility to both pure ABS and the ABS/PMMA bilayer. This characteristic makes the bilayer particularly suitable for applications requiring a balance of strength and ductility.
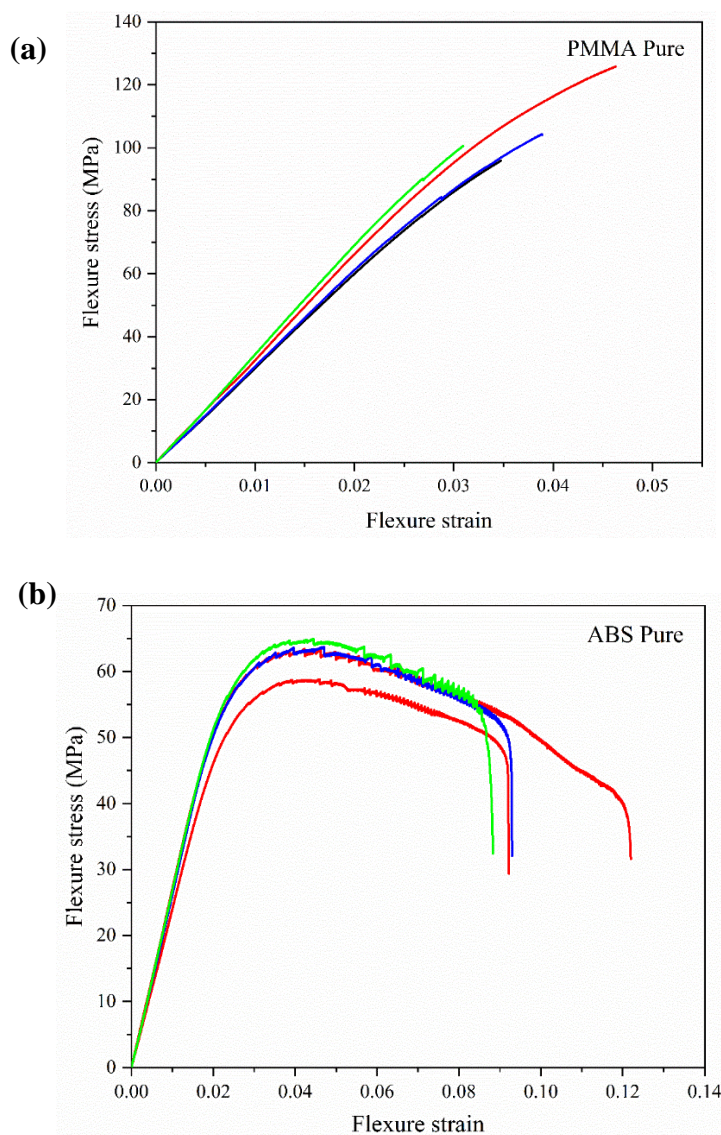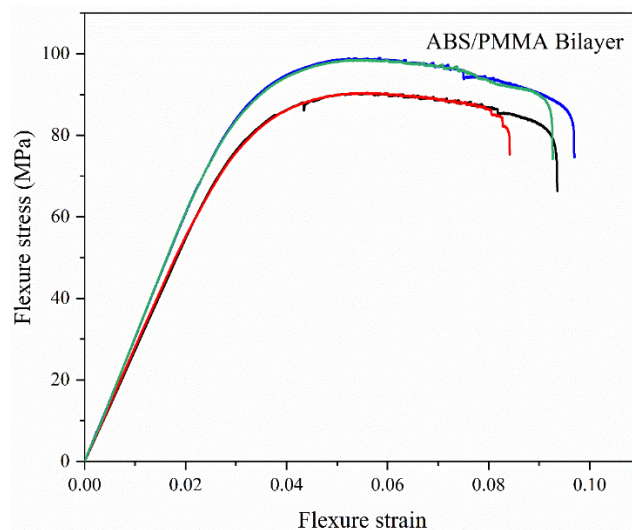
Figure 4-16: Flexure stress - flexure strain curves of three-point bending tests of polymers; a) PMMA, b) ABS, and c) ABS/PMMA bilayer.

Table 4-3 provides a comprehensive summary of the flexural properties of the three polymers, including PMMA, ABS, and ABS/PMMA bilayer. The table details the bending stress, bending strain, and bending modulus for each material. These properties were determined using standard deviation calculations to ensure the reliability and accuracy of the results. Statistical analyses were carried out using Microsoft Office tools, facilitating accurate data handling and analysis. Comparison of these flexural properties highlights the distinct mechanical behaviors of the polymers, emphasizing the high strength and brittleness of PMMA, the ductility of ABS, and the balanced performance of the ABS/PMMA bilayer. These detailed data are essential for understanding the suitability of these materials for various technical applications.

Table 4-3: Flexural properties of ABS, PMMA, ABS/PMMA bilayer.

Material	Flexure stress (MPa)	Flexure strain	Flexure modulus (MPa)
PMMA pure	106.65 ±13.20	0.038± 0.0058	3187.38±231.70
ABS pure	62.59±4.70	0.089± 0.051	2543.63±265.98
ABS/PMMA bilayer	94.54±4.81	0.091± 0.0054	2908.37±188.34

4.3.5. Impact Strength

The results of notched impact tests carried out on ABS/PMMA bilayer samples are shown in Figure 4-17 The impact strength of the bilayer at room temperature (25 KJ/m²) is comparable to that of pure ABS, as reported by several researchers [92], [152].

Notably, impact strength shows an upward trend with increasing temperature, indicating an improvement in polymer ductility. This increased ductility of the ABS/PMMA bilayer is mainly attributed to the high proportion of ABS in the bilayer, which takes advantage of the high impact strength of the ABS polymer. These results suggest that the ABS/PMMA bilayer retains the beneficial properties of ABS while potentially offering additional benefits in applications requiring both high-impact resistance and flexibility at different temperatures.
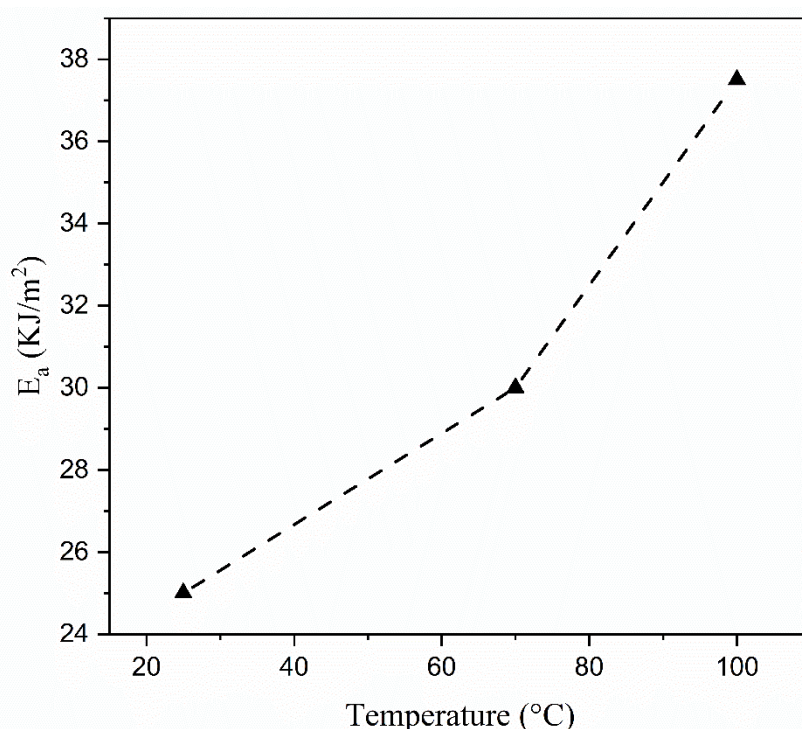
Figure 4-17: Energy absorption at different temperatures.

4.3.5.1. SEM images of impact test

Fractography analyses were conducted on the ABS/PMMA bilayer using the Izod impact test at different temperatures (23°C, 70°C, and 100°C), as illustrated in Figure 4-18 to Figure 4-20. Examination of the SEM surfaces of the ABS/PMMA structure at room temperature reveals a ductile fracture pattern, with an impact strength of 25 kJ/m^2. The ABS layer exhibits fibrils terminating in wave formations, with the number of waves increasing and converging towards the end of the specimen fracture. The PMMA layer displays crazes following the initial cracking, intensifying towards the end of the sample, leading to less ductile fracture. At 70°C, the material becomes more shock-absorbing,

with an impact of 30.5 kJ/m^2, and there's a reduction in cracking and crazing in the PMMA layer, accompanied by the disappearance of waves in the ABS layer. Features such as cusps and microcracks in the pre-fatigue flow also diminish. In particular, a small parabolic cavitation is observed (Figure 4-19), centered around the 30 µm well with an elliptical particle. At 100°C, the ABS/PMMA polymer becomes rubber-like, effectively absorbing shock increases of 37.5KJ/m^2. The PMMA layer structure shows complete fracture and remains largely unchanged from lower temperatures, showing no cracks or crazing. Conversely, the ABS structure displays distinct zones, including parabolic cavities distributed more widely between 40-110 µm on the ABS layer surface, most of these cavities are located inside the ribs. These Ribs and spaces between ribs originate from the specimen's center and conclude in hackles and striations, leading to ductile rupture in the ABS layer's end. Furthermore, no rupture was observed at the end of the ABS layer, indicated by the ellipse zone, which extends to the beginning of the PMMA layer that has undergone complete fracture. This suggests that the ABS layer has reached a high level of performance and toughness.

The ABS/PMMA bilayer structure exhibited ductile fracture (25 KJ/m^2) upon impact at room temperature (23°C). However, as the temperature increased to 100°C, the impact strength reached (37.5 KJ/m^2), and this ductile fracture transitioned into a ductile and super-plastique (rubber) fracture, inducing a shift in the polymer's behavior. This resulted in distinctive behaviors observed in both the ABS and PMMA layers during the impact test. Remarkably, the PMMA layer showed minimal response to the impact test, in contrast to the ABS layer, which displayed strength, toughness, and shock absorption, particularly with increasing temperatures. The layer avoided complete failure (refer to Figure 4-20), and the small particles in the cavities can be attributed to the presence of butadiene, serving as a rubbery (i.e. Poly Butadiene of ABS) curing agent established in the reactor [92], [130].
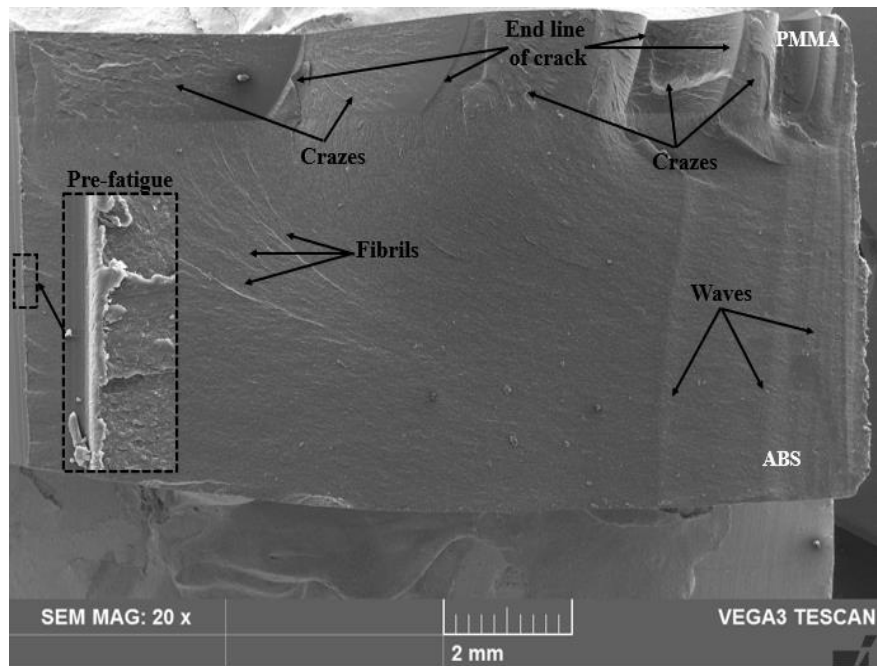
Figure 4-18: SEM image of ABS/PMMA structure after notched Izod impact at 23°C.
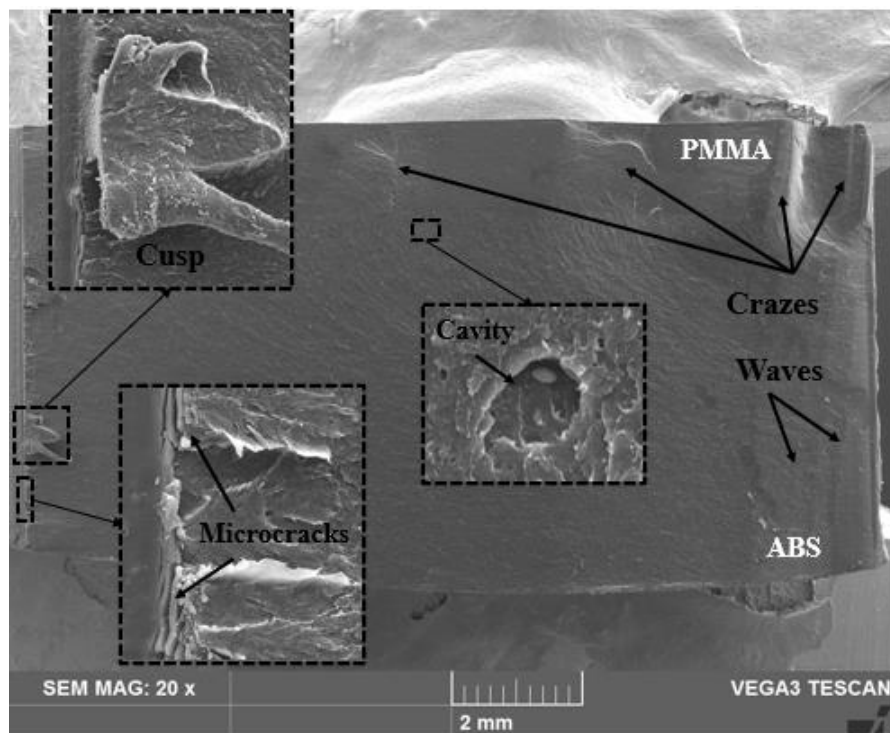
Figure 4-19: SEM image of ABS/PMMA structure after notched Izod impact at 70°C.
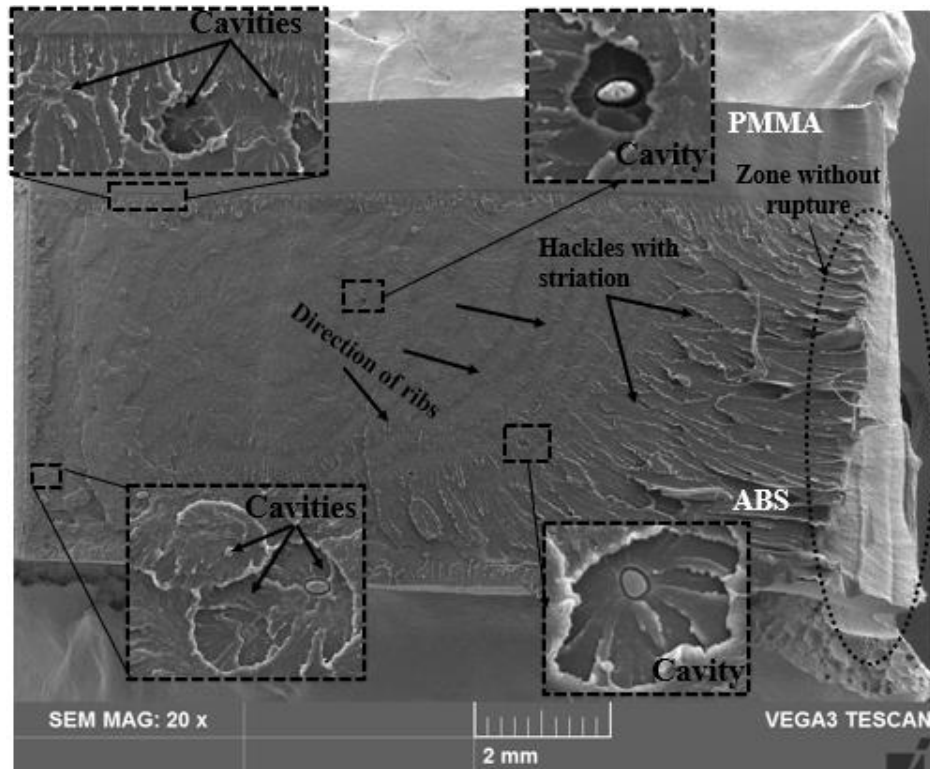
Figure 4-20: SEM image of ABS/PMMA structure after notched Izod impact at 100°C.

4.4.   Hardness and tribology of ABS/PMMA bilayer sheet

4.4.1. Hardness results
4.4.1.1.   Shore Hardness

Shore D hardness was measured for four commercial polymers: ABS/PMMA bilayer, ABS/PMMA blend, pure ABS and pure PMMA, in accordance with ISO standards 868/7619. The results, presented in Table 4-4, reveal distinct hardness characteristics for each material. The hardness of the ABS side of the ABS/PMMA bilayer corresponds to that of pure ABS, while the PMMA side has a hardness identical to that of pure PMMA. In the case of the ABS/PMMA blend, the hardness value lies between those of ABS and PMMA, reflecting a balanced combination of the properties of the two materials. It is particularly interesting to note that the PMMA layer has a higher hardness than the ABS layer, underlining PMMA's greater resistance to surface deformation. These results underline the distinct mechanical characteristics of each polymer, and provide valuable insights for applications requiring specific levels of hardness and material performance.

Table 4-4: Shore D hardness properties of ABS/PMMA bilayer, ABS/PMMA blend, pure ABS and pure PMMA.

Specimens		Shore Hardness (type D)
ABS/PMMA bilayer	ABS side	76±1
	PMMA side	85±2
ABS/PMMA blend (80/20)		81±0
Pure ABS		74±1
Pure PMMA		88±1

4.4.1.2. Vickers microhardness

The microhardness results for the ABS and PMMA layers in this polymer bilayer reveal significant differences in the hardness of these materials. Figure 4-21 illustrates the microhardness distribution under different loadings in the ABS layer and the PMMA layer, showing different diagonal lengths as a function of the delayed time ratio (observation time/dwell time) for four loading levels: 10 g, 25 g, 50 g, 100 g and 300 g.
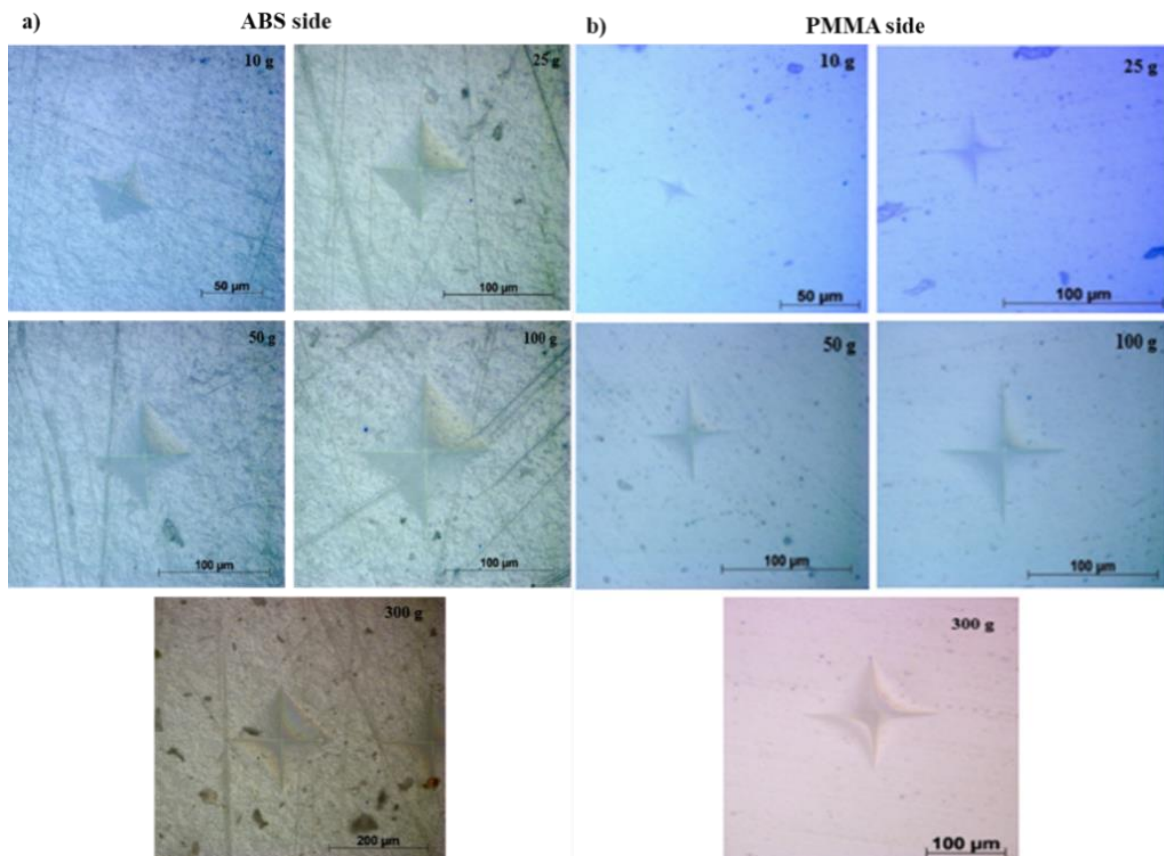
Figure 4-21: Optical microscope images of 10 g, 25 g, 50 g, 100 g, and 300 g indents: (a) ABS side and b) PMMA side

Microscopic images show variable diagonal indentations from the hardness test, indicating that ABS is softer and more ductile in nature, which may contribute to its ability to absorb energy and deform plastically under stress. In contrast, PMMA is characterized as brittle and hard, prone to fracturing in similar situations, making it less suitable for applications requiring high-impact resistance.

The analysis of microhardness and diagonal length data presented in Figure 4-22.a and Figure 4-22.b reveal**s** significant insights into the performance of ABS and PMMA under varying loads. For ABS, hardness values increased by 58% (from 64 MPa to 110 MPa) as the applied load increased from 10g to 50g. Beyond this point, the hardness of ABS stabilized despite further load increases, remaining consistent between 50g and 300g. In contrast, the hardness of PMMA exhibited greater variability. At an initial load of 10g, PMMA demonstrated a high hardness value of 173 MPa, which decreased to 160 MPa at 25g. Subsequently, PMMA's hardness increased again to 170 MPa at 300g. This indicates that PMMA is generally harder than ABS, but its hardness shows less stability across different loads compared to ABS. Additionally, the diagonal length of these polymers increased with the applied force. Notably, the diagonal length of ABS was consistently higher than that of PMMA under the same loads. This observation supports the conclusion that PMMA is harder than ABS, as the greater diagonal length of ABS under identical conditions suggests that PMMA resists deformation more effectively.
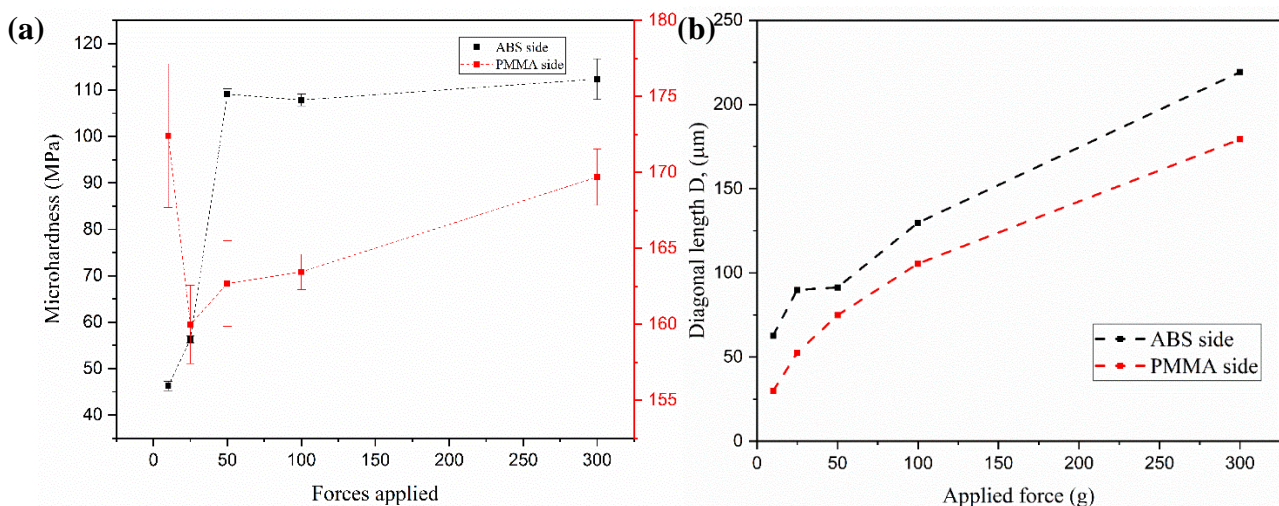
Figure 4-22: Microhardness Vickers results: a) the hardness of ABS side and PMMA side *vs*. load applied, b) the diagonal length effect of ABS side and PMMA side under different loads.

4.4.1.3. The comparison between shore hardness and Vickers microhardness of polymers

The two hardness tests, Shore D and Vickers are complementary in that they offer different perspectives on the mechanical properties of ABS/PMMA materials. While the Shore D test provides a general overview of surface hardness, the Vickers test offers a more detailed insight into how these materials respond to varying forces. The collective data indicate that PMMA is typically harder and more brittle, whereas ABS is softer, more ductile, and better suited to absorb impact. These differences are of paramount importance when considering the application of ABS/PMMA bilayers in a variety of industries, as the selection of material will depend on the specific mechanical demands of the final product. The Shore D method is an accurate and effective means of assessing surface properties, rendering it suitable for quality control and applications where surface characteristics are of paramount importance. In contrast, the Vickers method provides a more precise and comprehensive understanding of the material's hardness and its response to different stresses. This makes it the preferred method for research and applications that require detailed material characterization.

In summary, the Shore D method is precise for surface-level assessments, while the Vickers method provides a more comprehensive analysis of the material's mechanical behavior. Combining both methods offers a well-rounded view of the material's hardness and overall performance.

4.4.2. Coefficient of friction and wear of ABS/PMMA bilayer sheet

Figure 4-23 illustrates the COF as measured on both sides of the ABS/PMMA bilayer sheet. The data demonstrate that the frictional characteristics attained a stable equilibrium during the tribological evaluation, thereby providing a clear representation of the material's behavior under consistent testing conditions.

As can be seen from the friction results in Figure 4-23 illustrates that an increase in load applied to ABS and PMMA surfaces is accompanied by a corresponding increase in the COF. In particular, the ABS/PMMA bilayer shows a greater increase, indicating that the composite structure of the bilayer amplifies the friction response under high loads.

Additionally, the COF on the ABS surface is higher than on the PMMA surface, suggesting that ABS contributes more to the friction resistance in the bilayer than PMMA. These observations highlight the impact of bilayer material interaction on overall friction performance.
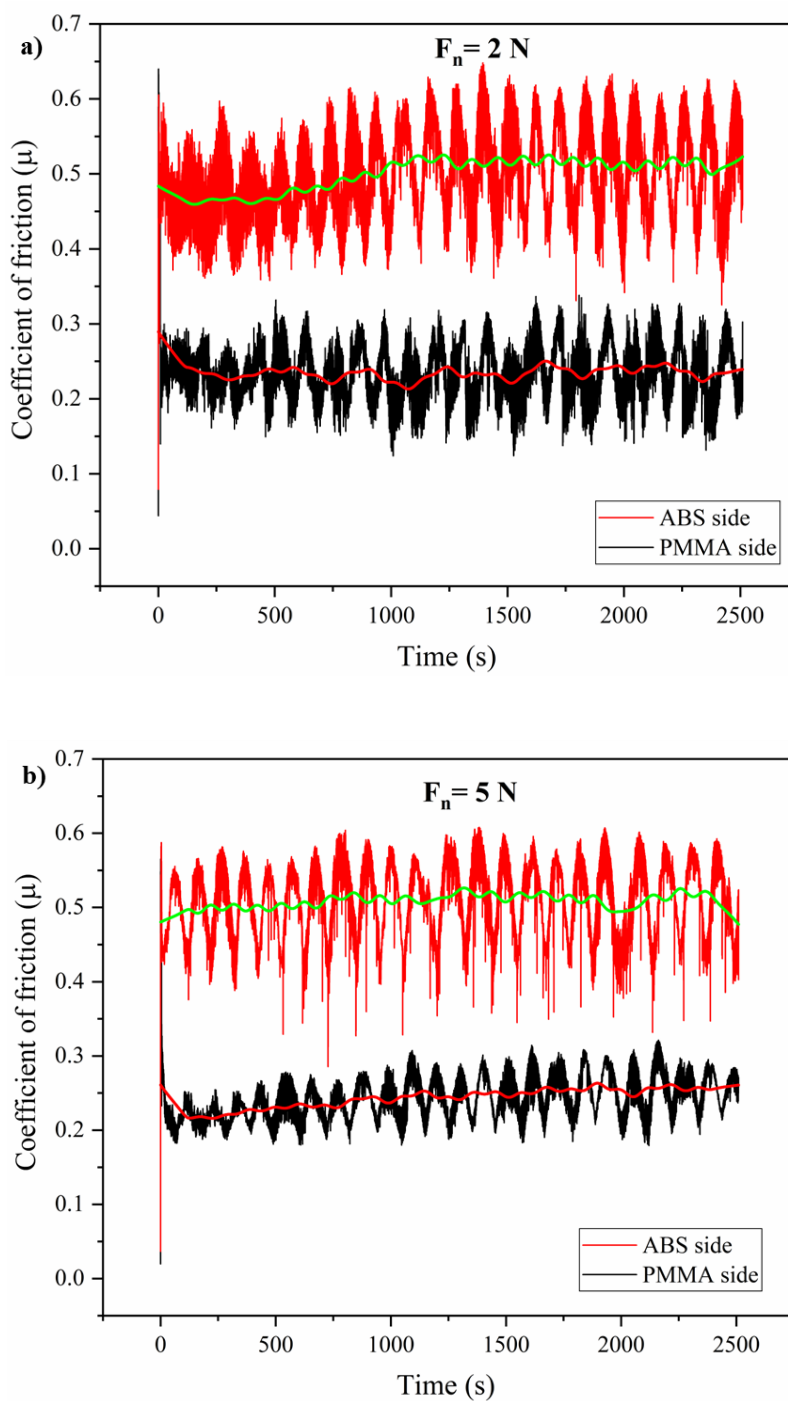
Figure 4-23: Coefficient of friction at different load for ABS/PMMA bilayer (both side ABS and PMMA)/Alumina: a) 2 N and b) 5 N.

Figure 4-24 and Figure 4-25 show 3D wear scars on ABS and PMMA surfaces, revealing a notable difference in wear volume. The PMMA wear scar is approximately six times deeper than that of ABS under a 2N load and four times deeper under a 5N load. In addition, the PMMA wear scar is approximately three times wider than the ABS scar at 2N and half as wide at 5N. This significant difference in wear depth and width suggests that PMMA, being harder and more brittle, tends to exhibit more pronounced wear under applied loads than ABS. The wider and deeper wear scars on PMMA indicate that it is less resistant to wear and deformation, reinforcing the brittleness of the material and highlighting its susceptibility to surface damage under higher loads. Conversely, the deeper, narrower wear scars on ABS reflect its more ductile nature Figure 4-24, which contributes to better resistance to wear and deformation in similar situations.
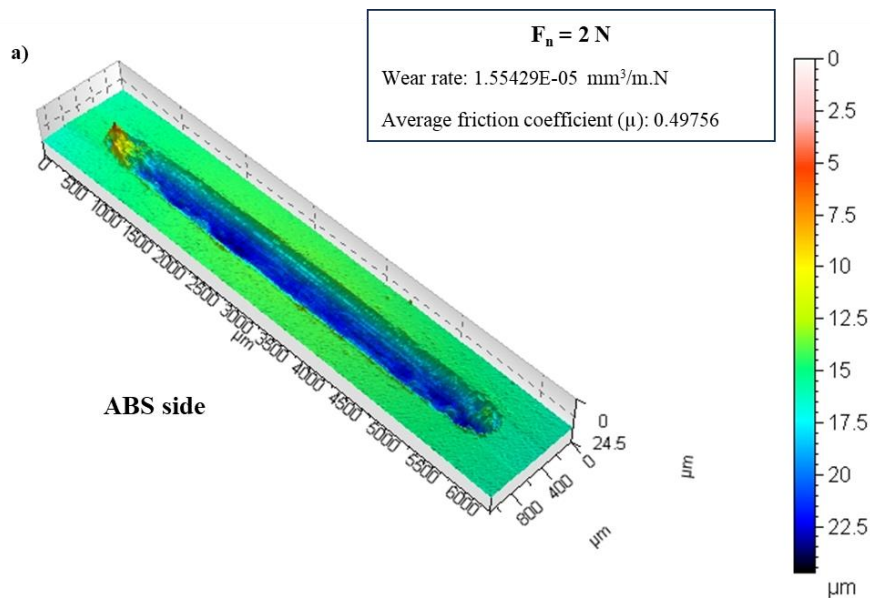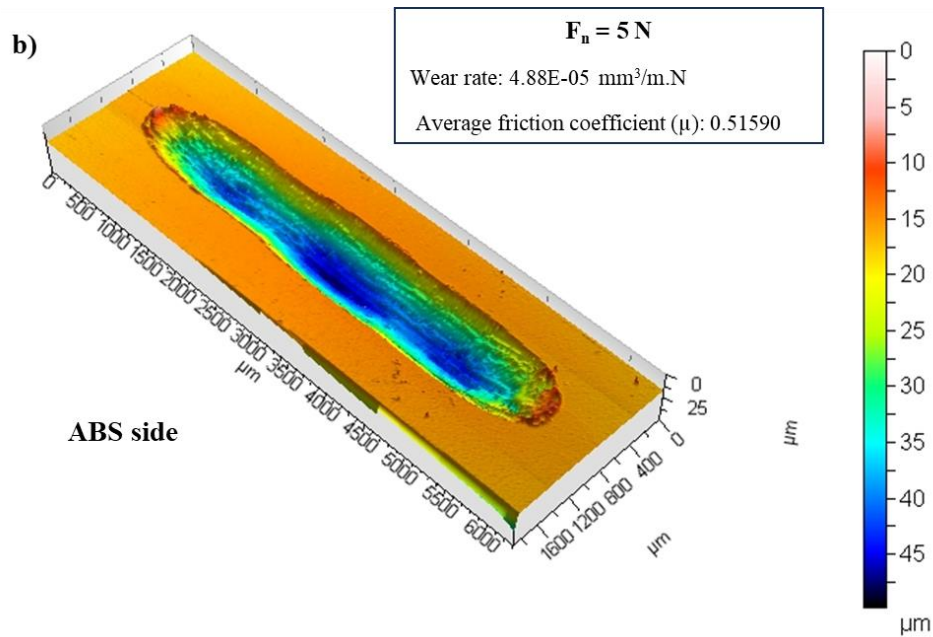
Figure 4-24: 3D wear-scar measurement of ABS side a) 2 N and b) 5 N.

Interestingly, the wear rate of ABS increases with load while that of PMMA decreases with load. This behavior is contrary to the common expectation that wear generally increases with load. This suggests that the wear mechanisms of these materials are significantly different under different loads.

The wave appearance observed on the PMMA side is more pronounced compared to the ABS side. This phenomenon is attributed to the stick-slip behavior occurring during the ball's contact with the PMMA surface. The intermittent stopping and starting of the ball create periodic waves on the PMMA side, which are less evident on the ABS side. This stick-slip effect results from the higher frictional forces and the increased brittleness of PMMA Figure 4-25, leading to more noticeable surface undulations. In contrast, the more consistent frictional response of ABS results in a smoother surface with fewer wave patterns. This difference highlights PMMA's sensitivity to frictional variations and its tendency to exhibit more pronounced surface deformations under dynamic loading conditions.

a)

$F_n = 2\ N$

Wear rate: 9.91434E-07 $mm^3/m.N$

Average friction coefficient (μ): 0.233197

PMMA side

b)

$F_n = 5\ N$

Wear rate: 5.61559E-07 $mm^3/m.N$

Average friction coefficient (μ): 0.24113
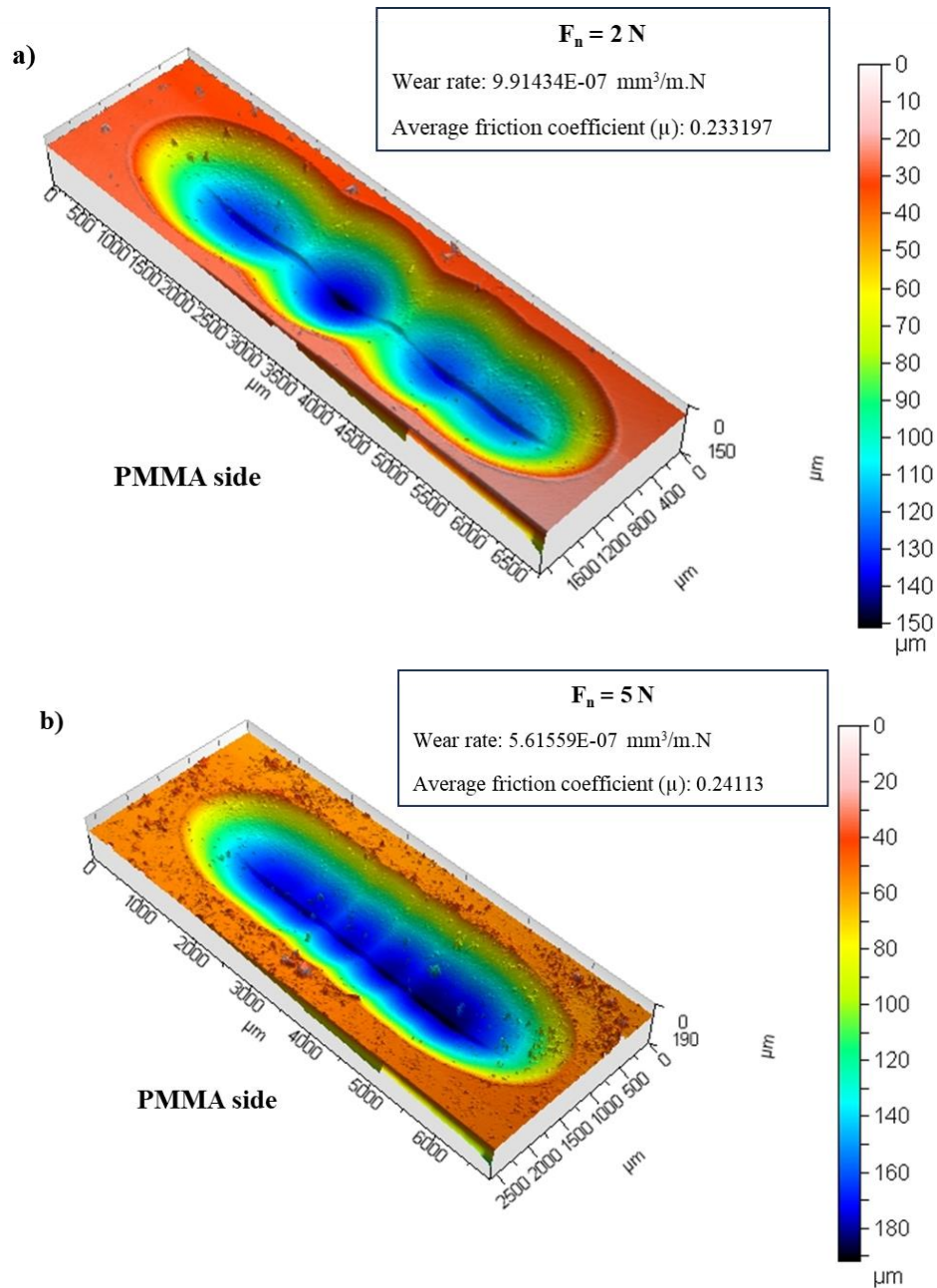
PMMA side

Figure 4-25: 3D wear-scar measurement of PMMA side a) 2 N and b) 5 N.

Figure 4-26 summarizes the dimensions of the wear marks on the ABS and PMMA layers of the two-layer foil under applied loads of 2 N and 5 N. On the ABS side, the width of the wear trace exhibited a continuous increase, ranging from 305 µm to 540 µm as the applied load increased, accompanied by a corresponding increase in trace depth. In contrast, the width of the wear trace on the PMMA side remained constant at 1020 µm, regardless of the load applied, with a similar trend observed in trace depth.
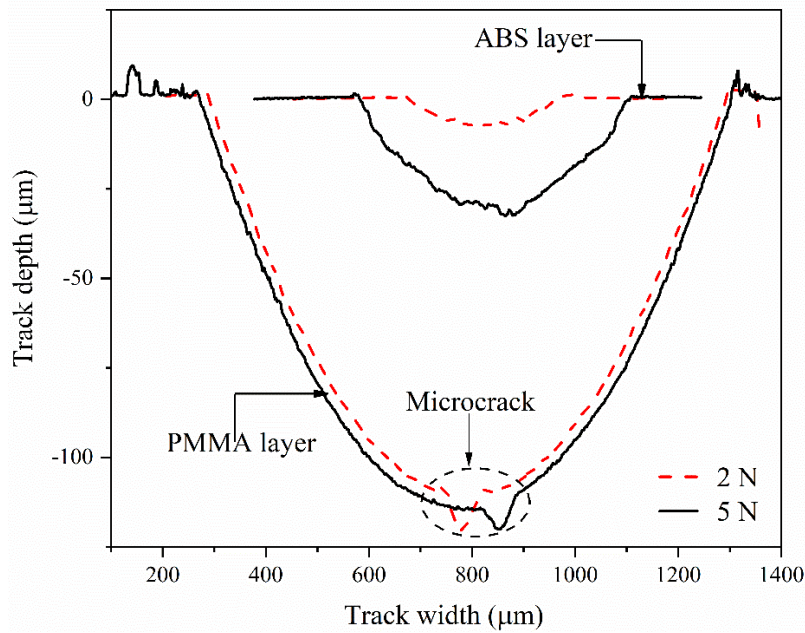
Figure 4-26: Typical depth profiles of experimental ABS/PMMA bilayer sheet after tribological testing.

The findings of the friction and wear testing demonstrate that the surface of ABS is more helpful to thermoforming processes than the smoother surface of PMMA. The matte texture of ABS facilitates superior adhesion and interaction with molds, thereby facilitating uniform contact during processing. In contrast, the smooth surface of PMMA presents a challenge in maintaining consistent contact with the mold, which may affect the quality and precision of the thermoformed product. This enhanced interaction with ABS underscores its utility in contexts where robust adhesion to the mold is paramount for attaining optimal manufacturing outcomes.

These observations are further corroborated by the disparate wear responses of the two layers under varying load conditions. As a ductile material, ABS demonstrates a gradual increase in wear track width and depth with increasing load, indicating its susceptibility to deformation and material loss. In contrast, PMMA, which is brittle and has a lower COF than ABS, maintains a constant width and depth of wear track under varying loads. Although this indicates that PMMA is resistant to substantial dimensional alterations, it also renders it susceptible to localized failures, such as the observed stick-slip phenomenon. The emergence of stick-slip on the PMMA side serves to highlight its brittleness, as the inability of the material to undergo plastic deformation results in intermittent oscillatory motion during sliding.

The contrasting wear behaviors of ABS and PMMA provide crucial insights into their performance characteristics within the bilayer structure. The load-dependent deformation of ABS suggests greater adaptability and interaction with mold surfaces, whereas the stability of PMMA, despite its brittleness, suggests limitations in applications requiring flexibility. These differences are of critical importance for determining the appropriate use of each material in applications involving friction, wear resistance, and durability, especially for processes like thermoforming that rely on surface adhesion and uniform contact.

4.4.3. Conclusion

The analysis of the results indicates that the ABS/PMMA bilayer exhibits strong thermal and mechanical properties, demonstrating high thermal stability. However, temperature variations significantly impact the material's mechanical behavior. As temperature increases, there is a noticeable decrease in the maximum elastic limit and Young's modulus, while the material shows a substantial increase in deformation at the break. Conversely, a higher deformation rate leads to rapid fracture and an increase in both Young's modulus and the elastic limit. The bilayer displays considerable flexibility (ductility) under bending and impact across different temperatures, attributed to the presence of ABS, which benefits from the toughness provided by acrylonitrile. On the other hand, PMMA is more brittle in bending but offers higher hardness compared to ABS. The COF for ABS is greater than that of PMMA, indicating ABS's suitability for contact applications involving the industries. Fractographic analysis reveals that the bilayer possesses significant ductility, with a strong interaction between the ABS and PMMA layers, resulting in overall satisfactory performance.

Conclusions & Perspectives

This thesis examines the characterization of an ABS/PMMA bilayer polymer, with a particular focus on its use in the thermoforming process. It includes a comprehensive literature review on thermoplastic polymer properties and the manufacturing steps for bathtubs. Furthermore, it investigates the influence of key factors such as temperature, rate, and friction on the interaction between the bathtub and the thermoforming process, to enhance understanding of the polymer's performance.

The initial part of the study examines the prevalent utilization of thermoforming techniques for thermoplastic polymer sheets in engineering contexts. These sheets are typically semi-finished products, manufactured through extrusion, injection molding, or analogous processes, which must then undergo processing at various stages. In the industrial context of the industrial sanitary materials company (EIMS), ABS/PMMA bilayer polymer is a key material utilized in the production of sanitary products, including bathtubs. The material undergoes several crucial steps during thermoforming, including clamping, where the sheet is heated to a specific temperature to ensure even distribution on both sides in the pre-stretching (bubbling) step. This is followed by the pre-stretching of the sheet to its final shape in the forming stage. Finally, cooling fans are activated to obtain the bathtub product, completing the process by stabilizing the material's shape. The behavior of the ABS/PMMA bilayer during this process is of great consequence, as it is directly related to temperature, strain rate, and contact conditions. An understanding of this behavior is essential for the optimization of the production process and the assurance of the quality and performance of the final product.

The second part of the study was dedicated to examining the behavior of amorphous polymers, with a particular focus on analyzing their performance in the thermoforming process and studying their interactions with other materials. The thermal properties of the ABS/PMMA bilayer were subjected to comprehensive analysis, with a specific focus on thermal stability and glass transition temperature. Furthermore, viscoelastic and mechanical properties were evaluated through dynamic mechanical analysis (DMA) and tensile tests conducted at varying temperatures and load rates. The tensile and impact test outcomes were then examined using scanning electron microscopy

(SEM), which facilitated the visualization of fracture surfaces and the investigation of interactions between the ABS and PMMA layers. Moreover, the ABS/PMMA bilayer was evaluated in comparison with pure ABS and pure PMMA, to determine the flexibility and mechanical performance of these materials. The hardness of the ABS/PMMA bilayer, as well as that of the pure ABS and pure PMMA materials, was determined using the Shore D and Vickers methods, thereby providing information on their surface resistance. Additionally, the wear rate and coefficient of friction of the ABS and PMMA layers were determined by tribological tests, which revealed significant differences in their frictional behavior. This comprehensive analysis provided important information on the material properties and performance of the ABS/PMMA bilayer in comparison with its components.

Based on the experimental results obtained, the characterization of the ABS/PMMA bilayer can be further refined by considering the following aspects:

- The ABS layer exhibits superior thermal stability in comparison to the ABS/PMMA bilayer and the PMMA layer. The glass transition temperature of the bilayer is determined to be 111.09°C, which represents an average of the glass transition temperatures of the individual ABS and PMMA layers.
- The viscoelastic properties obtained from the DMA tests display minimal variations as a function of frequency, and the glass transition temperature is found to be in accordance with the results obtained from the DSC analysis.
- Temperature and strain rate significantly influence the mechanical properties of the ABS/PMMA bilayer. As temperature increases, there is a marked reduction in yield stress, ultimate stress, and elastic modulus. The reduction in strength is more pronounced at lower strain rates, while at higher strain rates, the decrease in strength is less severe. This indicates that the bilayer's viscoelastic behavior is highly sensitive to temperature and strain rate, which in turn affects its stress and strain performance. Notably, the elastic modulus shows only slight variation with different strain rates across all temperatures.
- The viscoelastic behavior of the ABS/PMMA bilayer sheet follows a more regular pattern at lower strain rates, suggesting a more predictable response under these conditions.

- The fractography analysis of the ABS/PMMA bilayer following mechanical testing indicated that the tensile test data demonstrate a favorable interaction between the ABS and PMMA bilayers. At low strain rates, the bilayer exhibited a ductile rupture, while at high strain rates, it exhibited a brittle fracture. Additionally, the bilayer was observed to undergo ductile rupture at elevated temperatures.

- SEM images of the ABS/15% PMMA bilayer revealed that elevated temperatures enhance the ductility of the ABS/PMMA bilayer under tensile testing, whereas higher loading rates increase its brittleness. As temperatures rose, the ABS layer demonstrated increased impact strength and energy absorption, while the PMMA layer remained susceptible to brittle fracture.

- The results of the three-point bending test revealed that PMMA exhibited brittle behavior, in comparison to ABS, which demonstrated high elongation at break, indicative of ductile behavior. The ABS/PMMA bilayer thus exhibits a combination of superior bending strength and notable ductility, largely attributable to the butadiene content of ABS, which represents a significant advantage for thermoforming processes.

- The comparative analysis of the Shore D and Vickers hardness tests has yielded significant insights into the mechanical properties of ABS/PMMA materials. While the Shore D test effectively measures surface hardness, the Vickers test provides a more nuanced understanding of the material's response under varying forces. The findings indicate that PMMA exhibits higher hardness and brittleness than ABS, which is softer and more ductile.

- The analysis of the friction and wear of the ABS/PMMA bilayer sheet reveals significant distinctions in the behavior of each material under variable loads. The COF increases with increased loads for both the ABS and PMMA surfaces, with the ABS/PMMA bilayer exhibiting a more pronounced friction response. The ABS component contributes more to the overall frictional resistance in the bilayer structure, while the PMMA component, due to its harder and more fragile nature, leads to significant wear.

References

[1] Y. Dong, R. J. T. Lin, and D. Bhattacharyya, "Determination of critical material parameters for numerical simulation of acrylic sheet forming," *J. Mater. Sci.*, vol. 40, no. 2, pp. 399–410, 2005, doi: 10.1007/s10853-005-6096-0.

[2] G. Gruenwald, *Thermoforming: a plastics processing guide*. Routledge, 2018.

[3] J. Cha, H. Y. Song, K. Hyun, and J. S. Go, "Rheological measurement of the nonlinear viscoelasticity of the ABS polymer and numerical simulation of thermoforming process," *Int. J. Adv. Manuf. Technol.*, vol. 107, no. 5–6, pp. 2449–2464, 2020, doi: 10.1007/s00170-020-04979-7.

[4] Bart VAN MIEGHEM, "An intelligent experimental approach for the optimisation of the process parameters for the thermoforming of plastics and composites," Arenberg Doctoral School, 2015.

[5] A. Erner, "Etude experimentale du thermoformage Assiste Par poincon d'un melange de polystyrenes," Ecole des Mines de Paris, 2005.

[6] O. Ekşi and H. Üstünel, "Application of parabolic blending for the estimation of thickness distribution in thermoformed products," *J. Elastomers Plast.*, vol. 53, no. 6, pp. 583–598, 2021, doi: 10.1177/0095244320959801.

[7] J. Cha, M. Kim, D. Park, and J. S. Go, "Experimental determination of the viscoelastic parameters of K-BKZ model and the influence of temperature field on the thickness distribution of ABS thermoforming," *Int. J. Adv. Manuf. Technol.*, vol. 103, no. 1–4, pp. 985–995, 2019, doi: 10.1007/s00170-019-03408-8.

[8] J. L. Throne, *Understanding Thermoforming*. Germany: Hanser, 2008.

[9] Peter W. Peter, *Fundamentals of Plastics Thermoforming*. Morgan & CLaypool, 2009.

[10] G. Sala, D. Cassago, and L. Di Landro, "A numerical and experimental approach to optimise sheet stamping technologies: Polymers thermoforming," *Mater. Des.*, vol. 23, no. 1, pp. 21–39, 2002, doi: 10.1016/S0261-3069(01)00037-1.

[11] B. V. Pierre G. Lafleur, *Polymer Extrusion*. Wiley, 2014.

[12] J. P. Tim A. Osswald and Hernández-Ortiz, *Polymer processing :modeling and simulation*, no. 37. Germany: Hanser Publishers, 2006.

[13] K. Christian, "Solids Conveying , Melting and Melt Conveying in Single Screw Extruders and Extrusion Dies," Johannes Kepler University Linz, 2021.

[14] J. Vlachopoulos and N. D. Polychronopoulos, *Understanding rheology and technology of polymer extrusion*. 2019.

[15] S. Deshmukh *et al.*, "Extrusion of highly filled flexible polymer sheet," *Polym. Eng. Sci.*, vol. 60, no. 11, 2020, doi: 10.1002/pen.25509.

[16] D. Feldman, *Thermoforming, by James L. Throne, Hanser, Munich and Vienna*, vol. 25, no. 9. 1987. doi: https://doi.org/10.1002/pol.1987.140250914.

[17] M. Biron, *Aide-mémoire Transformation des matières plastiques*, Dunod. paris, 2010.

[18] Ben Moore, "In-Cycle Control of the Thermoforming Reheat Process," McGill University, 2002.

[19] J. J. M. Cormont, "Differences between amorphous and crystalline plastics with respect to thermoforming," *Adv. Polym. Technol.*, vol. 5, no. 3, pp. 209–218, 1985, doi: https://doi.org/10.1002/adv.1985.060050305.

[20] D. Hylton, "Laboratory techniques for predicting material thermoformability: a review," *SPE Antec , Montr.*, pp. 580–583, 1991.

[21] H. Münstedt, S. Kurzbeck, and J. Stange, "Importance of elongational properties of polymer melts for film blowing and thermoforming," *Polym. Eng. Sci.*, vol. 46, pp. 1190–1195, 2006.

[22] M. Yamaguchi and K.-I. Suzuki, "Enhanced strain hardening in elongational viscosity for HDPE/crosslinked HDPE blend. II. Processability of thermoforming," *J. Appl. Polym. Sci.*, vol. 86, no. 1, pp. 79–83, 2002, doi: https://doi.org/10.1002/app.10915.

[23] P. J. Martin *et al.*, "Biaxial characterisation of materials for thermoforming and blow moulding," *Plast. rubber Compos.*, vol. 34, no. 5–6, pp. 276–282, 2005.

[24] D. Laroche and F. Erchiqui, "Experimental and Theoretical Study of the Thermoformability of Industrial Polymers," *J. Reinf. Plast. Compos.*, vol. 19, no. 3, pp. 230–239, Feb. 2000, doi: 10.1177/073168440001900303.

[25] D. Laroche and F. Erchiqui, "Experimental and theoretical study of the thermoformability of industrial polymers," *Annu. Tech. Conf. - ANTEC, Conf. Proc.*, vol. 1, no. January 1999, pp. 676–680, 1998, doi: 10.1177/875608799901500404.

[26] C. P. J. O'Connor, G. Menary, P. J. Martin, and E. McConville, "Finite element analysis of the thermoforming of Polypropylene," *Int. J. Mater. Form.*, vol. 1, no. SUPPL. 1, pp. 779–782, 2008, doi: 10.1007/s12289-008-0291-x.

[27] N. Martin, J. F. Lappin, E. Harkin-Jones, and P. J. Martin, "The Use of hot Impact Testing in the Simulation of the Plug Assisted Thermoforming Process," 2000.

[28] B. Hegemann, "Deformationsverhalten von Kunststoffen beim Thermoformen - experimentelle und virtuelle Bestimmung-," pp. 1–111, 2004.

[29] H. C. P. Lau, S. N. Bhattacharya, and G. Field, "Melt strength of polypropylene: Its relevance to thermoforming," *Polym. Eng. Sci.*, vol. 38, pp. 1915–1923, 1998.

[30] D. Hylton, "Thermoforming Index - A New Test for Sheet," in *Thermoforming Quarterly*, 2011, pp. 12–14.

[31] M. N. Charalambides, L. Wanigasooriya, G. J. Williams, and S. Chakrabarti, "Biaxial deformation of dough using the bubble inflation technique. I. Experimental," *Rheol. Acta*, vol. 41, no. 6, pp. 532–540, 2002, doi: 10.1007/s00397-002-0242-2.

[32] A. J. De Vries and C. Bonnebat, "Uni- and biaxial stretching of chlorinated pvc sheets. A fundamental study of thermoformability," *Polym. Eng. \& Sci.*, vol. 16, no. 2, pp. 93–100, 1976, doi: https://doi.org/10.1002/pen.760160206.

[33] C. Galliot and R. H. Luchsinger, "Uniaxial and biaxial mechanical properties of ETFE foils," *Polym. Test.*, vol. 30, no. 4, pp. 356–365, 2011, doi:

doi.org/10.1016/j.polymertesting.2011.02.004.

[34] K. Y. T. R. M. G. M. C. G. A. P. J. Martin C. W. Tan and E. M. A. Harkin-Jones, "Biaxial characterisation of materials for thermoforming and blow moulding," *Plast. Rubber Compos.*, vol. 34, no. 5–6, pp. 276–282, 2005, doi: 10.1179/174328905X64803.

[35] D. J. Hitt and M. Gilbert, "A machine for the biaxial stretching of polymers," *Polym. Test.*, vol. 13, no. 3, pp. 219–237, 1994, doi: 10.1016/0142-9418(94)90029-9.

[36] A. Dharia and D. Hylton, "Novel method for rapid determination of thermoformability," in *Annual Technical Conference Proceedings (ANTEC)*, 2005, pp. 1214–1219.

[37] F. Beilharz, C. Bonten, and P. Eyerer, "Influence of processing conditions on the thermoformability of PP-sheet material," in *SPE annual technical conference, Massachusetts, USA*, 2011, pp. 1–5.

[38] S. S. Morye, "A comparison of the thermoformability of a PPE/PP blend with thermoformable ABS. Part I: Small deformation methods," *Polym. Eng. Sci.*, vol. 45, pp. 1369–1376, 2005.

[39] B. Noria, "Calcul Des Propriétés Physiques Par Modélisation Moléculaire Des Copolymères," Université des Sciences et de la Technologie d'Oran Mohamed Boudiaf, 2016.

[40] B. M. Ouassini, "Étude Des Polymères Par Dynamiques Moléculaire," Universite Des Scienes et de la technologie Mohamed Boudiaf, 2015.

[41] M. Dupeux, *Aide-mémoire Science des matériaux*, Dunod. paris, 2004.

[42] C. Paris, "Etude et Modélisation de la Polymérisation Dynamique de Composites à Matrice Thermodurcissable," Génie Mécanique et Mécanique des Matériaux, 2011.

[43] K. Friedrich, "Polymer composites for tribological applications," *Adv. Ind. Eng. Polym. Res.*, vol. 1, no. 1, pp. 3–39, 2018, doi: 10.1016/j.aiepr.2018.05.001.

[44] EIMS, "Entreprise industrielle de matriel sanitaire (EIMS-Miliana), Algeria," 2024.

[45] L. R. Schmidt and J. F. Carley, "Biaxial stretching of heat-softened plastic sheets using an inflation technique," *Int. J. Eng. Sci.*, vol. 13, no. 6, pp. 563–578, 1975, doi: 10.1016/0020-7225(75)90091-9.

[46] Sven Engelmann, *Advanced Thermoforming Methods, Machines and Materials, Applications and Automation*. Germany: Wiley, 2012.

[47] B. Van Mieghem, F. Desplentere, A. Van Bael, and J. Ivens, "Improvements in thermoforming simulation by use of 3D digital image correlation," *Express Polym. Lett.*, vol. 9, no. 2, pp. 119–128, 2015, doi: 10.3144/expresspolymlett.2015.13.

[48] S. Kommoji, R. Banerjee, N. Bhatnagar, and A. K. Ghosh, "Studies on the stretching behaviour of medium gauge high impact polystyrene sheets during positive thermoforming," *J. Plast. Film Sheeting*, vol. 31, no. 1, pp. 96–112, 2015, doi: 10.1177/8756087914538443.

[49] H. Zhang, F. Che, T. Lin, and W. Zhao, *Modeling, analysis, design, and tests for electronics packaging beyond moore*. Woodhead Publishing, 2019.

[50] A. G. Dastidar, "Modeling and simulation of thermoforming," Université de Lille, 2022.

[51] R. McCool and P. J. Martin, "The role of process parameters in determining wall thickness distribution in plug-assisted thermoforming," *Polym. Eng. Sci.*, vol. 50, no. 10, pp. 1923–1934, 2010.

[52] D. Marathe *et al.*, "Effect of plug temperature on the strain and thickness distribution of components made by plug assist thermoforming," *Int. Polym. Process.*, vol. 31, no. 2, pp. 166–178, 2016.

[53] R. A. Morales, M. V Candal, O. O. Santana, A. Gordillo, and R. Salazar, "Effect of the thermoforming process variables on the sheet friction coefficient," *Mater. Des.*, vol. 53, pp. 1097–1103, 2014.

[54] B. Van Mieghem, J. Ivens, and A. Van Bael, "Consistency of strain fields and thickness distributions in thermoforming experiments through stereo DIC," *Exp. Tech.*, vol. 40, pp. 1409–1420, 2016.

[55] K. Kouba, O. Bartos, and J. Vlachopoulos, "Computer simulation of thermoforming in complex shapes," *Polym. Eng. Sci.*, vol. 32, no. 10, pp. 699–704, 1992.

[56] H. F. Nied, C. A. Taylor, and H. G. Delorenzi, "Three-dimensional finite element simulation of thermoforming," *Polym. Eng. Sci.*, vol. 30, no. 20, pp. 1314–1322, 1990.

[57] H. G. DeLorenzi and H. F. Nied, "Blow molding and thermoforming of plastics: finite element modeling," *Comput. Struct.*, vol. 26, no. 1–2, pp. 197–206, 1987.

[58] M. Elmeguenni, "Effet de la triaxialité sur le comportement et la rupture du polyéthylène haute densité : approches expérimentales et numériques.," *Thèse*, p. 227, 2010.

[59] M. Carrega, *Aide-mémoire Matières plastiques*, Dunod. paris, 2009.

[60] Julie VERA, "Texturation de surface de pièces polymères injectées à partir de la structuration submicronique du moule," Ecole doctorale Matériaux de Lyon, 2017.

[61] A. A. Abdel-Wahab, S. Ataya, and V. V. Silberschmidt, "Temperature-dependent mechanical behaviour of PMMA: Experimental analysis and modelling," *Polym. Test.*, vol. 58, pp. 86–95, 2017, doi: 10.1016/j.polymertesting.2016.12.016.

[62] N. Berrahou, A. Mokaddem, B. Doumi, S. Hiadsi, N. Beldjoudi, and A. Boutaous, "Investigation by molecular dynamics simulation of the glass transition temperature and elastic properties of amorphous polymers PMMA, PMAAM and PMMA co PMAAM copolymers," *Polym. Bull.*, vol. 73, no. 11, pp. 3007–3017, 2016, doi: 10.1007/s00289-016-1637-z.

[63] P. Weiss, "La chimie des polymères," *Univ. Médicale Virtuelle Francoph.*, 2010.

[64] P. Combette and I. Ernoult, "Physique des polymeres-Tome 1: Structure, fabrication, emploi," *Collect. Enseign. des Sci. Hermann éditeurs*, 2005.

[65] J. H. Gibbs and E. A. DiMarzio, "Nature of the glass transition and the glassy

state," *J. Chem. Phys.*, vol. 28, no. 3, pp. 373–383, 1958.

[66] M. Chanda and S. K. Roy, *Plastics technology handbook*. CRC press, 2006.

[67] M. Tsige and P. L. Taylor, "Simulation study of the glass transition temperature in poly (methyl methacrylate)," *Phys. Rev. E*, vol. 65, no. 2, p. 21805, 2002.

[68] Kenny B. Lipkowitz Thomas R. Cundari, *Reviews in Computational Chemistry 25*. John Wiley & Sons, 2007.

[69] J. S. Reinaldo, L. M. Pereira, E. S. Silva, T. C. P. Macedo, I. Z. Damasceno, and E. N. Ito, "Thermal, mechanical and morphological properties of multicomponent blends based on acrylic and styrenic polymers," *Polym. Test.*, vol. 82, p. 106265, 2020, doi: 10.1016/j.polymertesting.2019.106265.

[70] D. A. Brown, E. W. Lee, C. T. Loh, and S. T. Kee, "A New Wave in Treatment of Vascular Occlusive Disease: Biodegradable Stents-Clinical Experience and Scientific Principles," *J. Vasc. Interv. Radiol.*, vol. 20, no. 3, pp. 315–324, 2009, doi: 10.1016/j.jvir.2008.11.007.

[71] M. Arzhakov, *Relaxation in Physical and Mechanical Behavior of Polymers*. CRC Press, 2019.

[72] Swallowe and Mol, *Mechanical properties and testing of polymers*. Springer Netherlands, 1999.

[73] S. Turner, *Mechanical testing of plastics*, 2nd editio. George Godwin (London), 1983.

[74] Y. E. Prawatya, "Multivariate optimisation and statistical process control of polymer triboelectric charging," Université de Poitiers, 2018.

[75] N. K. Myshkin, M. I. Petrokovets, and A. V. Kovalev, "Tribology of polymers: Adhesion, friction, wear, and mass-transfer," *Tribol. Int.*, vol. 38, no. 11-12 SPEC. ISS., pp. 910–921, 2005, doi: 10.1016/j.triboint.2005.07.016.

[76] A. Abdelbary, *Wear of polymers and composites*. Woodhead Publishing, 2015.

[77] R. Brown, *Handbook of polymer testing: short-term mechanical tests*. Shropshire, UK: Rapra Technology Limited, 2002.

[78] H. Wu *et al.*, "On the Application of Vickers Micro Hardness Testing to Isotactic Polypropylene," *Polymers (Basel).*, vol. 14, no. 9, pp. 1–16, 2022, doi: 10.3390/polym14091804.

[79] R. SEDLÁK, "Development of advanced ceramic – graphene platelet nanocomposites," Technical university of košice, 2018.

[80] H. Wu, G. Ma, and Y. Xia, "Experimental study of tensile properties of PMMA at intermediate strain rate," *Mater. Lett.*, vol. 58, no. 29, pp. 3681–3685, 2004, doi: 10.1016/j.matlet.2004.07.022.

[81] G. H. Michler, *Atlas of Polymer Structures*. Munich: Hanser, 2016.

[82] D. M. Kulich, S. K. Gaggar, V. Lowry, and R. Stepien, "Acrylonitrile–Butadiene–Styrene Polymers," in *Encyclopedia of Polymer Science and Technology*, John Wiley & Sons, Ltd, 2001. doi: https://doi.org/10.1002/0471440264.pst011.

[83] Mohammad Mahmoud Safwat Fareed NAGY, "Statistical methods for improving quality in thermoforming processes," Menoufiya University, 2013.

[84] M. A. Dundar, "Strain Rate Dependence And Impact Behavior Of Abs (acrylonitrile-Butadiene-Styrene) Amorphous Thermoplastic," School of Wayne State University, 2017.

[85] A. Alonso, M. Lázaro, D. Lázaro, and D. Alvear, "Thermal characterization of acrylonitrile butadiene styrene-ABS obtained with different manufacturing processes," *J. Therm. Anal. Calorim.*, vol. 148, no. 20, pp. 10557–10572, 2023, doi: 10.1007/s10973-023-12258-2.

[86] S. Küchler, *Materials and Design*. 2017. doi: 10.5040/9781474259071.ch-001.

[87] M. F. Ashby, "Introduction : material dependence," *Mater. Environ.*, pp. 1–126, 2021.

[88] S. Palaniyappan, D. Veeman, K. Rajkumar, K. Vishal, R. Kishore, and L. Natrayan, "Photovoltaic Industrial Waste as Substitutional Reinforcement in the Preparation of Additively Manufactured Acrylonitrile Butadiene Styrene Composite," *Arab. J. Sci. Eng.*, vol. 47, no. 12, pp. 15851–15863, 2022, doi: 10.1007/s13369-022-06806-5.

[89] S. Ponsuriyaprakash, P. Udhayakumar, and R. Pandiyarajan, "Mechanical characterization and morphological behavior of a novel composite of ABS polymer strengthened by cellulose," *J. Chinese Inst. Eng. Trans. Chinese Inst. Eng. A*, vol. 45, no. 3, pp. 255–265, 2022, doi: 10.1080/02533839.2022.2034055.

[90] H. Kita, M. Higuchi, A. Miura, and J. Moalli, "morphology and fractography: Fractography of abs," in *Plastics Failure Analysis and Prevention, Plastics Design Library*, William Andrew Publishing, 2001, pp. 121–125.

[91] S. A. Madkour, S. Tirkes, and U. Tayfun, "Development of barite-filled acrylonitrile butadiene styrene composites: Mechanical, thermal, melt-flow and morphological characterizations," *Appl. Surf. Sci. Adv.*, vol. 3, no. November 2020, p. 100042, 2021, doi: 10.1016/j.apsadv.2020.100042.

[92] R. Marissen *et al.*, "The effect of material defects on the fatigue behaviour and the fracture strain of ABS," *J. Mater. Sci.*, vol. 36, no. 17, pp. 4167–4180, 2001, doi: 10.1023/A:1017960704248.

[93] C. Federico, "Coupled temperature and strain rate effects on non-linear mechanical behaviour of amorphous polymers : Experimental characterisation and modelling of strain rate-temperature superposition To cite this version," Parir Sciences and Letters Research University, 2019.

[94] L. Mascia, *Polymers in Industry from A–Z*. Germany: Wiley, 2012.

[95] U. Ali, K. J. B. A. Karim, and N. A. Buang, "A Review of the Properties and Applications of Poly (Methyl Methacrylate) (PMMA)," *Polym. Rev.*, vol. 55, no. 4, pp. 678–705, 2015, doi: 10.1080/15583724.2015.1031377.

[96] J. M. E, *Physical Properties of Polymers Handbook*, vol. 199, no. Part_1. 2007. doi: 10.1524/zpch.1997.199.part_1.128.

[97] M. KUTZ, *Handbook of Materials Selection*. New York: Wiley, 2002.

[98] A. Nabhan, M. Taha, and N. M. Ghazaly, "Filler loading effect of Al2O3/TiO2 nanoparticles on physical and mechanical characteristics of dental base composite (PMMA)," *Polym. Test.*, vol. 117, no. July 2022, 2023, doi:

10.1016/j.polymertesting.2022.107848.

[99] A. Fouly, A. Nabhan, and A. H. Badran, "Mechanical and Tribological Characteristics of PMMA Reinforced by Natural Materials," *Egypt. J. Chem.*, vol. 65, no. 4, pp. 543–553, 2022, doi: 10.21608/EJCHEM.2021.98063.4572.

[100] D. W. Van Krevelen and K. Te Nijenhuis, *Properties of polymers: their correlation with chemical structure; their numerical estimation and prediction from additive group contributions*. Elsevier, 2009.

[101] C. Y. Zhi, Y. Bando, W. L. Wang, C. C. Tang, H. Kuwahara, and D. Golberg, "Mechanical and thermal properties of polymethyl methacrylate-BN nanotube composites," *J. Nanomater.*, vol. 2008, no. 1, 2008, doi: 10.1155/2008/642036.

[102] A. Charvet, "Study of mechanical properties and damage mechanisms in plasticized cellulose acetate polymers," 2019.

[103] C. Gauthier, A. L. Durier, C. Fond, and R. Schirrer, "Scratching of a coated polymer and mechanical analysis of a scratch resistance solution," *Tribol. Int.*, vol. 39, no. 2, 2006, doi: 10.1016/j.triboint.2005.04.014.

[104] H. Pelletier, C. Gauthier, and R. Schirrer, "Influence of the friction coefficient on the contact geometry during scratch onto amorphous polymers," *Wear*, vol. 268, no. 9–10, 2010, doi: 10.1016/j.wear.2010.01.003.

[105] S. Aid, A. Eddhahak, S. Khelladi, Z. Ortega, S. Chaabani, and A. Tcharkhtchi, "On the miscibility of PVDF/PMMA polymer blends: Thermodynamics, experimental and numerical investigations," *Polym. Test.*, vol. 73, pp. 222–231, 2019, doi: 10.1016/j.polymertesting.2018.11.036.

[106] I. S. Baulin, V. V Yatsenko, and O. M. Kasperovich, "Thermoformation of composite sheets on the basis of abs–plastics with high surface luster," 2012.

[107] K. Schneider and T. Seelig, "Numerical aspects of failure modeling of amorphous thermoplastics," in *Proc. Appl. Math. Mech*, 2014, pp. 133–134. doi: 10.1002/pamm.201410054.

[108] L. Li *et al.*, "Enhanced energy storage performance with high temperature stability in ABS-PLZST composites," *J. Alloys Compd.*, vol. 966, no. March, p. 171308, 2023, doi: 10.1016/j.jallcom.2023.171308.

[109] M. Asif *et al.*, "High energy ion irradiation effect on electrical and optical properties of polymers," *Radiat. Phys. Chem.*, vol. 192, no. September 2021, p. 109931, 2022, doi: 10.1016/j.radphyschem.2021.109931.

[110] M. Z. Rahman, M. Rahman, T. Mahbub, M. Ashiquzzaman, S. Sagadevan, and M. E. Hoque, "Advanced biopolymers for automobile and aviation engineering applications," *J. Polym. Res.*, vol. 30, no. 3, 2023, doi: 10.1007/s10965-023-03440-z.

[111] K. Venkata Chalapathi, M. N. Prabhakar, D. W. Lee, and J. il Song, "Development of thermoplastic self-healing panels by 3D printing technology and study extrinsic healing system under low-velocity impact analysis," *Polym. Test.*, vol. 119, no. January, p. 107923, 2023, doi: 10.1016/j.polymertesting.2023.107923.

[112] B. Acherjee, A. S. Kuar, S. Mitra, D. Misra, and S. Acharyya, "Experimental investigation on laser transmission welding of PMMA to ABS via response surface

modeling," *Opt. Laser Technol.*, vol. 44, no. 5, pp. 1372–1383, 2012, doi: 10.1016/j.optlastec.2011.12.029.

[113] S. A. Ashter, "Thermoforming of Single and Multilayer Laminates," Elsevier, 2014.

[114] M. B. J. Rösler, H. Harders, *Mechanical Behaviour of Engineering Materials*, Metals, Ce. Springer, 2007. doi: 10.1007/978-94-017-2231-5.

[115] O. K. Gohatre, M. Biswal, S. Mohanty, and S. K. Nayak, "An effective sustainable approach towards recycling and value addition of waste poly(vinyl chloride) and acrylonitrile butadiene styrene (ABS) recovered from electronic waste (e-waste)," *J. Polym. Res.*, vol. 28, no. 9, pp. 1–16, 2021, doi: 10.1007/s10965-021-02678-9.

[116] R. Xiao and T. D. Nguyen, "An effective temperature theory for the nonequilibrium behavior of amorphous polymers," *J. Mech. Phys. Solids*, vol. 82, pp. 62–81, 2015, doi: 10.1016/j.jmps.2015.05.021.

[117] W. M. Cheng, G. A. Miller, J. A. Manson, R. W. Hertzberg, and L. H. Sperling, "Mechanical behaviour of poly(methyl methacrylate)," *J. Mater. Sci.*, vol. 25, no. 4, pp. 1931–1938, 1990, doi: 10.1007/bf01045745.

[118] E. M. Arruda, M. C. Boyce, and R. Jayachandran, "Effects of strain rate, temperature and thermomechanical coupling on the finite strain deformation of glassy polymers," *Mech. Mater.*, vol. 19, no. 2–3, pp. 193–212, 1995, doi: 10.1016/0167-6636(94)00034-E.

[119] J. Jancar, R. S. Hoy, E. Jancarova, and J. Zidek, "Effect of temperature, strain rate and particle size on the yield stresses and post-yield strain softening of PMMA and its composites," *Polymer (Guildf).*, vol. 63, pp. 196–207, 2015, doi: 10.1016/j.polymer.2015.03.001.

[120] A. Mimaroglu, O. F. Yenihayat, and A. Celebi, "The influence of thermal history, strain rate and sample geometry on the deformation behaviour of polymers: use of the thermovision technique," *Mater. Des.*, vol. 16, no. 4, pp. 199–203, 1995, doi: 10.1016/0261-3069(95)00037-2.

[121] M. Shirinbayan, J. Fitoussi, F. Kheradmand, A. Montazeri, P. Zuo, and A. Tcharkhtchi, "Coupling effect of strain rate and temperature on tensile damage mechanism of polyphenylene sulfide reinforced by glass fiber (PPS/GF30)," *J. Thermoplast. Compos. Mater.*, vol. 35, no. 11, pp. 1994–2008, 2022, doi: 10.1177/0892705720944229.

[122] A. D. Mulliken and M. C. Boyce, "Mechanics of the rate-dependent elastic-plastic deformation of glassy polymers from low to high strain rates," *Int. J. Solids Struct.*, vol. 43, no. 5, pp. 1331–1356, 2006, doi: 10.1016/j.ijsolstr.2005.04.016.

[123] J. Li *et al.*, "Tensile Behavior of Acrylonitrile Butadiene Styrene at Different Temperatures," *Adv. Polym. Technol.*, vol. 2020, pp. 1–10, 2020, doi: 10.1155/2020/8946591.

[124] P. Y. Huang, Z. S. Guo, and J. M. Feng, "General Model of Temperature-dependent Modulus and Yield Strength of Thermoplastic Polymers," *Chinese J. Polym. Sci. (English Ed.*, vol. 38, no. 4, pp. 382–393, 2020, doi: 10.1007/s10118-020-2360-7.
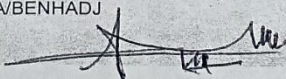
[125] H. Louche, F. Piette-Coudol, R. Arrieux, and J. Issartel, "An experimental and modeling study of the thermomechanical behavior of an ABS polymer structural component during an impact test," *Int. J. Impact Eng.*, vol. 36, no. 6, pp. 847–861, 2009, doi: 10.1016/j.ijimpeng.2008.09.007.

[126] J. Richeton, S. Ahzi, K. S. Vecchio, F. C. Jiang, and R. R. Adharapurapu, "Influence of temperature and strain rate on the mechanical behavior of three amorphous polymers: Characterization and modeling of the compressive yield stress," *Int. J. Solids Struct.*, vol. 43, no. 7–8, pp. 2318–2335, 2006, doi: 10.1016/j.ijsolstr.2005.06.040.

[127] L. Li, Y. Zhang, L. Sun, and H. Hu, "Effects of strain rate and temperature on the mechanical behavior of polymethyl methacrylate (PMMA)," *Polym. Bull.*, vol. 80, no. 8, pp. 8685–8702, 2023, doi: 10.1007/s00289-022-04472-z.

[128] I. Al-hydary, L. Manocha, and P. George, "Preparation and characterization of PMMA-ABS Blend," *Iraqi J. Mech. Mater. Eng.*, vol. 12, no. 4, pp. 709–722, 2012.

[129] H. Kuleyin, R. Gümrük, and S. Çalişkan, "The effect of ABS fraction on the fatigue behavior of PMMA/ABS polymer blends," *Mater. Today Commun.*, vol. 33, no. July, 2022, doi: 10.1016/j.mtcomm.2022.104139.

[130] J. Ma, "The Influence of Processing Conditions on the Mechanical Properties of Poly(Acrylonitrile-Butadiene-Styrene)/ Poly(Methyl Methacrylate) (ABS/PMMA) Blends," *J. Macromol. Sci. Part B Phys.*, vol. 62, no. 4, 2023, doi: 10.1080/00222348.2023.2207897.

[131] A. Khledj, M. H. Miloud, M. Mendas, and I. Zidane, "Temperature-dependent tensile test of ABS / 15 % PMMA bilayer polymer," in *The Third Doctoral Symposium on Technology: Process, Mechanical and Electrical Engineering DST'03-2023*, 2023, pp. 1–2.

[132] A. Khledj, M. H. Miloud, M. Mendas, and P. Hvizdoš, "Mechanical characterisation and morphological properties of ABS / 15 % PMMA bilayer polymer," in *First International Congress on Mchanical Engineering*, Constantine, Algeria, 2023, pp. 219–224.

[133] M. M. Khledj Abdelwahab, Mohamed HADJ MILOUD, "Caractérisation mécanique du feuille polymère multicouche Acrylonitrile Butadiène Styrène – 15 % poly (Méthacrylate du méthyle) utilisé en thermoformage," in *The Second Doctoral Symposium on Technology: Process, Mechanical and Electrical Engineering*, 2022, pp. 71–72.

[134] A. Khledj, M. H. Miloud, M. Mendas, and I. Zidan, "Comparative Analysis of Three Polymers : ABS , PMMA , and ABS / 15 % PMMA bilayer in Three-Point Bending," in *The 5 th International Seminar on Avanced Mecahnical Technologies*, Tlemcen, Algeria, 2024, pp. 3–6.

[135] Y. W. Leong, S. Yamaguchi, M. Mizoguchi, H. Hamada, U. S. Ishiaku, and T. Tsujii, "The effect of molding conditions on mechanical and morphological properties at the interface of film insert injection molded polypropylene-film/ polypropylene matrix," *Polym. Eng. Sci.*, vol. 44, no. 12, pp. 2327–2334, 2004, doi: 10.1002/pen.20260.

[136] L. M. Wittmann and D. Drummer, "Mechanical properties of thermoformed multilayer parts containing non thermoformable materials," *J. Plast. Film Sheeting*, vol. 38, no. 4, pp. 608–628, 2022, doi: 10.1177/87560879221093977.

[137] X. Ji, F. Gao, Z. Geng, and D. Li, "Fabrication of thermoplastic polyurethane/polylactide shape-memory blends with tunable optical and mechanical properties via a bilayer structure design," *Polym. Test.*, vol. 97, no. November 2020, p. 107135, 2021, doi: 10.1016/j.polymertesting.2021.107135.

[138] Z. Chen *et al.*, "Parameter optimization for PETG/ABS bilayer tensile specimens in material extrusion 3D printing through orthogonal method," *Int. J. Adv. Manuf. Technol.*, vol. 127, no. 1–2, pp. 447–458, 2023, doi: 10.1007/s00170-023-11515-w.

[139] Y. Xu, J. Qin, J. Shen, S. Guo, and K. Lamnawar, "Scratch behavior and mechanical properties of alternating multi-layered PMMA/PC materials," *Wear*, vol. 486–487, no. August, p. 204069, 2021, doi: 10.1016/j.wear.2021.204069.

[140] R. B. P. JOSEPH D. MENCZEL, *Thermal analysis of polymers Fundamentals and Applications*. Hoboken, New Jersey: Wiley, 2009.

[141] ISO 527-2, "Plastics - Determination of tensile properties-Part 2: Test conditions for moulding and extrusion plastics," *ISO*, 2012.

[142] ISO 2580-1, "Plastic- Acrylonitrile-butadiene-styrene (ABS) moulding and extrusion materials- part 1: Designation system and basis for specifications," *ISO*, 2015.

[143] Iso 178, "Plastics - Determination of flexural properties," *Int. Stand.*, vol. 2013, no. 1, 2010.

[144] Roger Brown, *Handbook of Polymer Testing Short-Term Mechanical Tests*. Shropshire, UK: Rapra Technology Limited, 2002.

[145] "https://websrv.saske.sk/imr/vedecke-divizie/divizia-keramickych-a-nekovovych-systemov/pristroje/."

[146] A. O. Bouakkaz, A. Albedah, B. B. Bouiadjra, S. M. A. Khan, F. Benyahia, and M. Elmeguenni, "Effect of temperature on the mechanical properties of polypropylene–talc composites," *J. Thermoplast. Compos. Mater.*, vol. 31, no. 7, pp. 896–912, 2018, doi: 10.1177/0892705717729016.

[147] K. P. Menard and K. Peter, *Dynamic mechanical analysis : a practical introduction*. New York: CRC Press LLC, 1999.

[148] M. Foster, B. Love, R. Kaste, and P. Moy, "The Rate Dependent Tensile Response of Polycarbonate and Poly-methylmethacrylate," *J. Dyn. Behav. Mater.*, vol. 1, no. 2, pp. 162–175, 2015, doi: 10.1007/s40870-015-0020-8.

[149] M. A. Dundar, G. S. Dhaliwal, E. Ayorinde, and M. Al-Zubi, "Tensile, compression, and flexural characteristics of acrylonitrile–butadiene–styrene at low strain rates: Experimental and numerical investigation," *Polym. Polym. Compos.*, vol. 29, no. 5, pp. 331–342, 2021, doi: 10.1177/0967391120916619.

[150] N. Brown and I. M. Ward, "Load drop at the upper yield point of a polymer," *J. Polym. Sci. Part A-2 Polym. Phys.*, vol. 6, no. 3, pp. 607–620, 1968.

[151] L. Schanzel, "Phase field modeling of fracture in rubbery and glassy polymers at

finite thermo-viscoelastic deformations," Universität Stuttgart, Stuttgart, 2015.

[152] G. Ozkoc, G. Bayram, and E. Bayramli, "Impact essential work of fracture toughness of ABS/polyamide-6 blends compatibilized with olefin based copolymers," *J. Mater. Sci.*, vol. 43, no. 8, pp. 2642–2652, 2008, doi: 10.1007/s10853-008-2483-7.

Annex 1

The technical data sheet of the ABS/PMMA bilayer sheet used for thermoforming provides key information on the material properties.

EIMSanitaire Unité: MILIANA Structure : ETUDE ET METHODES C.F :451 Doc. 451 / 4.03	FICHE TECHNIQUE PLAQUE ACRYLIQUE

DÉSIGNATION : PLAQUE ACRYLIQUE ABS avec 15% de PMMA (Acrylonitrile butadiène styrène) a une excellente résistance aux rayures et une bonne résistance aux chocs. Il est adapté à la fois sous vide et sous pression

DIMENSION :

N° CODE	DÉSIGNATION PRODUIT	DIMENSION DE LA TOLE [mm]	EPAISSEUR (MM)	POIDS EN[Kg]
50610112	BAIGNOIRE 1700	1780 X 785	[4-5]	[6.1 - 6.6]
50610111	BAIGNOIRE 1600	1680 X785	[4-5]	[5.6 –6.1]
50610110	BAIGNOIRE 1400	1480 X 785	[4-5]	[5.3- 5.8]

Caractéristiques physiques typiques

Propriétés	Unité	Standard	Méthodes d'essais	Valeur
Densité*	g/cm3	ISO1183	-	1.11
Charpy sans encoche	KJ/m2	ISO 179	1fn poli **	>20
Contrainte à la limite élastique	MPa	ISO 527Type 1B	50 mm/min	>38
Module de flexion	MPa	ISO 527Type 1B	50 mm/min	>1800
HDT	oC	ISO 75	***	>100
Norme d'inflammabilité	Rating	UL94	2.0 mm	HB

*La densité mentionnée devrait être utilisée seulement comme guide. Cette valeur peut changer selon le type et la quantité des pigments ou additifs utilisés.

**polissage selon EN 15015 § 5.1.1

***conditions de recuit: 24h à 80°C, puis 16h à 23°C et 50% RH.

Pour les fardeaux de la plaque acrylique :
- Châssis en bois dur
- Filme en Nylon
- poids max du fardeau 800 KG

| ETABLIE PAR iliana Nom :BELKADI ABDELKADER Visa : T S Methode Fabrication	VERIFIEE PAR Nom : A/BENHADJ Visa :	DATE :03/01/2018 VERSION :00

Figure 1: The technical data sheet of the ABS/PMMA bilayer sheet used for thermoforming provides key information on the material properties
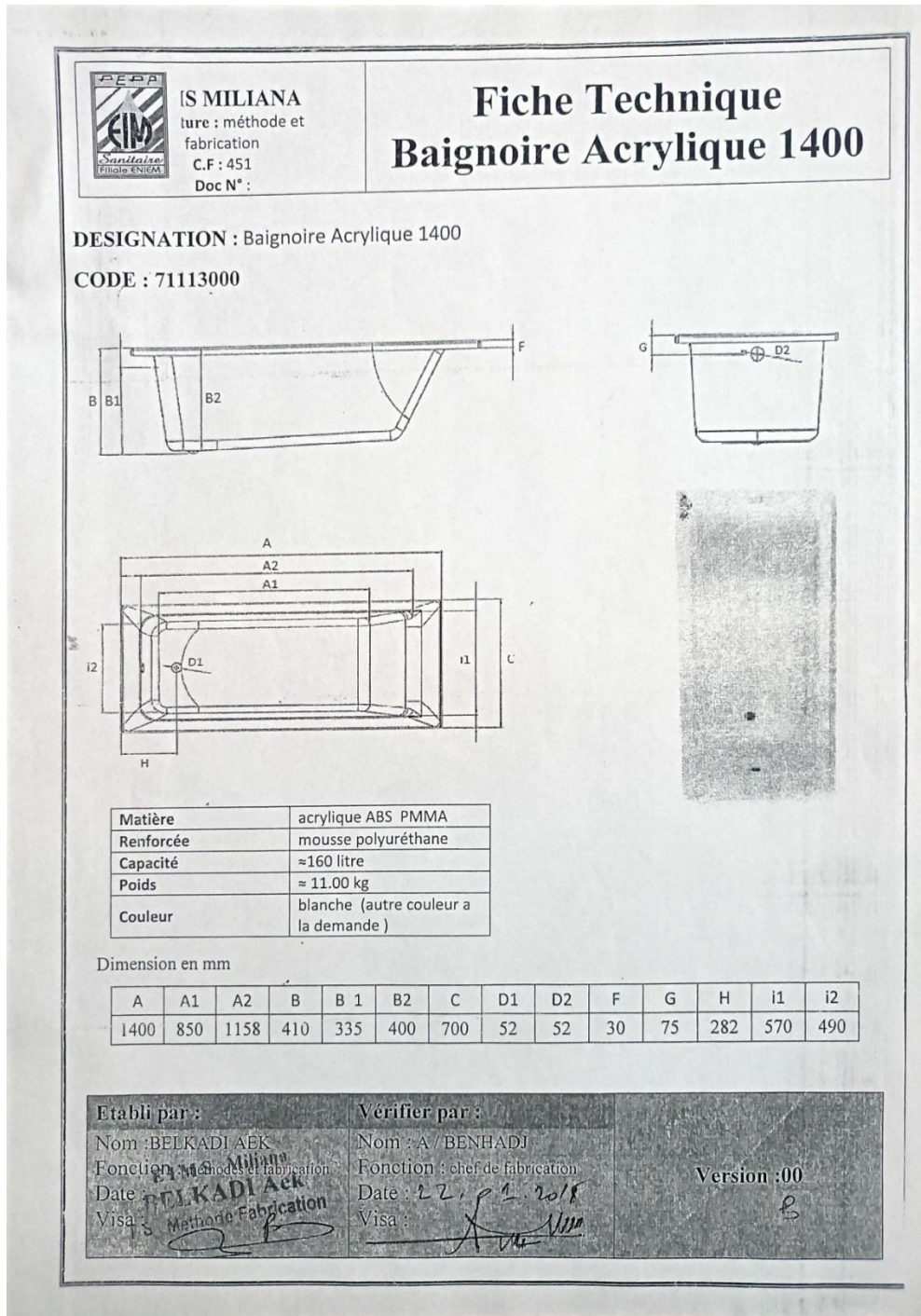
Figure 2: The geometry and dimensions of the 1400 bath, as provided by EIMS

Annex 2

The tensile tests were conducted at different temperatures and strain rates, with each condition subjected to five repeated trials. This rigorous testing approach ensures precise and reliable data on material performance. The results provide insights into the material's behavior under various thermal and deformation conditions.
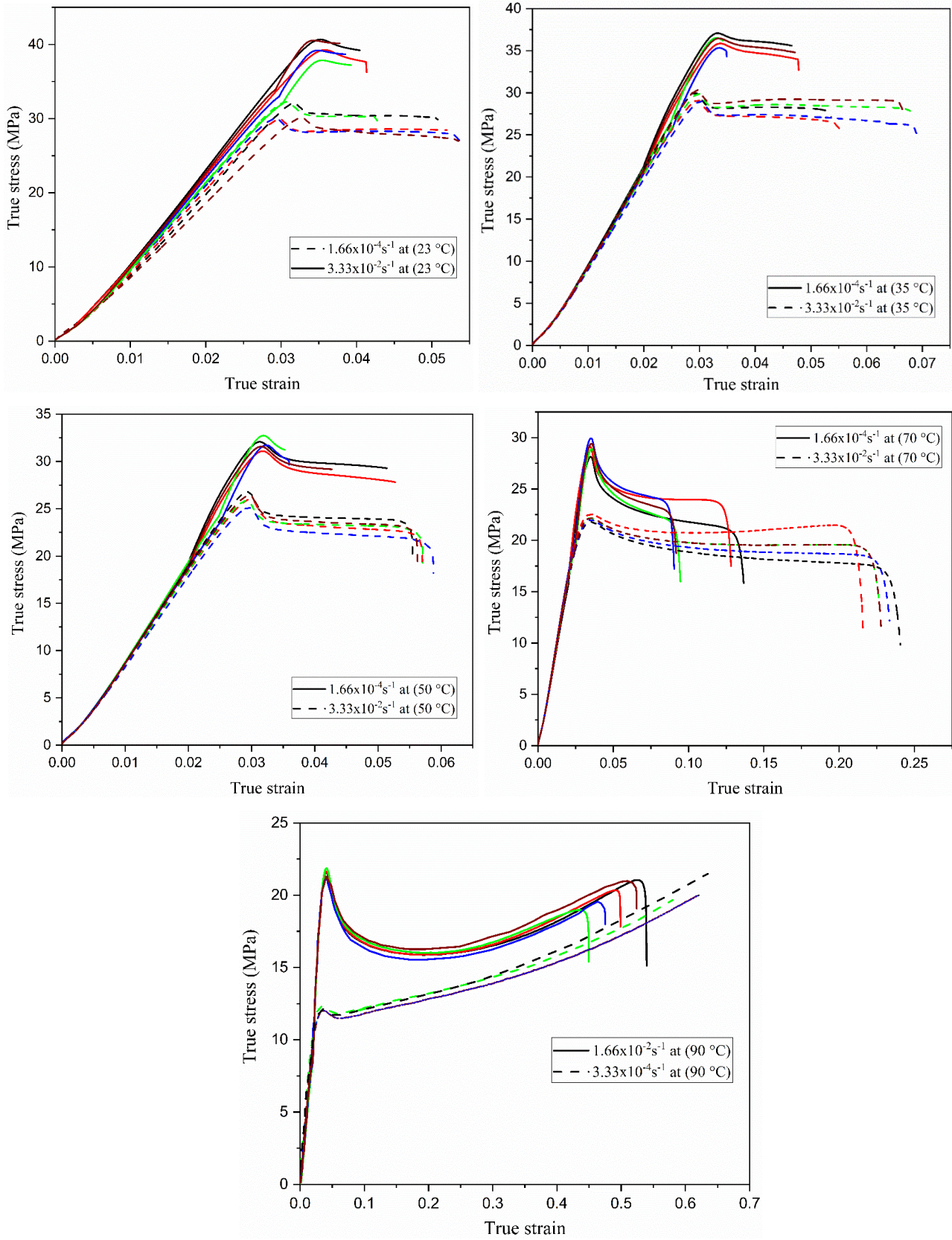
Figure 2: The result of tensile test at different temperatures *vs.* strain rates.